STUDY OF 2D KINETICS AND FORCE REGULATION IN T CELL RECOGNITION

A Dissertation

Presented to

The Academic Faculty

by

Jin Sung Hong

In Partial Fulfillment

of the Requirements for the Degree

Doctor of Philosophy in the

School of Mechanical Engineering

Georgia Institute of Technology

May of 2014

STUDY OF 2D KINETICS AND FORCE REGULATION IN T CELL RECOGNITION

Approved by:

Dr. Cheng Zhu, Advisor
Department of Biomedical Engineering
Georgia Institute of Technology and Emory University

Dr. Julia E. Babensee
Department of Biomedical Engineering
Georgia Institute of Technology and Emory University

Dr. Brian D. Evavold
Department of Microbiology and Immunology
Emory University

Dr. Melissa L. Kemp
Department of Biomedical Engineering
Georgia Institute of Technology and Emory University

Dr. Andres J. Garcia
Department of Mechanical Engineering
Georgia Institute of Technology

Date Approved: March 24, 2014

To my love Shinae Kim

ACKNOWLEDGEMENTS

The completion of this dissertation would not have been possible without the support and nurturing of the following people. I would like to express my deepest appreciation to my advisor and mentor, Dr. Cheng Zhu, for his guidance, encouragement, understanding, patience and support. He has taught me the mindset and the passion to do science. I would like to extend my sincere thanks to my committee members Drs. Julia Babensee, Andres Garcia, Mellissa Kemp, and Dr. Brian Evaold for their scientific suggestions and encouragement in the process of my whole thesis.

I am deeply indebted to the former and current Zhu lab members intellectually and morally. I thank former lab members including Dr. Jizhong Lou, Dr. Veronika Zarnistyna, Dr. Sergey Pryshchep, Dr. Fang Kong, Dr. Wei Chen, Dr. Jun Huang, Dr. Tao Wu, Dr. Xue Xiang, Dr. Jiangguo Lin, Dr. Jin Qian, William Madison Parks, and Dr. Lining Arnold Ju for their encouragement and helpful discussions in the lab. I cannot say more to the love and support from our current lab members including Dr. Jack Wei Chen, Dr. Baoyu Liu, Dr. Zhenhai Li, Dr. Ke Bai, Dr. Hyun-jung Lee, Kaitao Li, Yunfeng Chen, Loice Chingozha, Prithiviraj Jothikumar, Paul Cardenas-Lizana, Chenghao Ge, William Rittase, Václav Beránek, Fangyuan Zhou, Zhou Yuan, Muaz Rushdi, Aaron Rosado and Larissa Doudy. I specially want to thank Larissa Doudy for making a wonderful and conducive lab environment for all of us to do science and helping me with cell purification work.

I am grateful to the great collaboration with former and current Evavold lab members including Dr. Lindsay Edwards, Dr. Joe Sabatino, Jennifer Hoods, Jennifer Lori Blanchfiled, Shayla Shorter, Rakieb Andargachew, Anna Kersh, Ryan Martinez and Laurel Lawrence. I want to specially thank Laurel for all her contribution on keeping the mouse colony.

I also want to thank collaboration with Dr. Paul Allen's lab in Washington University (St. Louis) for SPR experiments and supplying 3.L2 mouse. I want to specially thank NIH tetramer Core Facility at Emory University for providing reagents for this research. Without the reagents this research would not have been possible. I also want to thank other collaborators, Dr. Khalid Salaita and Yun Zhang for DNA force probe study.

Thanks should also go to friends that I met in Atlanta including the members of NCA, Nabi ministry, and Korean-ME grad students. They have been a great part of my life in Atlanta spiritually and morally. I cannot forget my parents and parents-in-law in South Korea, and my dearest wife Shinae Kim for their unstoppable prayers and encouragement. Lastly, I praise my Lord and savior Jesus Christ for allowing this opportunity to seek and enjoy His wonderful creation.

TABLE OF CONTENTS

LIST OF TABLES

LIST OF FIGURES

LIST OF SYMBOLS AND ABBREVIATIONS

2D	Two dimension(al)
3D	Three dimension(al)
A_cK_a	Effective affinity
A_ck_{on}	Effective on-rate
APC	Antigen presenting cell
APL	Altered peptide ligand
BFP	Biomembrane force probe
BSA	Bovine serum albumin
CD	Cluster of differentiation
CTL	Cytotoxic T lymphocytes
CRAC channel	Calcium-release-activated calcium channel
DAG	Diacylglycerol
CREB protein	Cyclic-AMP responsive-element-binding protein
cTEC	Cortical thymic epithelial cells
EAS45	Experimental additive solutions 45
EC_{50}	Half maximal effective concentration
EDTA	Ethylenediamine tetraacetic Acid
FACS	Fluorescence-activated cell sorting
FBS	Fetal bovine serum
FRET	Fluorescence resonance energy transfer
FTOC	Fetal thymic organ culture
ICAM-1	Intercellular adhesion molecule-1
InsP3	Inositol-1,4,5-trisphosphate
InsP3Rs	InsP3 receptors
ITAMs	Immunoreceptor tyrosine based activation motifs

ITK	Interleukin-2-inducible T-cell kinase
k	stiffness or spring constant
K_a	Affinity
K_d	Dissociation constant
k_{on}	On-rate
k_{off}	Off-rate
LAT	Linker for activation of T cells
Lck	Src kinase p56lck
LFA-1	lymphocyte function-associated antigen-1
mAb	Monoclonal antibody
MHC	Major histocompatibility complex
m_l	Site density of ligand
m_r	Site density of receptor
mTEC	Medullary thymic epithelial cells
NFAT	Nuclear factor of activated T cells
NFκB	Nuclear factor-κB
P_a	Adhesion probability (frequency)
PBS	Phosphate buffered saline
PE	Phycoerythrin
PLCγ1	Phospholipase Cγ1
pMHC	Peptide complexed with MHC
PP2	4-amino-5-(4-chloro-phenyl)-7-(t-butyl) pyrazolo [3,4-d] pyrimidine
PZT	Piezoelectric translator
RBC	Red blood cell
RT	Room temperature

s	Seconds
SEM	Standard error of the mean
SLP76	Src-homology-2-domain-containing leukocyte protein of 76kDa
SPR	Surface plasmon resonance
STIM1	Stromal interaction molecule 1
TCR	T cell receptor
WT	Wild type
ZAP-70	Zeta-chain-associated protein kinase 70

SUMMARY

T cell activation and thymic selection are thought to be determined by the binding propensity (avidity or affinity) of the T cell receptor (TCR) to its ligands. However, binding propensity quantified by previous 3D TCR–pMHC kinetics such as using tetramer staining or surface plasmon resonance (SPR) under estimate TCR–pMHC interaction due to neglecting physiological conditions. Recent studies considering membrane contribution in TCR–pMHC interaction reported 2D kinetics and force regulated bond dissociation kinetics have better prediction to biological responses in $CD8^+$ T cells. In this study, we further tested the findings in $CD4^+$ T cells and $CD4^+$ $CD8^+$ (double-positive, DP) thymocytes. We analyzed TCR–pMHC interaction for a well-characterized panel of altered peptide ligands (APLs) on multiple transgenic mouse TCR systems. Using ultrasensitive 2D mechanical assays, *in situ* 2D kinetic measurements show better sensitivity than the SPR 3D kinetic measurements in gauging the ligand potency and thymic selection. Furthermore, force-regulated bond lifetime of TCR–pMHC interaction amplifies the discrimination in recognition of APLs and thymic selection. When force was applied to TCR–pMHC–CD4/8 bonds, two distinct patterns emerged: agonist/negative selecting ligands formed CD4/8-dependent catch-slip bonds where lifetime first increased, reached a maximum, then decreased with increasing force, whereas antagonist/positive selecting ligands formed slip-only bonds where lifetime monotonically decreases with increasing force. Our results highlight an important role of mechanical force in ligand discrimination and suggest a new mechanism for T cell activation and thymic selection that is distinct from previous models based on 3D measurements.

CHAPTER 1 INTRODUCTION

How do T cells recognize subtle difference in TCR ligands, initiate distinct intracellular signals, and induce the appropriate T cell function? is the central question for T cell immunity and central tolerance. The context in which to answer this question includes the complexity of surface molecules on the cell membrane, and the following signaling events across the cell membrane and inside of the cells. Furthermore, T cells are constantly exposed to a physical environment by cell motility and/or cellular cytoskeleton activity. However, previous techniques used to characterize TCR–pMHC interaction only focus on TCR–pMHC binding in the extracellular domain of TCR–pMHC interaction which fail to incorporate other physiological components such as co-receptor contribution and force regulation. In this study following objectives, central hypotheses, and specific aims are proposed to better investigate T cell recognition mechanism using an ultrasensitive 2D mechanical assays.

1.1 Objectives

The main objective of this study is to better characterize *in situ* TCR–pMHC interaction with considering cellular component contribution, membrane restriction and physical force contribution to correlate with cellular function. Therefore, the central hypothesis of this thesis is co-receptor and force regulated 2D TCR-pMHC interaction determine T cell function. In order to fulfill the objective, three specific aims are performed with working hypotheses to test the central hypothesis.

1.2 Aims and hypotheses

Aim 1. Study 2D kinetics of TCR–pMHC interaction under force in an MHC class II system.

The working hypothesis for this aim is that *in situ* 2D kinetics and force regulation of TCR–pMHC interaction better define T cell response than previous 3D

methods in MHC class II system. This hypothesis is based on the recent report that observed 2D kinetic measurement of TCR–pMHC in MHC class I system which suggested 2D kinetic results are more relevant to predict the T cell response[1]. In addition, since T cells are continuously in physical environment we hypothesize that force regulation could be critical in TCR–pMHC interaction. The rationale for testing this hypothesis is that it will provide more strong evidence for the importance of 2D kinetic measurement and force contribution in TCR–pMHC interaction by testing an MHC class II system which may or may not show difference to the MHC class I system. For testing the hypothesis, we quantified 2D kinetic parameters of 3.L2 TCR to analogues of Hb_{68-76} ligand bound MHC II in naïve T cells to better predict the T cell response. We compared 2D and 3D measurements to confirm the differences and the advantage of 2D kinetic parameters. Lastly, we analyzed force regulation in TCR–pMHC interaction for T cell response.

Aim 2. Compare 2D kinetics of TCR–pMHC interaction and co-receptor cooperativity between naïve T cells and thymocytes.

The working hypothesis for this aim is that contribution of co-receptors and 2D kinetics may differ between naïve T cells and thymocytes. This hypothesis is based on previous studies that report co-receptor dependent increased thymocytes sensitivity[2-4]. Since T cell function and TCR expression differ during T cell maturity, we hypothesize TCR–pMHC interaction and co-receptor contribution may develop based on their maturation states. In order to test this hypothesis, we quantified and compared 2D kinetic parameters of 3.L2 and OT-I TCR binding to its respective APLs in naïve T cells and thymocytes. We compared the contribution of co-receptors in TCR–pMHC interaction for these systems. Lastly, we measured intracellular calcium signaling to compare the sensitivity between naïve T cells and thymocytes.

Aim 3. Study 2D kinetics of TCR–pMHC interaction under force for thymic selection.

The working hypothesis for this aim is that *in situ* 2D kinetics and force regulation of TCR–pMHC interaction better define thymic selection. This hypothesis is also based on the recent report that showed the importance of 2D kinetic measurement of TCR–pMHC in MHC class I system[1]. In addition, thymocytes are continuously moving and scanning in thymus encountering cortical (cTEC) and medulla thymic epithelial cells (mTEc)[5] that may expose a physical environment to TCR–pMHC interaction. Therefore, it is reasonable to suspect physical force could play an important role in TCR–pMHC interaction in thymic selection. The rationale for testing this hypothesis is that it will allow evidence for the importance of 2D kinetic measurement and may suggest force contribution in TCR–pMHC interaction on thymocytes. To test the hypothesis, we quantified zero-force 2D kinetic parameters of immature TCR–pMHC interaction for thymic selection. We analyzed force regulation in TCR–pMHC interaction for thymic selection. Lastly, we verified force regulation effect in thymic selection with endogenous ligands and in alternative systems.

CHAPTER 2 BACKGROUND

2.1 T cell immunology

2.1.1 T lymphocytes

T lymphocytes are a type of lymphocytes or white blood cells that are distinguished from other lymphocytes by the presence of T-cell receptor (TCR) on their membrane surface. The name "T lymphocytes" are derived from an organ that these cells get matured in, a thymus which starts with alphabet "T." T lymphocytes hold delicate mechanism in adoptive immunity as the last barrier of defense to pathogenic or viral invasion in human body. Current understanding of how T lymphocytes accomplish their adequate function in the immune system is fascinating but still insufficient. Clinical studies have shown that many immunodeficiency diseases, autoimmune diseases and transplant failures are due to malfunctioning and misunderstanding T cell immunity[6-8].

Lymphocytes first derive from lymphoid progenitor (one of the differentiated cell type from stem cells) in bone marrow through process called "lymphopoiesis"[9]. Some of these lymphocytes stay in the bone marrow to be differentiated to B lymphocytes and some migrate to the thymus to undergo development to be T lymphocytes. These lymphocytes in the thymus are called thymocytes and they undergo multiple stages to fully develop TCR, get positively selected base on their TCR binding with self antigens, and lastly decide their lineage to either be $CD4^+$ or $CD8^+$ naïve T cells[10, 11]. When fully maturated, naïve T cells now enter the circulation and peripheral lymphoid organs such as lymph nodes or spleen to perform their immunological activity. Most of them will monitor antigens expressed by pMHC on antigen presenting cells (APCs) for survival (i.e., immunological tolerance) or/and activation cues. Once they are exposed to a pathogenic antigen, these naïve T cells become effector T cells and undergo clonal expansion. The effector T cells will function as either releasing cytotoxic granule to kill

the specific cells directly ($CD8^+$ cytotoxic T cells) or releasing cytokines to trigger other immune cells like B cells for help ($CD4^+$ helper T cells)[8, 9]. After their activity they become memory T cells and reside in the body. Like such, throughout the life of a T lymphocyte (**Figure 2.1**), exposure to an antigen, whether it is self-antigen or pathogenic, is critical in determining thymic development, central tolerance, and T cell immunity. Therefore, T cell recognition is important in both thymic development and T cell activation.

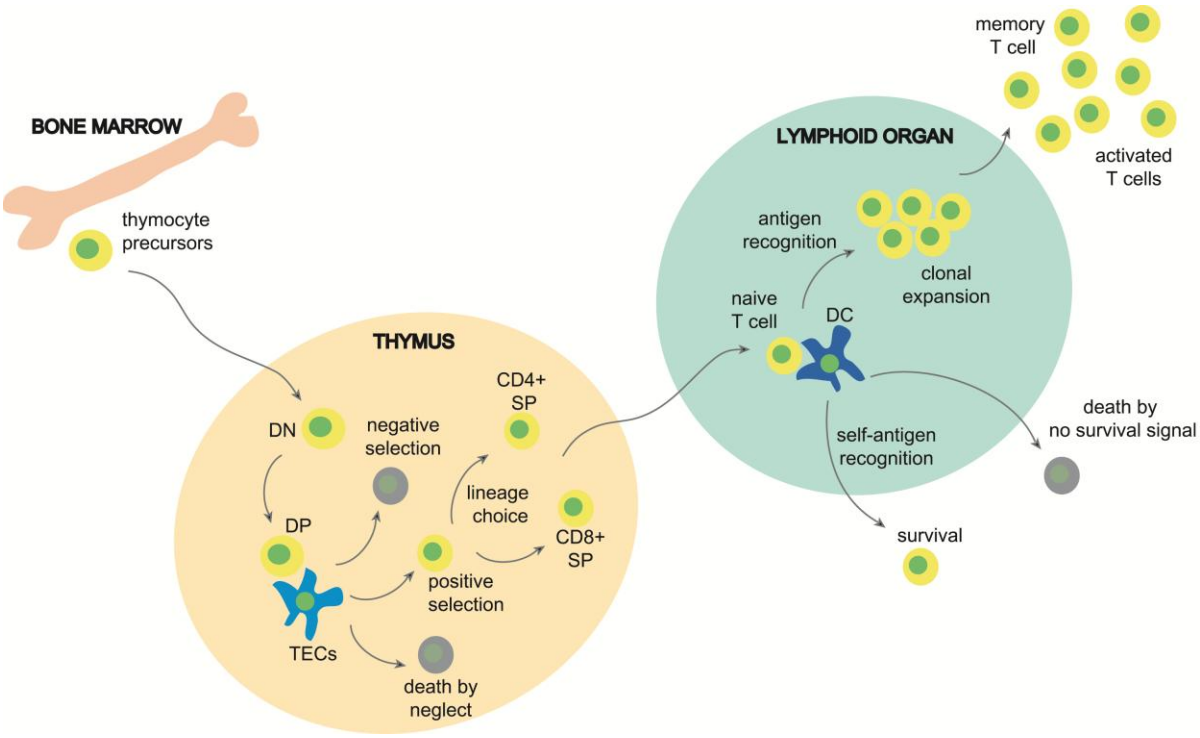

Figure 2.1: Life of a T cell
Thymocyte precursors enter thymus to undergo multiple stages of encountering cTECs and mTECs for thymic selection and lineage selection. When fully matured, T cells migrate to the periphery lymphoid organs constantly monitoring antigen on APCs. When pathogenic antigen is detected, naïve T cells undergo clonal expansion and become activated T cells and memory T cells.

2.1.2 TCR/CD3 complex

TCR/CD3 complex plays an important role in differentiation, survival and function of T cells by engaging with pMHC (**Figure 2.2**). TCR is a heterodimer and the

two chains are linked by disulfide bonds. The extracellular portion is slightly less than 10nm[9]. Each of the chain has N-terminal variable domain and constant Ig-like domain in the extracellular portion, followed by a transmembrane domain and a short cytoplasmic tail at the C-terminal end. At the variable domain, there is the complementarity determining region which binds with the pMHC[9]. There are two lineages of T cells depending on the heterodimer combination. About 95% of the T cells have αβ TCR and about 5% of the T cells have γδ TCR[9]. The TCR normally associates with invariant chains of CD3 complex compose of εδ and εγ heterodimers, and ζζ homodimer. This association is stabilized by polar interaction between CD3 molecules that have negatively charged transmembrane region and TCR that has positively charged transmembrane region[9]. Since TCR have short cytoplasmic tail that lack signaling domain, CD3 complex is critical in signaling cascade. There are 10 immunoreceptor tyrosine based activation motifs (ITAMs) in the cytoplasmic tail of CD3 heterodimersand ζζ homodimer that become phosphorylated after TCR engagement[9, 12].

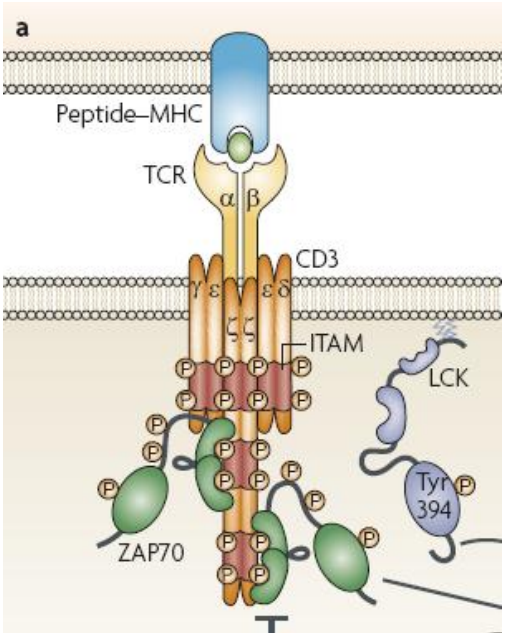

Figure 2.2: TCR/CD3 complex engaging with pMHCTCR is a heterodimer complexed with three dimers of CD3 which has 10 ITAMs in total for intracellular signaling. Once pMHC binds to TCR/CD3, Lck is brought to TCR/CD3 complex to phosphorylate

ITAMS allowing ZAP70 to bind and further initiate signaling cascade (adapted from Acuto et al., Nat. Rev. Immunol., 2008)[12].

2.1.3 Co-receptors CD4 and CD8

Along with TCR/CD3 complex, co-receptors CD4 and CD8 play important roles in the TCR–pMHC interaction. It is known that co-receptors bind also on the MHC molecule to bring Src family tyrosine kinase $p56^{lck}$ or Lck to the TCR/CD3 complex to trigger the signaling cascades[9, 12, 13]. CD4 is a single chain glycoprotein that has 4 immunoglobulin domains (D1, D2, D3, and D4). The D1 domain interacts with the β2 domain of a MHC II molecule[14, 15] and the cytoplasmic C-terminal end interacts with Lck molecules. On the other hand, CD8 is a αβ heterodimer transmembrane glycoprotein that have immunoglobulin variable (IgV)-like extracellular domain connected to the membrane by a thin stalk. The extracellular IgV-like domain of an α chain interacts with the α3 portion of a Class I MHC molecule and the cytoplasmic tail recruits Lck molecules to the TCR/CD3 complex. CD4 and CD8 are expressed on different subpopulation of T cells that have different functions. CD4 is restricted to an MHC class II expressed on T helper cells, and CD8 is restricted to an MHC class I expressed on cytotoxic T cells (or cytotoxic T lymphocytes, CTL)[9, 16].

2.1.4 pMHC

TCR–pMHC interaction is the main initial event that leads to the specific T cell response[9]. MHC has two general classes depending on the components and the peptide it presents (**Figure 2.3**). MHC class I molecules consist of two polypeptide chains, α and β2-microglobulin that are linked non-covalently[9]. Among 3 domains in α chain (α1, α2, and α3), the α1 and α2 domain make a pocket to hold endogeneous antigen peptide that are cleaved by proteosome whereas the α3 is the site for CD8 binding. Normally the peptide that is presented by MHC class I molecule is 8-10 amino acids long[9]. On the

other hand, MHC class II molecules comprise of αβ heterodimers that have peptide binding pocket at the α1 and β1 domain. The peptides that are expressed by MHC class II molecules are exogeneous antigen fragments that are degraded in the endosome which are at least 13 amino acid residues long[9]. The β2 domain on MHC class II molecule serves as the binding site for CD4[9].

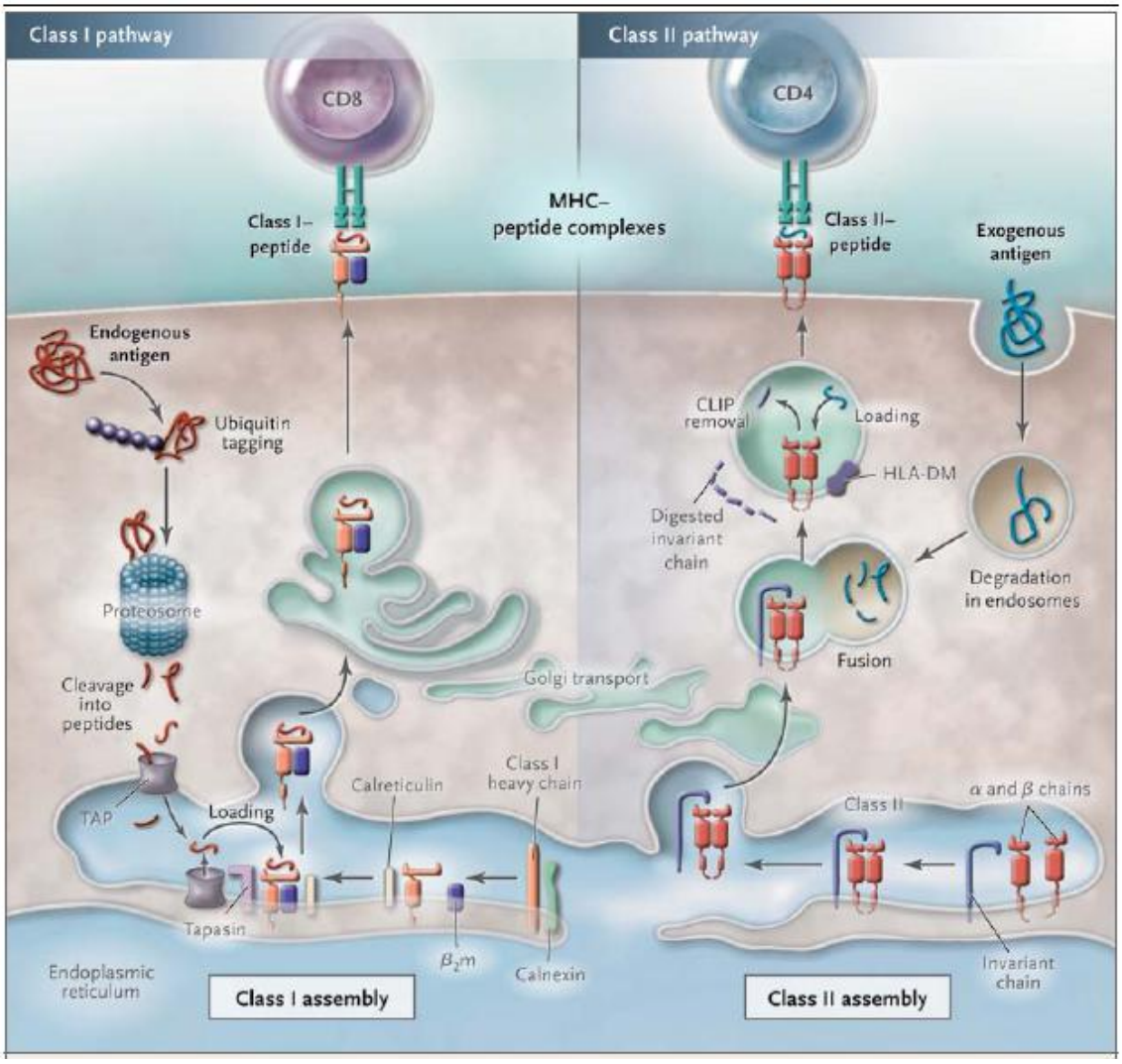

Figure 2.3: Generation of pMHC class I and class II For MHC class I molecule, endogenous antigen fragment of 8-10 amino acids is presented by two polypeptide chains, α and β2-microglobulin. For MHC class II molecule, exogenous antigen fragment of 13 amino acids is presented by αβ heterodimers (adapted from Nankivell et al., N. Engl. J. Med., 363:1451-62)[8].

2.1.5 Calcium mediated intracellular signaling

Once a pMHC get engaged to a TCR/CD3 complex, intracellular signaling molecules get involved to further direct the T cell response[17-22]. As TCR–pMHC interacts, CD4/CD8 co-receptors are recruited to form a synapse with the TCR–pMHC binding complex[17, 23, 24]. As this complex is formed, Src family tyrosine kinase Lck which is linked to cytoplasmic tail of the co-receptors get recruited to initiate the signaling. The Lck phosphorylates ITAMs on cytoplasmic domains of CD3s and ζ chains and allow a docking site for ζ-chain-associated protein kinase of 70 kDa (Zap70) to bind. This initiates phosphorylation of adaptor proteins, such as Src-homology-2-domain-containing leukocyte protein of 76kDa (SLP76) and linker for activation of T cells (LAT). This leads to the recruitment and activation of the TEC kinase interleukin-2-inducible T-cell kinase (ITK) and phospholipase Cγ1 (PLCγ1). In addition, binding of G-protein-coupled chemokine receptors results in the activation of PLCβ. The PLCβ and PLCγ1 catalyse the hydrolysis of the membrane phospholipid phosphatidylinositol-4,5-bisphosphate (PtdIns(4,5)P2) to inositol-1,4,5-trisphosphate (InsP3) and diacylglycerol (DAG). The InsP3 binds to the InsP3 receptors (InsP3Rs) for the release of ER stored Ca^{2+}. The decrease of stored Ca^{2+} in ER is detected by stromal interaction molecule 1 (STIM1), which in turn activates calcium-release-activated calcium (CRAC) channels in the plasma membrane like the Orai1[18]. As Ca^{2+} influx through the activated CRAC channel, the increased concentration of intracellular Ca^{2+} activates Ca^{2+} dependent enzymes, such as calcineurin, and thereby some transcription factors, such as nuclear factor of activated T cells (NFAT), nuclear factor-κB (NFκB) and cyclic-AMP responsive-element-binding (CREB) protein (**Figure 2.4**)[13, 19, 21, 25, 26].

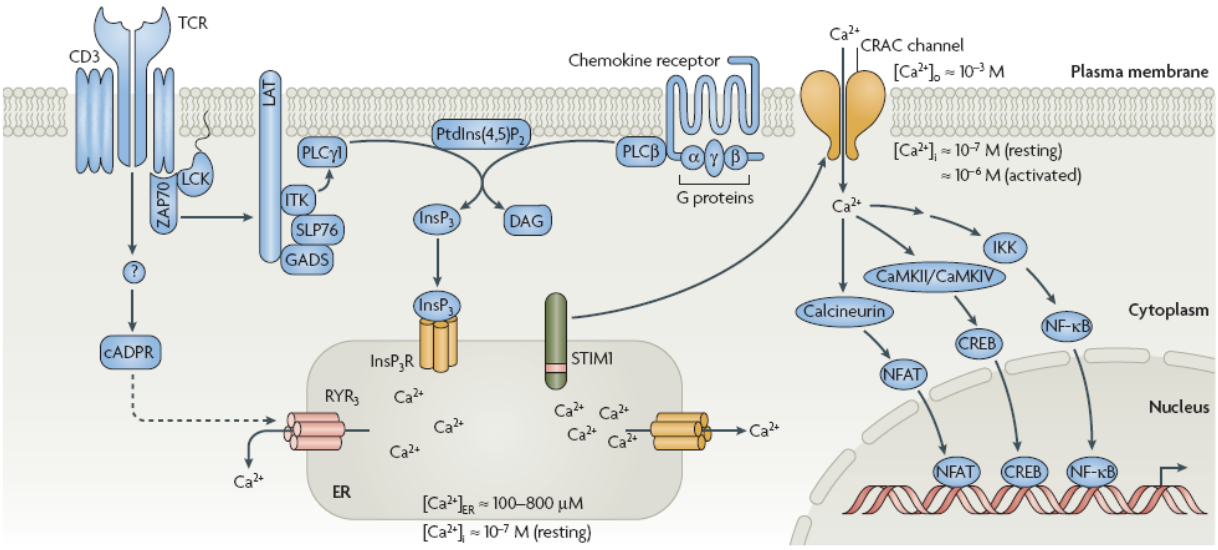

Figure 2.4: Calcium mediated intracellular signaling pathway in T cells As TCR–pMHC–CD4/8 complex forms, Lck is recruited to phosphorylate ITAMs to allow docking of Zap70. This initiates phosphorylation of SLP76 and LAT, and activates ITK and PLCγ1. Together with PLCβ, PLCγ1 catalyse the hydrolysis of PtdIns(4,5)P2 to InsP3 and DAG. InsP3 binds to InsP3 receptors (InsP3Rs) for the release of ER stored Ca^{2+}. STIM1 detects drop of Ca^{2+} in ER, then activates CRAC channels in the plasma membrane like Orai1 for Ca^{2+} influx. These Ca^{2+} activate calcineurin, and thereby some transcription factors, NFAT, NFκB and CREB (adapted from Feske et al., Annu. Rev. Immunol., 2009)[19].

2.2 T cell recognition and the previous research

2.2.1 TCR–pMHC interaction in T cell recognition

In molecular level, TCR–pMHC interaction is the key to T cell recognition. Although their affinity is about 100~1000 times lower than antibody-antigen interaction, they possess high sensitivity and specificity. TCR can sense few antigenic pMHCs out of a sea of self-pMHCs (10-100 out of 100,000 in MHC class I) and also able to respond to single amino acid difference in a short peptide sequence[27]. Unlike other surface adhesion molecules such as integrin or selectin, TCR discriminates pMHCs for its relevant response.

2.2.2 T cell discrimination model

Several models have been proposed to describe T cell discrimination[27, 28]. Kinetic proofreading proposes that half life of TCR–pMHC binding determines ligand discrimination. However, there are outliers that have long half life but weak T cell response. TCR occupancy model proposes that number of TCR bound at a single time point is critical for ligand discrimination. However, in physiological condition we know that only few antigens are available and also previous study show that only a single ligand can activate T cell response. Serial triggering model suggests that number of TCR engagement over a period of time is the key for ligand discrimination. However, this model contradicts with the kinetic proofreading model where strong ligand with long half life cannot trigger many TCR. Thus, optimal dwell-time model proposes that there is optimal dwell-time that could enable serial triggering for strong ligands. However, this model is only tested in a mutant TCR system. Lastly, confinement time model combines on- and off-rate suggesting rapid rebinding is the key for ligand discrimination. However, these models are all based on non-physiologic measurements or mathematical calculations that have no supportive data. This is because T cell is a highly sophisticated system that cannot be explained from one aspect of observation or a conclusion. Also there are limitations of current state of experiment methods or tools that restrict the full understanding of T cell behavior[18, 28].

2.2.3 Limitations of 3D measurements in TCR–pMHC interaction

TCR–pMHC interaction has intrigued many because of its low affinity (K_d ~1-100μM) but high specificity and sensitivity[29-31]. Among many attempts to characterize the TCR–pMHC interaction, the most widely used method is using surface plasmon resonance (SPR) technique with soluble molecules in flow-governing conditions which only consider the interaction of extracellular domain of the TCR–pMHC[30-36]. These

analyses show the dissociation kinetics ("off-rate") are the best predictor for the T cell response, with the agonist pMHC having a slower off-rate than the antagonist[32]. However, these analyses over simplifies the TCR-pMHC interaction. In microenvironment, not only TCR and pMHC but other components contribute in TCR–pMHC interaction such as co-receptor binding to MHC and CD3 complex associates with TCR. Also, these molecules are constraint on 2-dimensional (2D) cellular membrane restricting the molecular movement only in lateral direction. In addition, how proximal signaling molecules are segregated to break the balance of activation and inhibition signaling and how TCR-pMHC interaction transports the information through the membrane to the cytoplasmic tail are important considering factors in studying TCR–pMHC interaction. Lastly, extracellular/environmental contributions like cell migration or retrograde actin flow can apply physical force to TCR–pMHC interaction[37]. In fact, now TCR is thought as a mechanosensor since it can be triggered by mechanical force[38]. Therefore, there is a new need for understanding TCR-pMHC interaction with considering these contributions.

2.2.4 2D measurements of TCR–pMHC interaction

Up to now, two techniques has been used to measure the 2D kinetics of the TCR–pMHC interaction: one based on single-molecule Förster resonance energy transfer (FRET) by Mark Davis' group[39], and the other based on the membrane stretch of a red blood cell (RBC) in a micropipette adhesion frequency assay by Cheng Zhu's group[1, 40-43]. Huppa et al.[39] studied FRET between lipid bilayer-anchored pMHC and TCR on $CD4^+$ T cells. The FRET readout between the fluorophore-labeled pMHC (MCC:I-E^k) and 5c.c7 TCR allowed the calculation of binding parameters. Their results showed that 2D binding kinetics were faster than their 3D counterparts and that 2D kinetics did not change with blockade of the CD4 co-receptor. Similarly using the micropipette adhesion frequency assay, Huang and our group[1] found that 2D TCR binding kinetics were faster

than their 3D counterparts and correlated well with T cell activation levels to altered peptide ligands in the $CD8^+$ OT-I system (**Figure 2.5**). Not only did the 2D kinetics correlate well, but they also had a much larger dynamic range than the 3D kinetics.

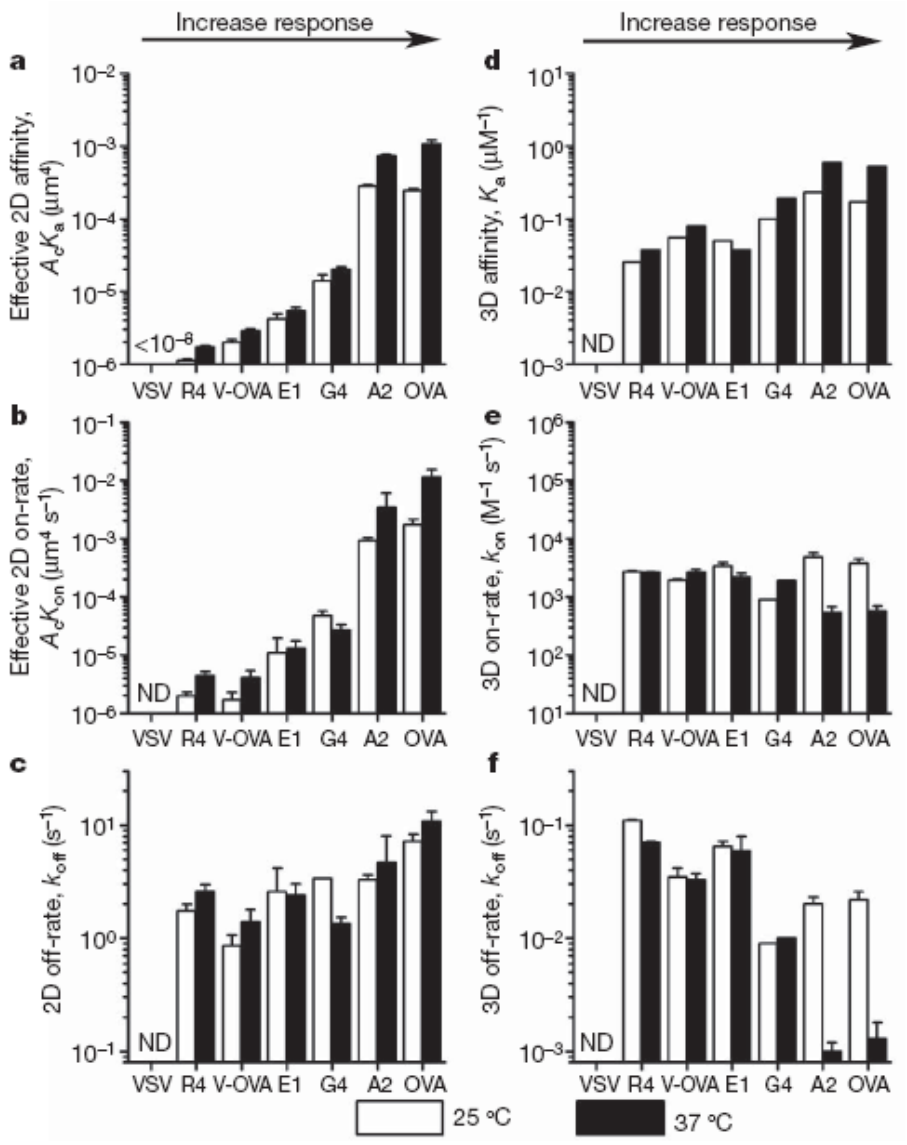

Figure 2.5: Comparison of 2D and 3D kinetics Affinities (A, D), on-rates (B, E), and off-rates (C, F) of the OT-I TCR interacting with indicated pMHCs are measured with adhesion frequency assay and compared with that of the 3D data (D-F) measured with SPR (adapted from Huang et al., Nature, 2010)[1].

Furthermore, CD8 affinity[40] and its cooperativity[41] was measured using micropipette adhesion frequency assay. These studies reported the basal affinity of CD8

co-receptor binding to MHC class I H-2K^b (2.8~5.7 x 10^{-6} μm^4) and H-2D^b (0.1~0.5 x 10^{-6} μm^4) (**Figure 2.6**)[40], and cooperative binding of CD8 after approximately one-second of delay on TCR–pMHC interaction (**Figure 2.7**)[41]. In essence, CD8 form a trimeric interaction with TCR–pMHC resulting in an abrupt increase in binding. In comparison, there is currently no comparable analysis for the CD4 co-receptor.

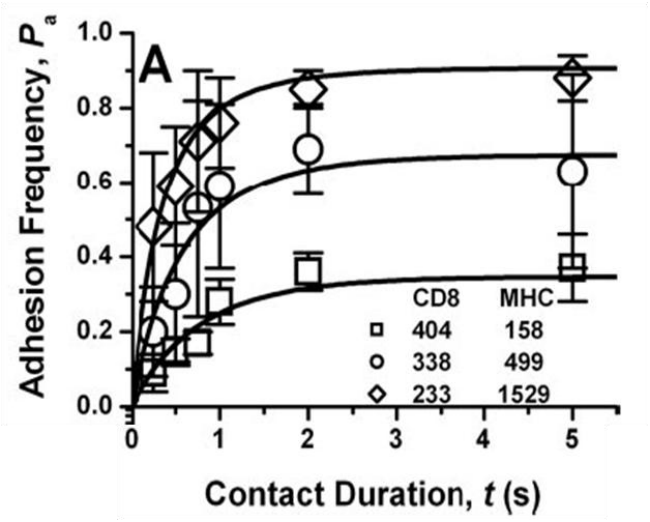

Figure 2.6: Adhesion frequency of CD8 binding to H-2K^{b}Different level of adhesion frequency of CD8 binding to H-2K^b is measured with altering the density of MHC molecule on the RBC (adapted from Huang et al, J. Immunol., 2007)[40].

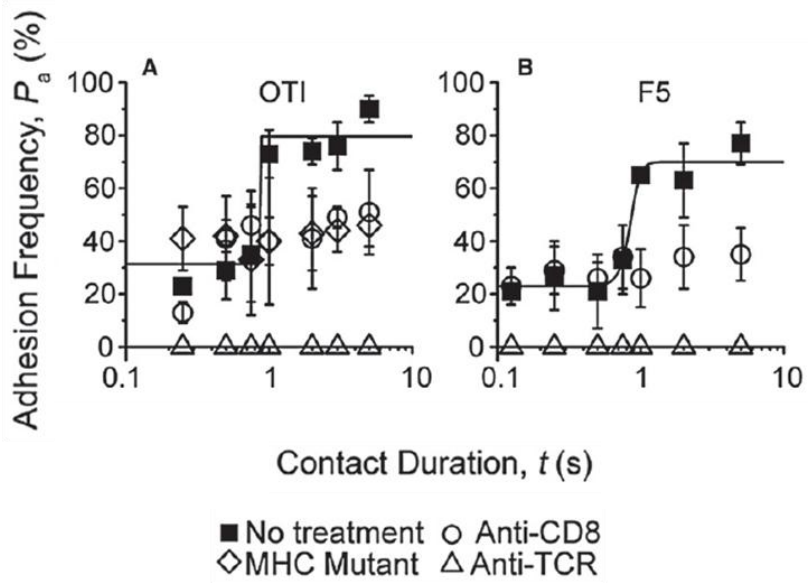

Figure 2.7: Two-stage kinetics of TCR–pMHC–CD8 trimolecular interaction

Adhesion frequency data of OT-I (A) and F5 (B) system show synergistic increase of adhesion frequency after one-second delay. These characteristics are CD8 dependent since anti-CD8 antibody or using MHC mutant eliminate the synergy (adapted from Jiang et al., Immunity, 2011)[41].

2.3 Thymic selection and the previous research

2.3.1 Thymic selection

Thymocytes undergo multiple stages in thymic development to select-out fully equipped mature T cells for T cell immunity and central tolerance. One of the key check-points in the thymic development is the positive and negative selection[44, 45] (**Figure 2.8A**). As the thymocytes engage with self-pMHCs on the cortical (cTEC) and medulla thymic epithelial cells (mTEc), they decide whether to live or die based on the binding propensity (avidity or affinity) to the self-ligand. First, thymocytes that do not have enough specificity to self antigen undergo apoptosis process. This is called "death by neglect[46]." The ones with the "over-the-threshold" binding propensity will be deleted from the repertoire (thymocyte apoptosis, lineage deviation, and receptor editing) as "negative selection or clonal deletion." Negative selection offers a key mechanism for self-tolerance since it removes the self-reactive T cells from the immune system that could potentially cause autoimmune disease in periphery[6, 7]. Thus, only the thymoyctes that have TCRs with optimal binding propensity to self-ligands will be positively selected. This process is called "positive selection[47]." In addition to mentioned conventional thymic selection, non-conventional thymic selection[48] for $CD4^+CD25^+Foxp3^+$ regulatory T cells (Tregs)[49], Natural Killer T cells (NKT cells)[50], and CD8αα intestinal intraepithelial lymphocytes (iIELs)[51] can occur from "agonist selection," where high affinity TCR can be replaced to low affinity TCR by receptor editing or functionally inactivated (anergy)[45]. However, we still lack the understanding of how the thymocytes

distinguish the ligand strength and how signaling is initiated to facilitate in a totally different cell behavior.

2.3.2 Previous research on thymic selection

2.3.2.1 Receptor-ligand kinetics

Since TCR–pMHC interaction is critical in initiating the engagement and further translating the signaling cascade, studies have been conducted to identify a clear selection threshold parameter. One attempt was to characterize the selection threshold in kinetic parameters. The basic assumption of this approach is that occupancy time of single TCR determines the selection. This model is called "affinity model" and is based on "kinetic proofreading" model. Hogquist et al.[47] used fetal thymic organ culture (FTOC) and showed that some variant of antigenic peptides induce positive selection. Alam et al.[33] measured kinetics of these ligands using SPR and correlated to the thymic selection. The kinetics of positive and negative selecting peptide showed some difference but whether there is a naturally occurring kinetic threshold for selection was questionable. Using SPR, tetramer staining, and photoaffinity labeling, only minimal difference (at most 2~3 times difference) was observed between the positive and negative selection ligands[52-54]. Although the differences in kinetic parameters were small, the threshold for two CD8 systems (T1 and S14) coincided to a constant of $K_d = 6\mu M$[53] (**Figure 2.8B**). For a CD4 system (3.L2), all the negative selecting ligands had half-lives of 2s or greater[54]. In addition to the affinity threshold that were identified in thymus, King et al.[55] recently showed that the same affinity threshold plays a role in maintaining peripheral tolerance in an autoimmune model. All together, it seems like the TCR affinity threshold exist and affects the peripheral immunity, but the magnitude of difference in affinity or kinetic parameters are smaller than expected which still leave the question of how thymocytes recognize these minute differences.

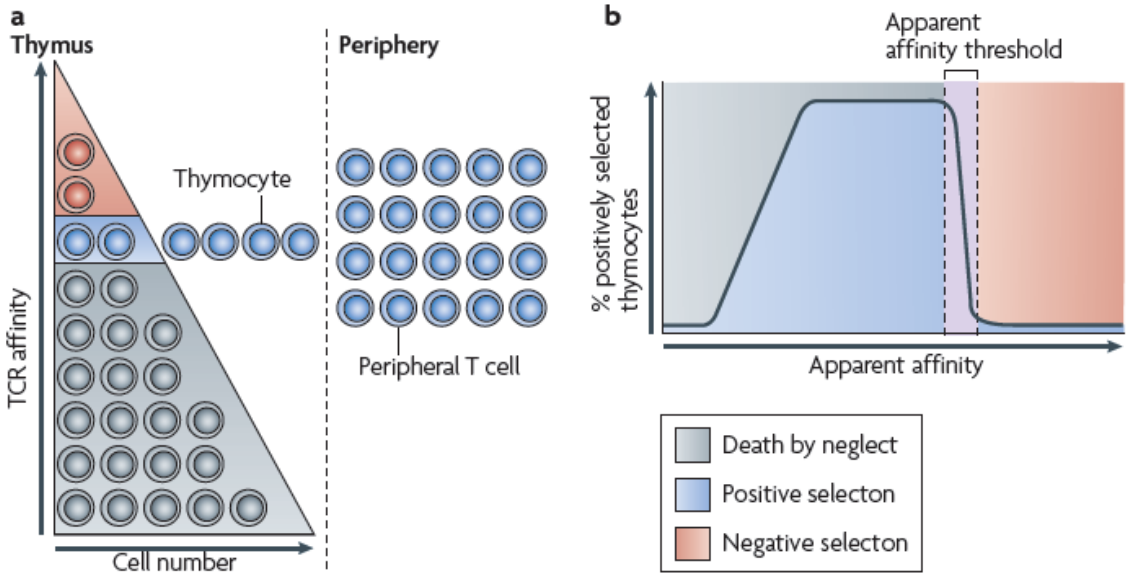

Figure 2.8: Thymic selection depends on T-cell receptor affinity for self pMHC Peripheral T cells are generated through the selection of self‑restricted and self-tolerant
thymocytes in the thymus. T cells that have TCRs that do not bind self-pMHC complexes and therefore do not receive a survival signal die by neglect; those with low affinity TCR to self pMHC complexes induces survival and differentiation (positive selection); whereas those with high affinity TCR to self-pMHC complexes induces cell death by apoptosis (negative selection) (A). Whether a self antigen induces positive or negative selection is defined by an apparent affinity threshold (K_d ~6 μM)[53] of TCR–pMHC interaction (B) (adapted from Palmer et al., Nat. Rev. Immunol., 2009)[10].

2.3.2.2 TCR complex

Another attempt to characterize a selection threshold is identifying changes in TCR complex. Many groups have studied CD3 conformational change to relate to thymic selection but it was not sufficient for a discriminating factor. Although negative selecting ligands induced conformational change in CD3 that activated programmed cell death[56], in another study both positive and negative ligands enabled the exposure of a cryptic polyproline sequence in CD3ε that suits as a binding site for SH3.1 domain of cytosolic adaptor protein Nck[57]. In addition to CD3, co-receptors have also been considered in thymic selection. From mutant mouse experiments, CD3δ and α-CPM were identified to be critical in positive selection[58] and further studies showed that CD8 associates with

TCR through CD3δ and α-CPM[59]. Therefore, we know that CD3 and co-receptor like CD8 is important in thymic selection but these studies do not yet give a concluding understanding of how they can decide selection process.

2.3.2.3 Signaling

In addition to the receptor-ligand kinetics and the TCR complex change, thymocyte signaling has been studied for thymic selection. Many groups were successful to observe qualitative differences in signaling kinetics (Ca^{2+}, Erk, LAT, Ras etc.) and compartmentalization[44, 52]. While Ca^{2+}, Erk, and LAT had transient peak activation and gradual decay for negative selection, those had a gradual increase in signaling kinetics for positive selection[44]. Also, while Ras/MAPK signaling molecules localized on the T cell membrane for negative selection, signaling localization was in the cytoplasmic golgi for positive selection[52]. In other studies, Nck recruitment and MINK correlated well with negative selection[60], voltage-gated sodium channel (VGSC) was essential for the positive selection[61], and thymocyte expressed molecule involved in selection (Themis) show close correlation with thymic selection[62-64].

2.4 Motivations for the research

Although 3D measurements, such as SPR or tetramer staining, have provided information to study TCR–pMHC interaction so far, the native cellular environment differs from the conditions under which those experiments are performed. Whereas the native TCR is restricted to lateral 2D movement in a plasma membrane, SPR uses surface-immobilized ligands to detect binding with soluble receptor molecules which have freedom of 3D movement. In addition, cellular components (e.g., co-receptors or other membrane proteins) or motions (e.g., migration, actin radial flow, membrane deflection) could actively restrict or promote TCR binding to pMHC in a force dependent

manner. Thus, examining 2D TCR–pMHC binding kinetics in the more physiological membrane environment may yield important insights to T cell biology[1, 39]. This study attempts to answer how TCR discriminate ligand potency and decide thymic selection in more physiological condition with considering co-receptor CD4 or CD8 contribution.

2.5 Significance

The fundamental mechanism of T cell activation and thymic selection are the central question in T cell immunity. We know the TCR–pMHC interaction combined with co-receptor contribution initiates the T cell recognition. However, the fundamental understanding of TCR–pMHC interaction is still not fully understood. In an attempt to provide more physiological characterization of TCR–pMHC interaction, this study considers 2D kinetics and physical force regulation in TCR–pMHC interaction which has not been well characterized before. Overall, this research contributes with a novel finding in T cell immunology and provides a scientific and clinical significance.

CHAPTER 3 MATERIALS AND METHODS

3.1 T cells and proteins

3.1.1 T cells

We used transgenic 3.L2, OT-I, and 2C mouse housed at the Emory University Department of Animal Resources facility in an experiment that followed protocol approved by the Institutional Animal Care and Use Committee of Emory University. The transgenic 3.L2 mouse expressed I-E^k MHC-restricted 3.L2 TCR specific to murine hemoglobulin (Hb) epitope 64-76 and the transgenic OT-I mouse expressed H-$2K^b$ MHC-restricted OT-I TCR specific to the chicken ovalbumin (OVA) epitope 257–264. We purified the naïve T cells from a mouse spleen using a $CD4^+$ T cell isolation kit (Miltenyi Biotec) and pre-selected DP thymocytes from a mouse thymus with $CD53^-$ $CD4^+$ $CD8^+$ double positive (DP) thymocyte enrichment by the magnetic bead immunoaffinity cell sorting (MACS) according to the manufacturer's instructions (**Figure 3.1**). CD53 is a cell surface glycoprotein in a tetraspanin family that is known to contribute to cell adhesion, migration, and signaling. Furthermore, CD53 is only expressed on single ($CD4^+$ or $CD8^+$) positive thymocytes. Since CD53 expression and positive selection strongly correlated, we selected CD53 as a purification marker[65]. In more detail, we incubated the cell suspension from the spleen and thymus with anti-CD4 negative selection magnetic beads and with anti-CD53 negative selection magnetic beads, respectively. Then we ran the mixture through a magnetic column for elution. We washed and stored the cells in RPMI 1640 (Cellgro) supplemented with 10% FBS (Cellgro), 2mM L-glutamine (Cellgro), 0.01M HEPES buffer (Cellgro), 100μg/ml gentamicin (Cellgro), and 2×10^{-5}M 2-β-mercaptoethanol (2-BM) (Sigma-Aldrich), the complete mixture of which is generally called R10, at room temperature (RT) for use of up to 24 hrs.

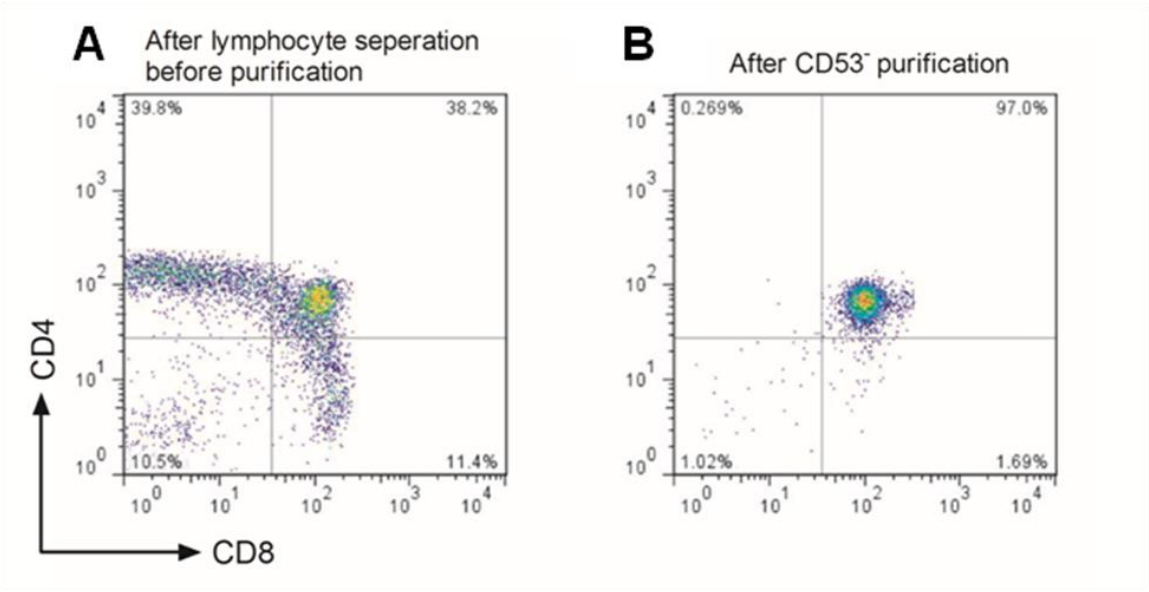

Figure 3.1: CD53$^-$ purification for DP 3.L2 thymocytes Since CD53 expression and positive selection strongly correlated, we selected CD53 as a purification marker. CD53$^-$ purification technique was used to enrich DP thymocytes (B) from the total thymocytes (A).

3.1.2 Proteins

For the ligands of this study, we received synthesized recombinant pMHC monomers from the National Institutes of Health Tetramer Core Facility at Emory University. For 3.L2, system, a murine hemoglobin (Hb)-derived APL sequence was tethered to a gene sequence of I-E^k (an MHC class II molecule), which generated a peptide bound to an MHC molecule after the plasmids were expressed in the clones[66]. The peptide sequences were murine Hb-derived peptides $Hb_{64\text{-}76}$ (GKKVITAFNEGLK, Agonist), T72 (GKKVITAFTEGLK, Weak agonist), I72 (GKKVITAFIEGLK, Antagonist), and A72 (GKKVITAFAEGLK, Weak antagonist)[36]. In addition, moth cytochrome *c* (MCC) peptide 88-103 (ANERADLIAYLKQATK) bound to IE^k were prepared in the same way for irrelevant control. For OT-I system, a chicken ovalbumin (OVA)-derived APL sequence was tethered to a gene sequence of H-2K^b or a mutant H-2K^b (replacing the α3 domain in mouse H-2K^b to the α3 domain of human HLA-A2). The

peptide sequences were chicken OVA-derived peptides $OVA_{257-264}$ (SIINFEKL, Agonist and negative selecting ligand), Q4 (SIIQFEKL, weak agonist and negative selecting ligand), Q4R7 (SIIQFERL, weak agonist and negative selecting ligand), T4 (SIITFEKL, weak agonist and negative selecting ligand), Q4H7 (SIIQFEHL, weak agonist and positive selecting ligand), and Q7 (SIINFEQL, weak agonist and positive selecting ligand), G4 (SIIGFEKL, weak agonist/antagonist and positive selecting ligand), $Cappl_{92-99}$ (ISFKFDHL, endogenous positive selecting ligand), $Catnb_{329-336}$ (RTYRYEKL, endogenous positive selecting ligand)[52, 67, 68]. In addition, vesicular stomatitis virus-derived nucleoprotein VSV_{52-59} (RGYVYQGL) bound to H-$2K^b$ was prepared in the same way for irrelevant control. For 2C system, SIYR (SIYRYYGL, super agonist and possible negative selecting ligand), dEV8 (EQYKFYSV, agonist and positive selecting ligand), EVSV (RGYVYQEL, weak agonist and possible positive selecting ligand), p2Ca (LSPFPFDL, endogenous positive selecting ligand) sequence was tethered to a gene sequence of H-$2K^b$ or H-$2K^{bm3}$ (two mutations in α1 domain at Asp77Ser and $Lys89Ala^{69}$) [35, 70-72]. All of the pMHC monomers were engineered to have a biotin tag on the C-terminus.

3.2 RBC preparation and site density measurement

3.2.1 RBC preparation and pMHC Coating

To anchor the pMHC monomers on the cell surface, we used human RBCs isolated from the whole blood of healthy volunteers according to a protocol approved by the Institutional Review Board of the Georgia Institute of Technology[1, 40, 41]. In more detail, 5ml of whole blood was drawn into an EDTA containing tube, overlaid onto 10ml of Histopaque (Sigma-Aldrich) and centrifuged five times in a PBS wash and twice with experimental additive solution 45 (EAS45) at RT. The isolated RBCs were stored in EAS45 at 4℃ for further use of up to two months.

Coating the pMHC onto the RBCs was conducted in three steps. First, we biotinylated RBCs with Biotin-XNHS (Calbiochem) according to the manufacturer's instruction. That is, we washed the prepared RBCs in PBS three times, incubated them in titrated Biotin-X-NHS at pH 7.2 for 30min at RT, and washed them in PBS with 1% BSA five times to remove the Biotin-X-NHS. In the second step, we coated the biotinylated RBCs with streptavidin molecules. We incubated the RBCs in 0.5mg/ml streptavidin (Pierce) for 30min at 4℃ and washed them in EAS45 three times. In the third step, we covalently linked the synthesized pMHCs with a single biotin on the C-terminus to the RBCs by the biotin-streptavidin interaction.

3.2.2 Site density measurement

Since the site density of the receptor and the ligand are crucial for calculating the 2D kinetics in the adhesion frequency assay, we measured their expression levels using flow cytometry analysis[1, 40, 41] and obtained the expression level using PE-conjugated antibodies: anti-mouse Vβ8.3 TCR antibody (1B3.3, BD Pharmingen), anti-mouse Vα2 TCR antibody (B20.1, BD Pharmingen), anti-mouse Vβ TCR antibody (F23.1, BD Pharmingen), anti-mouse CD4 antibody (GK1.5, eBioscience; RM-45, eBioscience), anti-mouse CD8 antibody (53-6.7, BD Pharmingen), anti-mouse H2-I-E^k monoclonal antibody (17-3-3, Santa Cruz ; 14-4-4s, BD Pharmingen), anti-mouse OVA257-264 (SIINFEKL) peptide bound H-$2K^b$ monoclonal antibody (25-D1.16, eBioscience), anti-mouse H-$2K^b$ monoclonal antibody (AF6-88.5, BD Pharmingen), and β-2-microglobulin antibody (S19.8, Santa Cruz Biotechnology). For isotype control, PE-conjugated antibodies were used: rat IgG2a κ (eBioscience), mouse IgG2a (Santa Cruz Biotechnology), and hamster IgG3 λ_1 (BD Pharmingen). We incubated the antibodies at 10μg/ml concentration in 100μl of FACS buffer (PBS without calcium and magnesium, 5mM EDTA, 1% BSA, 25mM HEPES, 0.02% sodium azide) at 4℃ for 30min; measured

the fluorescent intensity by the BD LSR II flow cytometer (BD Biosciences) (**Figure 3.2**); and calibrated the site density according to the BD QuantiBRITE PE standard beads (BD Biosciences).

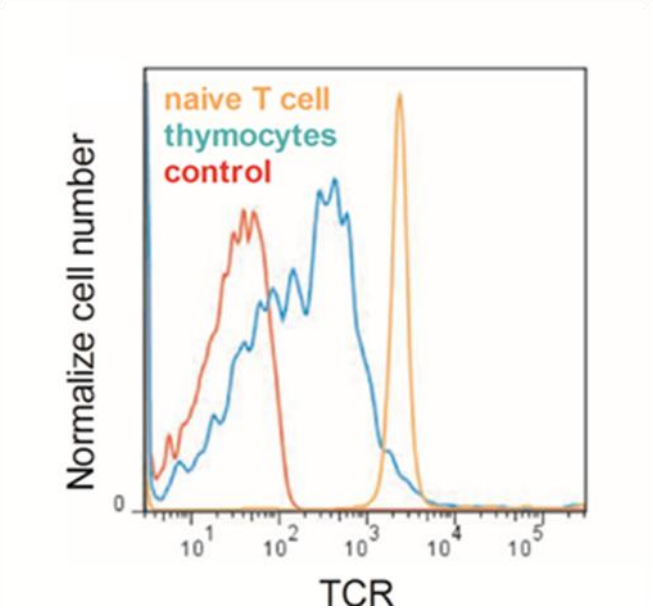

Figure 3.2: TCR expression level of OT-I naïve T cells and thymocytes An example of flowcytometry PE histogram using anti-mouse Vβ8.3 TCR antibody on OT-I naïve T cells and thymocytes. Site density of the receptor and the ligand were measured using specific antibodies with flowcytometry analysis. Fluorescent intensity from flowcytometry histogram was calibrated to site density using PE standard beads.

3.3 2D mechanical assays

3.3.1 Micropipette apparatus

We customized an inverted microscope (TMD Diaphot, Nikon) by mounting two identical sets of 3D mechanical manipulators (Newport) on each side of the microscope stage to hold apposing glass pipettes for capturing the cells (**Figure 3.3**). Because the pipettes were linked to a home-made manometer system, the applied suction pressure held the cells and controlled the contact of a pMHC presenting an RBC onto a T cell. A one-dimensional (1D) open-loop piezo actuator LVPZT (P840-1, Physik Instrumente) mounted on one side of the pipette allowed repeated approach and retract movements

controlled by voltage generation from LabVIEW software (National Instruments) and DAQ 6008 (National Instruments). Using an analog CCD camera (MTI DC330, Dage), we acquired real-time images at 30 frames per second and simultaneously observed them through a TV monitor and recorded them on a VHS cassette tape.

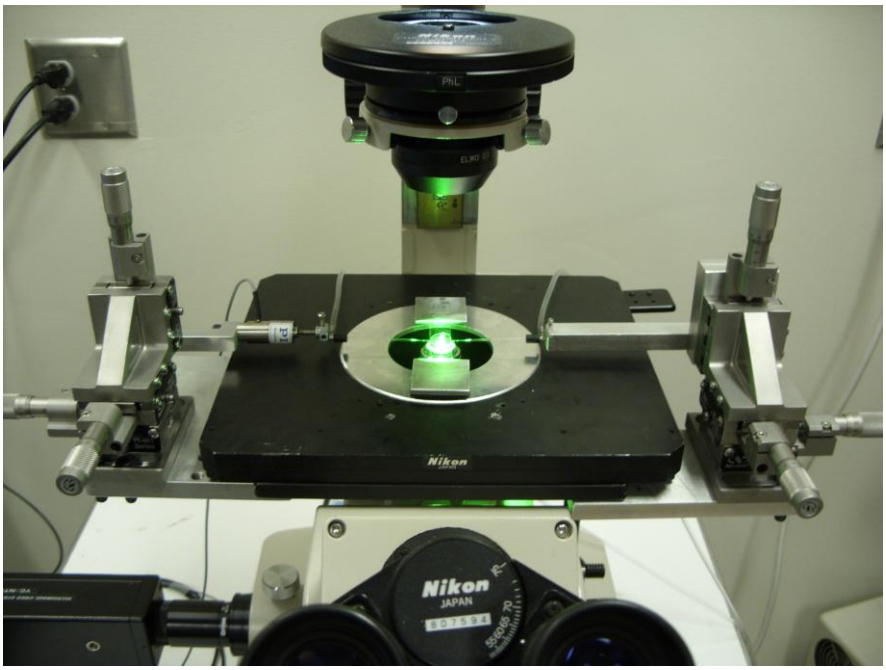

Figure 3.3: Micropipette setup An inverted microscope (TMD Diaphot, Nikon) was customized to have two sets of 3D mechanical manipulators (Newport) on each side of the stage with a home-made manometer system connection to hold apposing glass pipettes for capturing the cells.

3.3.2 Adhesion frequency assay

Using the micropipette adhesion frequency assay[73], we measured the 2D kinetics of the TCR-pMHC interaction. Two micropipettes held a single purified T cell on one side (glass pipette with a ~2μm inner diameter) and a single pMHC-coated RBC on the other (a glass pipette with a ~1μm inner diameter) (**Figure 3.4A**) in a chamber filled with an L-15 medium (Sigma-Aldrich) plus 5mM HEPES and 1% BSA. While a controlled piezoactuator linked to the pipette on the RBC side generated a repeat approach-retract

cycle, we observed binary events of adhesion (either 1, which represents the binding event shown in **Figure 3.4B**, or 0, which represents the no-binding event shown **Figure 3.4C**) by the deflection of the RBC membrane.

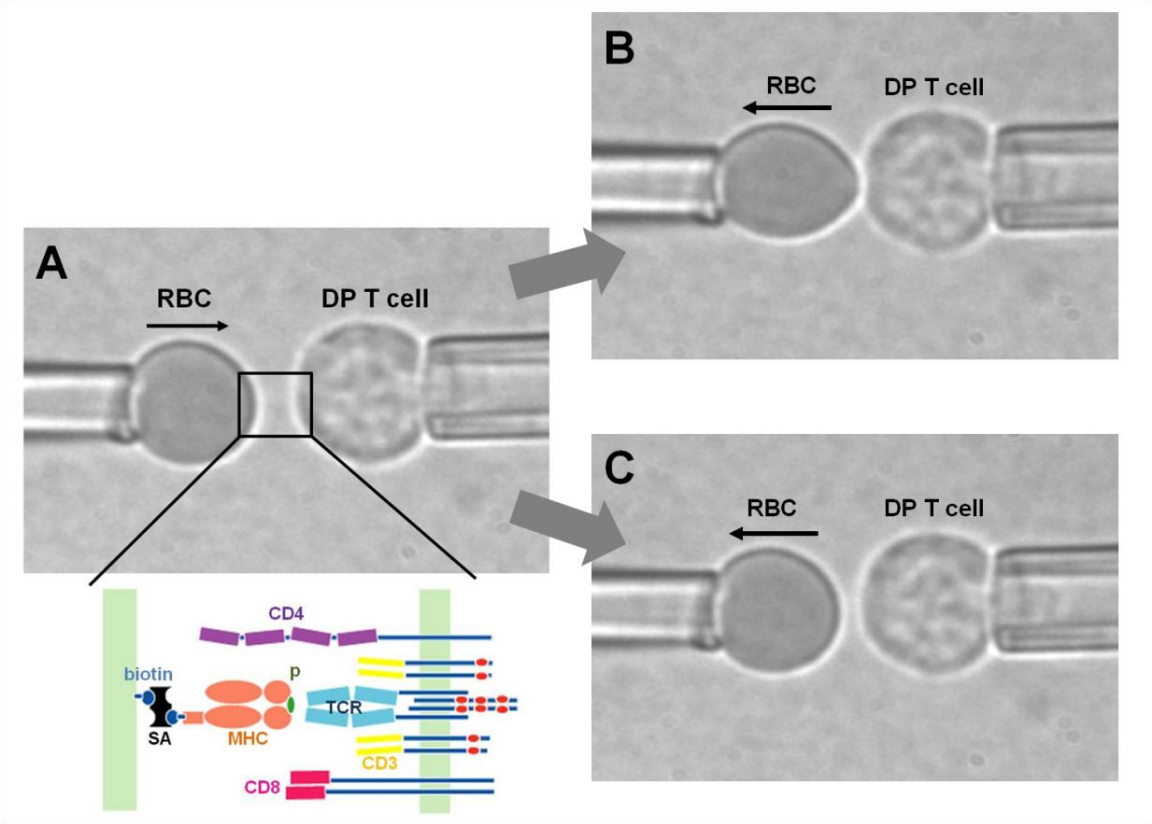

Figure 3.4: Micropipette adhesion frequency assay and thermal fluctuation assay
A single native T cell/thymocyte and a pMHC-coated RBC are held by two apposing micropipettes before the contact (A). The TCR, CD4, CD3 and the other native forms of molecules are presented on the native T cell/thymocyte surface. On the RBC surface, the biotinylated pMHC is linked to streptavidin to covalently bind to the 2D surfaces. For the adhesion frequency assay, we bring apposing cells to a contact for certain contact duration and retract to observe the adhesion frequency. Since binding events are binary, we can either observe a binding event from the elongation of the soft membrane of RBC (B) or no binding from no stretch events (C).

We repeated this approach-contact-retraction cycle 50 times for three to five cell pairs at each single contact duration (t_c) with a consistent contact area (A_c), resulting in a calculation of an adhesion frequency (P_a , mean ± SEM). Then we measured the site densities of the TCR (m_r) and the pMHC (m_l) from a flow cytometry analysis, derived the

results of P_a at different contact durations (0.1s-5s), and curve fitted the adhesion frequency curve with the least mean square method using the following probabilistic kinetic equation[73]:

$$P_a = 1 - \exp[-m_r m_l A_c K_a \{1 - \exp(-k_{off} t_c)\}] \quad (1)$$

We fit each binding curve using nonlinear regression to this probabilistic kinetic model for a single-step monovalent receptor ligand interaction. Since m_r, m_l, and P_a can be measured with varying t_c's with controlled A_c, the equation consisted of two unknown parameters, A_cK_a and k_{off}. We derived these parameters from the curve fit using the least mean square method (Excel Solver) and evaluated the data from repeated experiments (n≥3) with different TCR and pMHC densities.

To measure the non-specific adhesion, we conducted controlled experiments at a 5s contact duration for both 3.L2 naïve T cells and OT-I thymocytes. For 3.L2 naïve T cells we tested binding to (1) unmodified RBCs, (2) biotinylated RBCs, (3) biotinylated RBCs linked to streptavidin, (4) biotinylated RBCs linked to streptavidin and coated with irrelevant pMHC-I ($OVA_{257-264}$:H-$2K^b$), (5) biotinylated RBCs linked to sreptavidin and coated with irrelevant pMHC-II (MCC_{88-103}:IE^k), and (6) biotinylated RBCs linked to streptavidin and coated with antigenic Hb_{64-76}:IE^k (**Figure 3.5A**). Observed binding frequencies were less than 1% for unmodified RBCs, biotinylated RBCs (800μM biotinylated concentration), and biotinylated RBCs linked with streptavidin (4335 molecules/μm^2), about ~1% for $OVA_{257-264}$:H-$2K^b$ (1548 molecules/μm^2) , and less than 5% for MCC_{88-103}:IE^k (4140 molecules/μm^2). However, the observed frequency was ~75% for the specific antigen Hb_{64-76}:IE^k (TCR = 144 molecules/μm^2 and Hb_{64-76}:IE^k = 36 molecules/μm^2).

For OT-I thymocytes we tested binding to (1) unmodified RBCs, (2) biotinylated RBCs, (3) biotinylated RBCs linked to streptavidin, (4) biotinylated RBCs linked to streptavidin and coated with irrelevant peptide-mutant MHC-I (VSV:mH-$2K^b$), (5) biotinylated RBCs linked to streptavidin and coated with antigenic peptide-mutant MHC-

I ($OVA_{257-264}$:mH-$2K^b$), and (6) biotinylated RBCs linked to streptavidin and coated with antigenic peptide-wild type MHC-I ($OVA_{257-264}$:H-$2K^b$) (**Figure 3.5B**). Observed adhesion frequencies were less than 1% for unmodified RBCs, biotinylated RBCs (800μM biotinylated concentration), and biotinylated RBCs linked with streptavidin (4335 molecules/μm^2), and about ~1% for VSV:mH-$2K^b$ (604 molecules/μm^2). However, the adhesion frequencies for $OVA_{257-264}$:mH-$2K^b$ and $OVA_{257-264}$:H-$2K^b$ at the similar TCR and pMHC density (TCR = 9 molecules/μm^2 and Hb_{64-76}:IE^k = ~13 molecules/μm^2) were ~15% and ~53%, respectively.

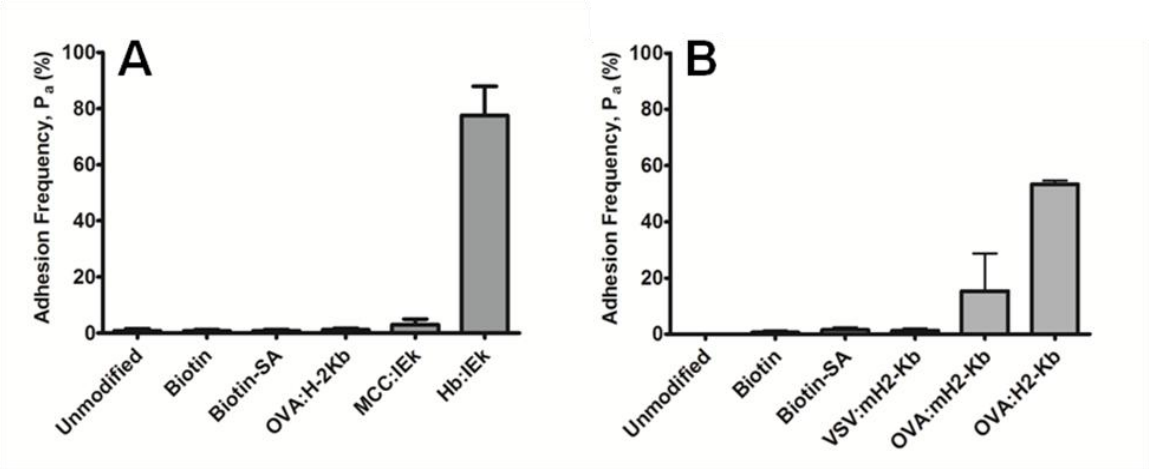

Figure 3.5: Non-specific adhesion control experiment
To measure the non-specific adhesion, we conducted controlled experiments at a 5s contact duration for 3.L2 naïve T cells and OT-I thymocytes. For 3.L2 naïve T cells, specific adhesion was tested with the unmodified RBCs, the biotinylated RBCs, the biotinylated RBCs linked with streptavidin, the biotinylated RBCs linked with streptavidin coated with irrelevant pMHC-I (OVA:H-$2K^b$), irrelevant pMHC-II (MCC:I-E^k), and antigenic Hb_{64-76}:I-E^k (A). For OT-I thymocytes, specific adhesion was tested with the unmodified RBCs, the biotinylated RBCs, the biotinylated RBCs linked with streptavidin, the biotinylated RBCs linked with streptavidin coated with irrelevant peptide-mutant MHC-I (VSV:mH-$2K^b$), antigenic peptide-mutant MHC-I ($OVA_{257-264}$:mH-$2K^b$), and antigenic peptide-wild type MHC-I ($OVA_{257-264}$:H-$2K^b$) (B). Each bar is presented as mean ± SEM (n≥5).

3.3.3 Thermal fluctuation assay

Using biomembrane force probe (BFP), we measured k_{off} by performing thermal fluctuation assay[74]. Because of BFP's high resolution and soft spring constant, thermal

fluctuation assay gave better measurement of k_{off} than adhesion frequency assay. BFP used RBC as a displacement sensor to detect TCR-pMHC bond formation using a high-speed CCD camera (**Figure 3.6A**). A RBC was held by a micropipette with controlled suction pressure to allow the RBC to have a spring constant of k_p = 0.15pN/nm[1, 74]. pMHCs were coated on a borosilicate bead (2-mm diameter, Duke Scientific) and attached to the apex of a RBC held on a micropipette. A native T cell held by an apposing micropipette was positioned to approach the bead with a certain distance to allow TCR-pMHC bond formation due to thermal fluctuation. A high-speed CCD camera (1,500 frames/s, Graftek Imaging) captured a well-defined greyscale profile of the edge of the bead to track the axial position of the bead with a 5nm spatial and 0.7ms temporal resolution. The bond formation and dissociation was detected by the reduction and resumption of the thermal fluctuations of the BFP bead[1, 74]. We were able to detect these bond lifetimes (t_b), i.e., from the instant of bond association to the instant of bond dissociation, by analyzing the displacement and the standard deviation of the bead movement (**Figure 3.6B**).

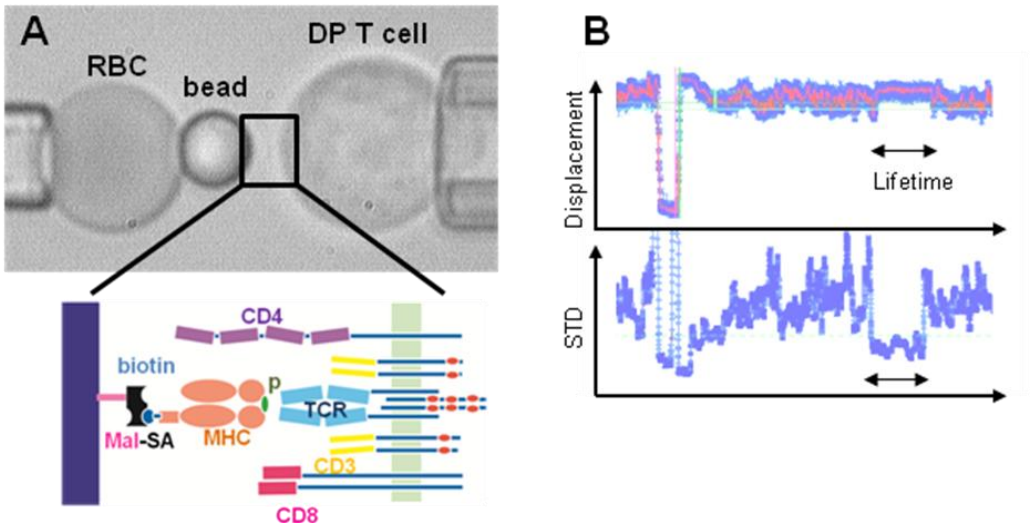

Figure 3.6: Thermal fluctuation assay
A single native T cell/thymocyte and a pMHC-coated bead are held by two apposing micropipettes before the contact (A). The TCR, CD4, CD3 and the other native forms of molecules are presented on the native T cell/thymocyte surface. On the bead surface, the biotinylated pMHC is linked to streptavidin to covalently bind to the 2D surfaces. For the

thermal fluctuation assay, we bring apposing cell and the bead to a certain distance to allow bond formation that gives reduction in the standard deviation of the bead movement (B).

Modeling the kinetic process as a single-step first order dissociation of a single monomeric TCR-pMHC bond, the probability P_b of a bond formed at time 0 to remain intact at time t_b is

$$P_b = \exp(-k_{off} t_b). \quad (2)$$

We can take a natural log to the linearized exponential function on right hand-side of this equation to plot the bond lifetime data as ln(number of events with a lifetime > t_b) versus t_b. We can then estimate k_{off} from the negative slope of the line (**Figure 3.7**).

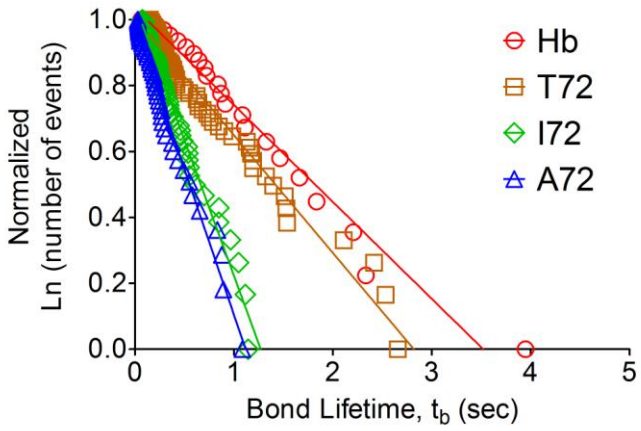

Figure 3.7: Bond lifetime distribution from thermal fluctuation assay in 3.L2 system
Using single-step first order dissociation model, the bond lifetime data was linearlized to plot ln(number of events with a lifetime > t_b) versus t_b to estimate k_{off} from the negative slope of the line.

3.3.4 Force-clamp assay

We measured force-dependent bond dissociation with using same BFP apparatus but with clamped-force applied to the TCR–pMHC bond[75-77]. The pipette holding the T cell was driven repeatedly to approach and make a contact with the bead at a 15pN compressive force for 0.2s for TCR-pMHC bond formation. After this brief contact, the

pipette was retracted at a 3μm/s speed (RBC spring constant of k_p = 0.3pN/nm, retraction speed 1000pN/s) to be held at a desired force (i.e., clamped-force) to wait for bond dissociation. At this point the adhesion was detected by a tensile force signal caused by RBC membrane deformation (i.e., displacement of the BFP beads). Lifetime was measured from the instant when the force reached the desired level to the instant of bond dissociation (**Figure 3.8A**). To avoid force drift over long time, a 10s cutoff was set to rupture bonds with lifetimes larger than 10s. After the bond dissociation, the program returned T cell held pipette to the original position for the next cycle. We repeated this cycle to obtain more than 300 lifetime events at a force range of 5-40pN for each TCR–pMHC interaction. We used 5-7 bins to segregate the force-lifetime data for presentation. In order to affirm the condition for monomeric interaction of more than 95%, the pMHC density on the beads were controlled to keep the adhesion frequency less than 20%[75, 77].

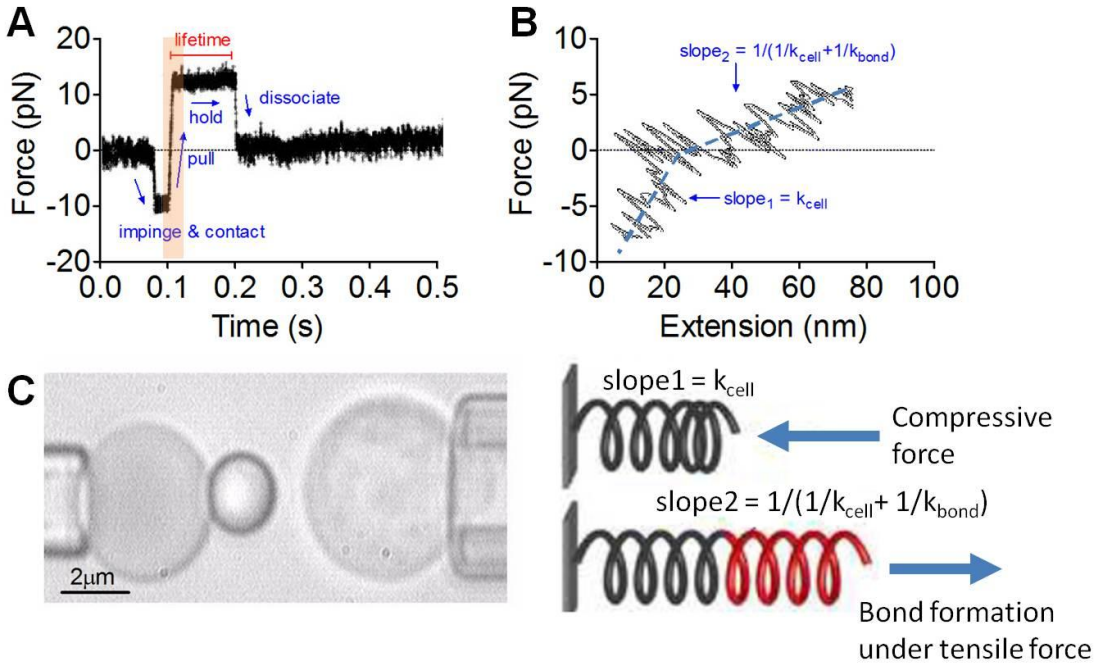

Figure 3.8: Force-clamp assay and stiffness analysis
The T cell was driven repeatedly to impinge, make a contact with the bead, then retract to be held at a desired force to wait for bond dissociation (A, C). Adhesion was detected by a tensile force signal caused by RBC membrane deformation and bond lifetime was measured from the instant when the force reached the desired level to the instant of bond

dissociation (A). In addition, the ramping phase of BFP cycles (shaded in A) can be zoom-in for force vs. extension curve (B). The slopes from this curve represent serially connected components: cells (slope1) and cell plus the molecular interaction (slope2). From linear curve fitting k_{cell} and k_{bond} are derived.

3.3.5 Stiffness analysis

We measured the stiffness of molecular bonds from the ramping phase of BFP test cycles[75, 78]. The ramping phase of BFP cycles (colored in **Figure 3.8A**) can be zoom-in to read force vs. extension curve (**Figure 3.8B**). The extension is the differential displacement between the BFP tracking system and the piezoelectric actuator feedback system. Therefore, the slope of this curve is the stiffness of serially connected components: cells (RBC and T cell) and the molecular interaction (TCR–pMHC) (**Figure 3.8C**). Two slopes appeared in the ramping phases: one ($slope_1$) from compressive force and the other with decreased slope ($slope_2$) from tensile force (**Figure 3.8B**). Since the slope under compression was higher, we assumed the molecular complex can resist tension but not compression, and the cellular spring has the same value regardless of whether the cell surface is in tension or compression. We verified this assumption with using purified molecules coated beads to measure k_{mol} and calculate tension k_{cell} from $slope_2$. Our data indicate that tension k_{cell} and compression k_{cell} are not significantly different (**Figure 3.9**). Therefore, with linear curve fitting of the data, we estimated k_{cell} from the $slope_1$ ($slope_1 = k_{cell}$) and calculated k_{bond} from $slope_2$ ($slope_2 = 1/(1/ k_{cell} + 1/k_{bond})$) (**Figure 3.8B**).

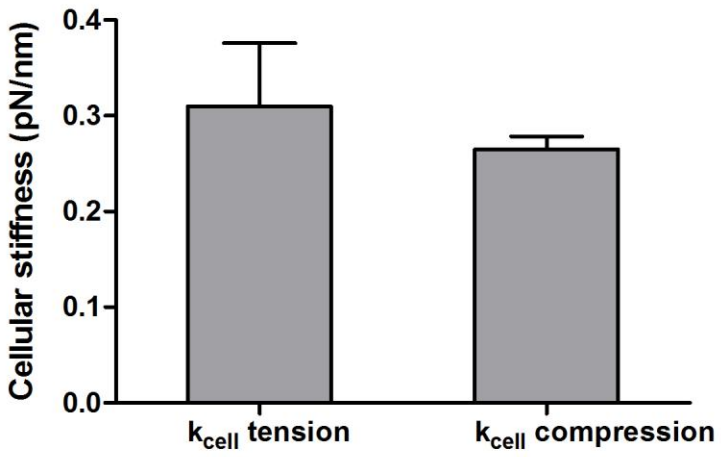

Figure 3.9: Cellular stiffness comparison
From purified molecules coated beads experiment, we measured k_{mol} to calculate tensile k_{cell} from $slope_2$ of force vs. extension curve and compared to the compressive k_{cell} from $slope_1$. No significant difference was observed (p=0.3). Bars are presented as mean ± SEM (n≥140)

3.4 3D Surface plasmon resonance

3D TCR–pMHC binding kinetics were analyzed using a Biacore 2000 surface plasmon resonance instrument[79] from Paul Allen's lab in Washington University in St. Louis. CM5 sensor chips (GE Healthcare) were activated with a 20minute pulse with a 1:1 mixture of 100mM N-hydroxysuccinimide (NHS) and 75mg/mL 1-ethyl-3-[3-dimethylaminopropyl] carbodiimide hydrochloride (EDC). NeutrAvidin (Pierce) was immobilized to the chip via amine coupling using a solution of ~100µg/mL NeutrAvidin in 20mM sodium citrate buffer pH 4.5. Unreacted NHS groups on the chip surface were blocked with a 6-minute pulse of 1M ethanolamine pH 8.5. Biotinylated pMHC monomer was then coupled to the chip to a total response level of ~1000 resonance units (RU). For binding analysis, concentration series of scTCR covering at least two orders of magnitude were injected in duplicate at 25°C over surfaces coupled with monomeric peptide:I-E^k, using a flow rate of 30µL/min. Running buffer for all experiments was HEPES-buffered saline (10mM HEPES, 3mM EDTA, 150mM NaCl and 0.005% Tween-20). All

sensorgrams were corrected for nonspecific binding by subtracting the response from a surface coupled with CLIP:I-E^k, and corrected for bulk flow effects by subtracting the response obtained from plain buffer injection.

Sensorgrams from scTCR concentration series injections were fitted to a 1:1 Langmuir binding model using BiaEvaluation version 4.1 to derive the 3D k_{off}, k_{on}, and K_a ($=1/K_d=k_{on}/k_{off}$). K_d and maximum response (R_{Max}) values for equilibrium binding analysis were obtained by plotting the equilibrium response (R_{eq}) at each concentration and fitting these data to a one-step binding model using GraphPad Prism version 6.0a for Macintosh (GraphPad Software, San Diego, CA). Scatchard plots were generated to confirm 1:1 binding stoichiometry by graphing R_{eq}/[TCR] versus R_{eq}.

3.5 Concurrent calcium imaging

In addition to the micropipette setup, we added fluorescent imaging capabilities to allow concurrent micromanipulation and calcium imaging (**Figure 3.10**). Two light sources were used to get bright field image (halogen lamp) and fluorescent image (xenon lamp). Since Fura2 required radiometric analysis, dual excitation filters (340 and 380 nm) were switched automatically using a filter wheel (Lambda LS, Sutter) and a controller (Lambda 10-3 controller, Sutter). With using dual channel imaging system (DC-2, Photometrics), the bright field wavelength filtered with 610nm red filter and the emission wavelength from Fura2 were separated to its respective cameras. A dichroic mirror with 565nm long-pass filter was used. A digital digital camera (CoolSNAP HQ2, Photometrics) and the NIS-Element software (Nikon) was implemented for fluorescent image acquisition and image analysis.

For loading the calcium indicator, T cells were loaded with 4μM Fura-2/AM, incubated for 30min at 37°C, washed twice with Ca^{2+} free PBS buffer (pH 7.4). Then, T cells and RBCs pre-coated with pMHC were transferred into L-15/HEPES media

(SIGMA) containing microscopic chamber. For simultaneous adhesion frequency assay and calcium imaging, each T cell and RBC pair was tested repeatedly for total 10 min of contact-retract cycles at a given contact duration.

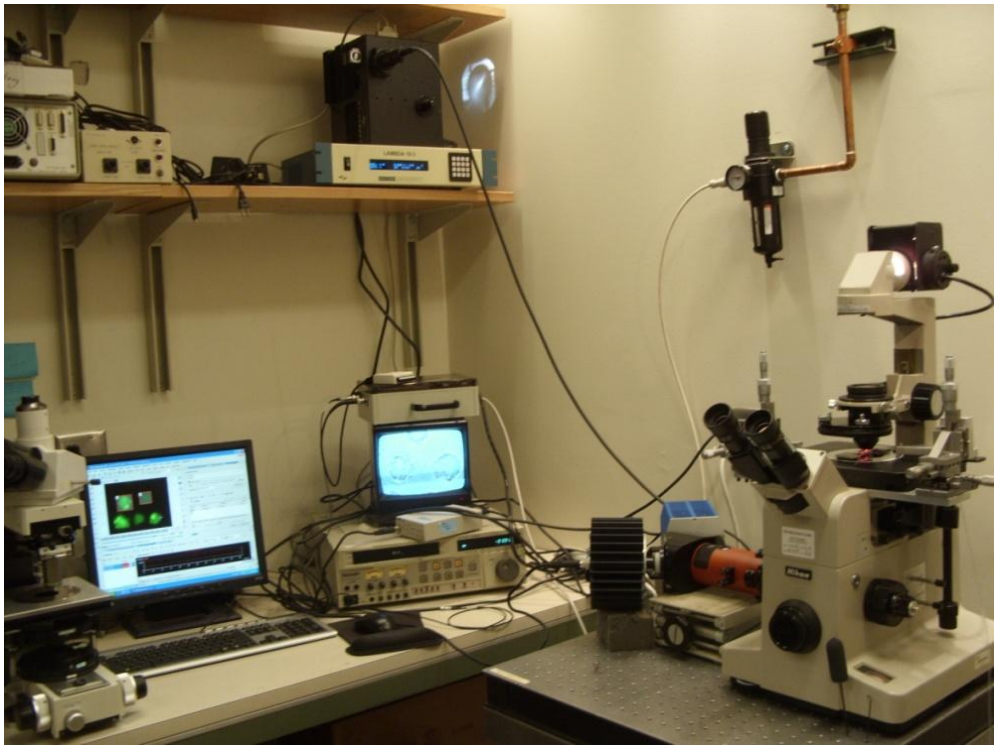

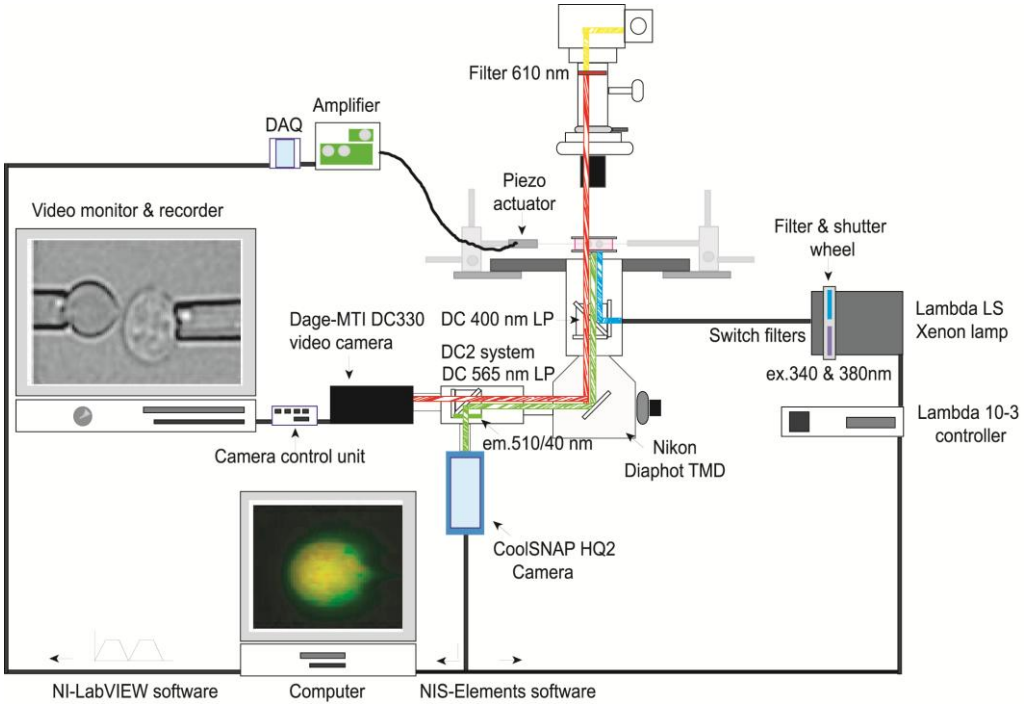

Figure 3.10: Concurrent micromanipulation and calcium imaging system An inverted microscope (TMD Diaphot, Nikon) was customized by mounting two sets of mechanical manipulators on the two sides of the stage. A piezo actuator is mounted on one side to drive micromanipulation of glass pipette for adhesion frequency assay. Concurrent detection of adhesion frequency and calcium signaling is enable by splitting the bright field light and Fura-2 excitation wave lengths. Decoupling the bright field and fluorescent images is obtained by using 610-nm long-pass filter for bright field light and DC2 system with 565 nm long-pass dichroic mirror for fluorescent imaging.

3.6 Blocking reagents

Prior to the CD4 blocking experiment, we used a purified anti-mouse CD4 monoclonal antibody (GK1.5, eBioscience) to incubate the T cells and injected them into the experiment chamber at the same concentration[39, 80]. That is, we incubated the purified 3.L2 T cells with the CD4 blocking antibody at 20μg/ml in 100μl for 30min in 4℃ and then tested them in the experiment chamber with the presence of 20μg/ml antibodies. For the 3.L2 TCR blocking experiment, we used an anti-3.L2 clonotypic antibody (CAb) donated by Dr. Brian Evavold at Emory University. We incubated the purified T cells at 50μg/ml in 100μl for 30min in 4℃, and then tested them in the experiment chamber in the presence of 50μg/ml CAb.

For the blocking of OT-I TCR and CD8, we incubated DP thymocytes with purified anti-mouse TCR Vα2 monoclonal antibody (B20.1, eBioscience) and CD8 monoclonal antibody (CT-CD8a, LifeSpan Biosciences), respectively, prior to the experiment and injected the antibodies into the experiment chamber to maintain the same antibody concentration[41]. That is, we incubated the purified DP thymocytes with antibodies at 50μg/ml in 100μl for 30min in 4°C and then tested them in the experiment chamber in the presence of antibodies with the same concentration.

For the inhibition of Lck, we used a Src tyrosine kinase inhibitor PP2 (4-Amino-5-(4-chlorophenyl)-7-(t-butyl)pyrazolo[3,4-d]pyrimidine) from Biomol (Plymouth Meeting, PA). We preincubated DP thymocytes with 10mM PP2 for 10min at 25℃ and

tested them during the next 10min with a continuous presence of PP2. Since PP2 is effective in only a 10-min window, we replaced the sample every 10min.

To disrupt microfilament organization, we used latrunculin A (Calbiochem). latrunculin A bind to monomeric G-actin to inhibit actin filament organization. We preincubated DP thymocytes in 1μM for 30min at 25℃ and then tested them in the experiment chamber in the presence of latrunculin A with the same concentration.

3.7 Statistical analysis

We statistically compared data using the Student's t-test or one-way ANOVA.

CHAPTER 4 IN SITU 2D KINETICS AND FORCE REGULATION OF TCR–pMHC INTERACTION IN CD4$^+$ T CELL FUNTION

4.1 Introduction

Previous study with using adhesion frequency assay showed CD8 cooperates to TCR–pMHC interaction in signaling dependent manner[41]. Also, recent reports suggested 2D kinetic results have wider dynamic range to predict the T cell response with faster on- and off-rate than the previous reported 3D kinetics[1, 39]. In addition, recent study shows that force regulates bond lifetime in TCR–pMHC interaction for T cell activation (Liu et al. Cell *in press*). Indeed TCR–pMHC interaction is exposed to a physical environment including cellular components (e.g., co-receptors or other membrane proteins) or cellular motions (e.g., migration, actin radial flow, membrane deflection) that could actively restrict or promote TCR binding to pMHC in a force dependent manner. Therefore, force regulation could be critical in TCR–pMHC interaction. In this chapter, we expanded the analysis of 2D TCR binding kinetics and contribution of force regulation to a class II-restricted T cell model. We anticipated testing the hypothesis of "*in situ* 2D kinetics and force regulation of TCR–pMHC interaction better define T cell response than previous 3D methods in MHC class II system." Three specific aims are tested: 1) Quantify 2D kinetic parameters of 3.L2 TCR to analogues of Hb68-76 ligand bound MHC II in naïve T cell to better predict the T cell response; 2) Compare 2D and 3D measurements to confirm the differences and the advantage of 2D kinetic parameters; 3) Analyze force regulation in TCR–pMHC interaction for T cell response.

To derive the *in situ* 2D kinetics, we used native T-cells purified from the 3.L2 TCR transgenic mouse system, and red blood cells (RBCs) covalently coated with purified cognate pMHC ($Hb_{64\text{-}76}$:I-E^k) or altered peptide ligands (APLs) in the

micropipette apparatus. The effective 2D affinity and the effective 2D on-rate positively correlated with the functional T cell response whereas the 2D off-rate showed negative correlation. Compared to previous 3D parameters, 2D parameters better correlated to a series of related pMHCs for this system. When force was applied to these TCR–pMHC interactions, agonist and weak agonist showed catch-slip bond and antagonists showed slip bonds. These findings indicate force regulation can contribute to ligand discrimination. Lastly, the results revealed that CD4 has a substantially lower affinity to MHC class II and did not cooperate to TCR binding under zero-force. However, under force-regulation CD4 contributes significantly to bond lifetime for the agonist ligand.

4.2 Results

4.2.1 Affinity of CD4 to I-E^k

Before analyzing the characteristics of TCR–pMHC interaction in 2D kinetics, we first wanted to verify the lack of CD4 contribution to TCR–pMHC binding. Although, CD4 has been previously shown to not contribute to TCR–pMHC binding by FRET experiments[39] and computational modeling[81], we conducted the adhesion frequency assay that have better sensitivity for verification. We tested the effect of blocking TCR and CD4 by pre-incubating T cells with the anti-3.L2 clonotypic antibody (CAb) and the CD4 blocking antibody (GK1.5) and then performed the adhesion frequency assay on naïve $CD4^+$ T cells against $Hb_{64\text{-}76}$:I-E^k-coated RBCs with the presence of the antibody in the experiment chamber. Adhesion frequency data showed that CAb treatment reduced the binding frequency but GK1.5 treatment did not (**Figure 4.1A**) indicating that TCR–pMHC interaction, but not CD4–MHC interaction, is the dominant factor in the binding frequency.

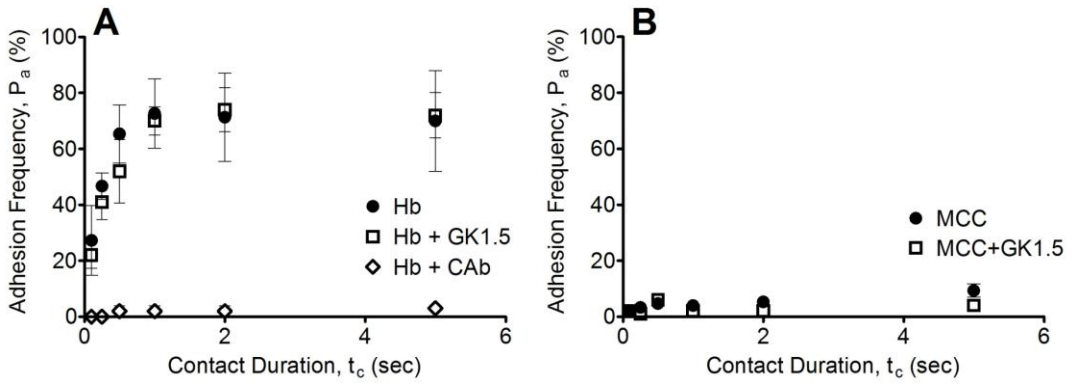

Figure 4.1: Contribution of CD4 in adhesion frequency The TCR blocking antibody (CAb) and the CD4 blocking antibody (GK1.5) were used to incubate the cells prior to the experiment, which was conducted in the presence of the antibody for the blocking treatment. The CAb treatment resulted in a drop in the binding frequency but the GK1.5 treatment did not affect the binding curve (A). In addition, the irrelevant peptide $MCC_{88\text{-}103}$:I-Ek was coated on the RBCs to test the binding frequency between the CD4 and I-Ek. Some binding was observed at the longer contact duration (5s) with a high site density over 4,000 molecules/μm2, but overall the binding was very low (<10%) (B). Because of the low binding frequency, blocking CD4 with GK1.5 did not produce a significant difference (B). The molecule densities tested at these representative data are as follows (TCR/μm^2:pMHC/μm^2): $Hb_{64\text{-}76}$ (116:34), $Hb_{64\text{-}76}$ + GK1.5 (116:34), $Hb_{64\text{-}76}$ + CAb (163:28), MCC (136:4483, 315 for CD4), and MCC + GK1.5 (136:4483, 315 for CD4). Each binding frequency measurement is presented as mean ± SEM (n≥3) from 50 touches each. The data are representative from at least two independent experiments.

In order to directly measure CD4 binding, we tested the binding frequency of the irrelevant $MCC_{88\text{-}103}$:I-E^k to CD4 (**Figure 4.1B**). We did observe binding at a longer contact duration (5s) with the highest possible site density on a RBC over 4,000 molecules/μm^2, but overall the binding was very low. The low binding between CD4 and MHC class II (I-E^k) yielded less than 7.0×10^{-8} μm^4 in 2D effective affinity. These results coincide with those of previous research confirming that CD4 does not enhance TCR binding[39, 42, 82]. Thus, we confirmed the lack of CD4 contribution supporting a dimeric interaction between the TCR and the pMHC. Here after, all of the measurements were derived using bimolecular interaction kinetic models, assuming that the adhesion frequencies and bond lifetimes were mediated by TCR–pMHC interactions with no CD4 contribution, as previously reported[39, 82].

4.2.2 Zero-force kinetic analysis of 3.L2 TCR–pMHC interaction

To compare with our previous zero-force analysis of the MHC class I-restricted TCR systems, we analyzed the 2D binding affinities and kinetic rates of the 3.L2 TCR (MHC class II-restricted). A series of well-characterized ligands were tested, including the wild-type peptide Hb_{64-76} and three APLs with a single amino acid alteration at residue 72 complexed with the mouse MHC class II I-E^k molecule[36, 83]. To reliably evaluate the distinct 2D affinities of Hb_{64-76} (agonist), T72 (weak agonist), I72 (antagonist), and A72 (weak antagonist), different pMHC densities were coated on the RBCs in order to obtain mid-ranged adhesion frequencies for all ligands (**Figure 4.2A**). We were then able to define 2D binding kinetics for all of the ligands (**Figure 4.2**, **Table 1**), including the weak antagonist A72 with lowest potency that was not previously detectable using SPR[36].

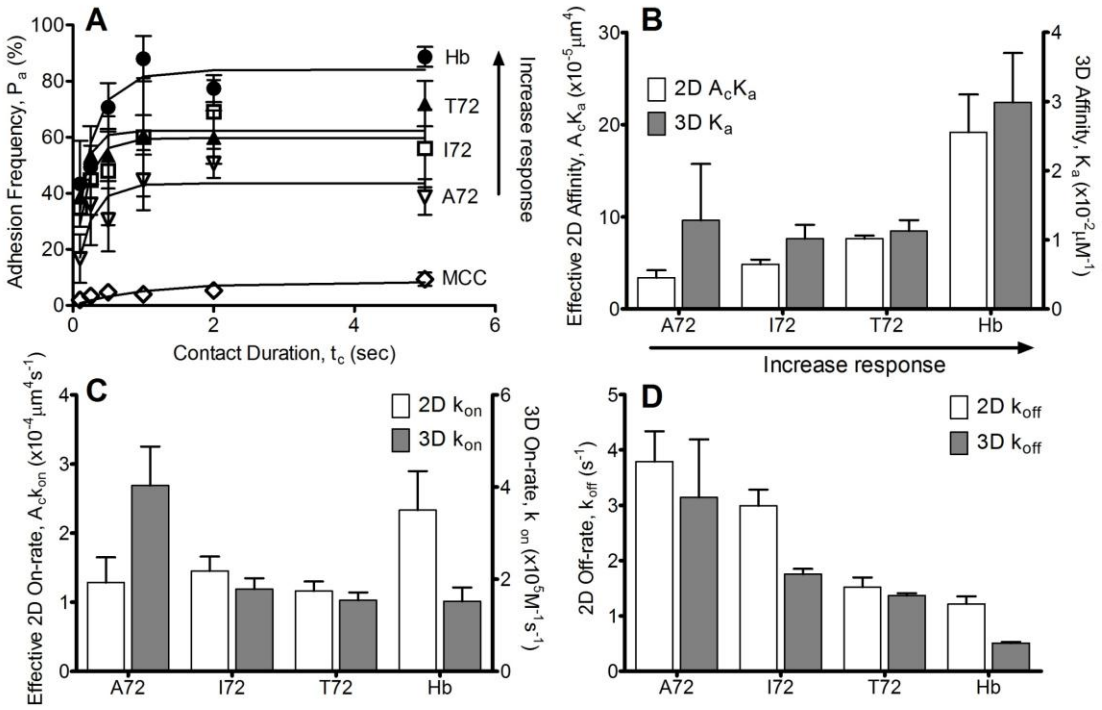

Figure 4.2: 2D kinetic measurements and the comparison between 2D vs. 3D kinetics The adhesion frequency assay was conducted through a different panel of

peptides (Hb_{64-76}, T72, I72, A72, and MCC (an irrelevant peptide)) (A). The measured 2D kinetics are compared to the 3D SPR data (B, C, D). Each 2D kinetic measurement is presented as mean ± SEM (n≥3). The data in (A) are representative from at least three independent experiments.

The 2D affinity was derived from the adhesion frequency curve-fitting data with a probabilistic kinetic equation that accounts for the different ligand densities (see *Materials and Methods*) (**Figure 4.2B**)[73]. The effective 2D affinity, A_cK_a, occurred over a 6-fold range (3.4-19.2 × 10^{-5} μm^4) with the agonist Hb_{64-76} displaying the highest affinity and the weakest antagonist A72 ligand the lowest affinity. In addition to the 2D off-rates derived from the adhesion frequency assay, the thermal fluctuation assay was also used, to obtain more accurate off-rate values from analysis of single-bond lifetime measurements[74, 84] (**Figure 4.2D**). These thermal fluctuation data show 2D off-rates, k_{off}, which also accurately reflected ligand potency ranging from the Hb_{64-76} to A72 with a range (1.22-3.79 s^{-1}). The effective 2D on-rate, A_ck_{on}, was calculated by multiplying the effective 2D affinity and the 2D off-rate (**Figure 4.2C**) and displayed a range (1.16-2.33 × 10^{-4} $\mu m^4 s^{-1}$) that reflected ligand potency. When comparing to OT-I system, the values of effective 2D affinity and on-rate for the tested ligands in 3.L2 system fall in the range of A2 (agonist) and G4 (weak agonist)[1]. However, 2D off-rate in 3.L2 system showed negative correlation to the ligand potency which was in opposite to that of the OT-I system[1].

Table 1: 2D kinetics and binding affinities of 3.L2 TCR–pMHC interactions from micropipette assay

Peptide	Sequence	Classification of Ligand	Effective 2D affinity, A_cK_a (μm^4)	Effective 2D on-rate, A_ck_{on} ($\mu m^4 s^{-1}$)	2D off-rate, k_{off} (s^{-1})
Hb_{64-76}	GKKVITAFNEGLK	Agonist	$19.2 \pm 4.1 \times 10^{-5}$	$2.33 \pm 0.56 \times 10^{-4}$	1.22 ± 0.14
T72	GKKVITAFTEGLK	Weak agonist	$7.6 \pm 0.3 \times 10^{-5}$	$1.16 \pm 0.14 \times 10^{-4}$	1.52 ± 0.17
I72	GKKVITAFIEGLK	Antagonist	$4.8 \pm 0.5 \times 10^{-5}$	$1.45 \pm 0.20 \times 10^{-4}$	2.99 ± 0.29
A72	GKKVITAFAEGLK	Weak antagonist	$3.4 \pm 0.8 \times 10^{-5}$	$1.29 \pm 0.36 \times 10^{-4}$	3.79 ± 0.55

4.2.3 Comparison of 2D and 3D kinetic parameters

Previously, Kersh et al.[36] reported SPR measurements for the tested panel of peptides using double-chain TCR. However, in order to directly compare with our 2D parameters, our collaborator Paul Allen's lab measured new 3D kinetic parameters with SPR method using single-chain TCR and peptides covalently linked I-E^k as in the 2D measurements (**Table 2**). Whereas Hb_{64-76} and T72 3D SPR measurements were readily calculated by simultaneous modeling of k_{on} and k_{off}, injection spikes coupled with extremely fast kinetics precluded successful curve fitting for I72 and A72. The 3D SPR measurements for these ligands were instead derived by separately modeling the k_{on} and k_{off} using data from the sensorgram corresponding to the highest scTCR concentration injection.

Table 2: 3D kinetics and binding affinities of 3.L2 TCR–pMHC interactions from SPR

Analyte / Ligand	k_{on} ($M^{-1}s^{-1}$)	k_{off} (s^{-1})	K_d (μM) k_{off}/k_{on}	Half-life (s)	K_d (μM) Equilibrium	*N*
scTCR / Hb_{64-76}:I-E^k	15,183 ± 3,017	0.508 ± 0.019	35.3 ± 0.82	1.36	28.73 ± 5.88	6
scTCR / T72:I-E^k	15,433 ± 1,711	1.37 ± 0.038	90.7 ± 1.28	0.51	73.71 ± 4.23	3
scTCR / I72: I-E^k	(28,100 – 14,000)*	(1.63 - 1.95)*		(0.355 - 0.425)	366 ± 18.7	3
scTCR / A72: I-E^k	(71,000 – 24,100)*	(1.12 - 4.61)*		(0.150 - 0.619)	1,309 ± 108	3

*3D k_{on} and k_{off} for I72 and A72 were derived by separate modeling using data from the sensorgram corresponding to the highest scTCR concentration injection.

Several differences were observed in comparison between the 2D and 3D kinetic parameters as shown in **Figure 4.2B-D** and **Figure 4.3**. First, the effective 2D affinity correlates with the peptide potency to activate T cell response[36, 83], showing a higher affinity for the agonist peptide and a lower affinity for the antagonist peptide (**Figure 4.2B**). Although the 2D and 3D affinities showed positive correlation ($p<0.05$), the high R^2 value (0.9) may be due solely to their much higher values for the agonist pMHC than the other three APLs, which could be resolved by the 2D, but not 3D, analysis (**Figure 4.3A**). For this reason, no correlation was observed between the 3D affinity and peptide potency (**Figure 4.2B**).

In the case of on-rate, the ligand potency positively correlated to the effective 2D on-rate (**Figure 4.2C**). However, the 3D on-rate showed an opposite trend: a high on-rate for the low potency ligands and a low on-rate for the high potency ligands (**Figure 4.2C**). Therefore, 2D and 3D on-rates poorly correlated ($R^2=0.14$, $p>0.5$) (**Figure 4.3B**). In the case of off-rates, the ligand potency negatively correlated to the 2D off-rate (**Figure 4.2D**) and the 3D off-rate also showed similar trend (**Figure 4.2D**). Therefore, 2D and 3D off-rates showed significant correlation ($R^2=0.87$, $p<0.1$) (**Figure 4.3C**).

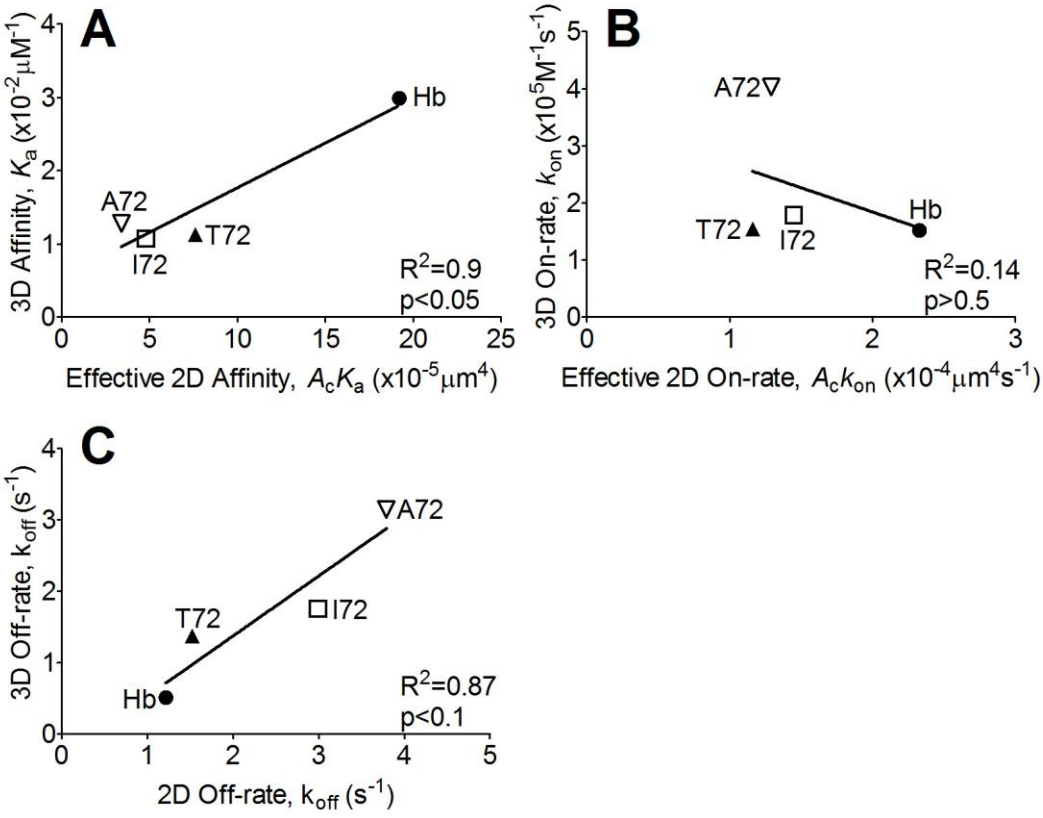

Figure 4.3: Correlation between 2D and 3D kinetics The effective 2D affinity shows a close correlation (R^2=0.9, p<0.05) to the 3D affinity but only due to high magnitude of the agonist Hb (A). The effective 2D on-rate poorly correlates (R^2=0.14, p>0.5) to the 3D measurements (B). Only the 2D off-rate showed a strong correlation (R^2=0.87, p<0.1) with the 3D measurements (C). The mean values were used for comparison for both 2D and 3D kinetics.

To further examine the functional correlation of the 2D kinetics of the 3.L2 TCR–pMHC interaction, we plotted functional T cell response against the effective 2D affinity (**Figure 4.4A**), on-rate (**Figure 4.4B**) and off-rate (**Figure 4.4C**). Because T cells can induce ligand dependent induction of B cell apoptosis, the ligand concentration required to generate 40% B cell apoptosis (EC_{40}) was chosen as a T cell response readout from the previous research[83]. Positive correlations were found for the effective 2D affinity (R^2=0.84) and 2D on-rate (R^2=0.36) (**Figure 4.4A and B**). With the 2D off-rate, negative correlations were observed (R^2=0.92) (**Figure 4.4C**). However, the correlation was

compressed compared to that of OT-I system only showing a single-log of magnitude 2D kinetics correlating to six-log of magnitude T cell response.

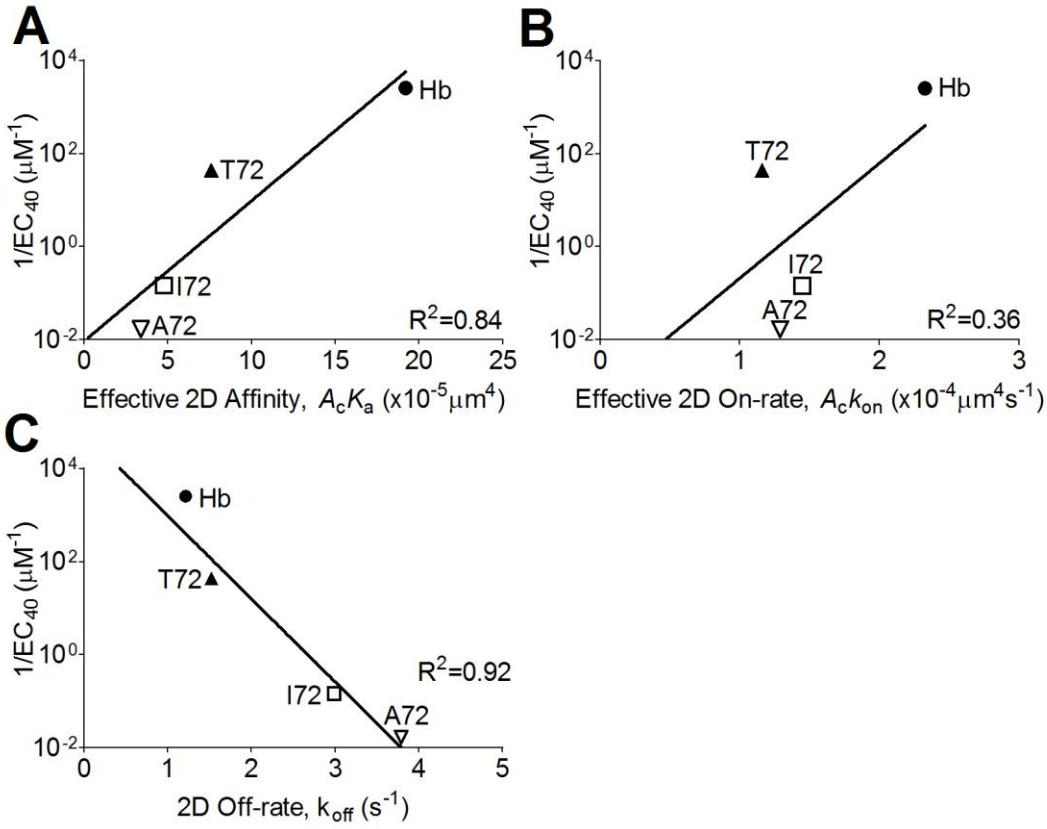

Figure 4.4: Correlation between 2D kinetics and T cell response The effective 2D affinity shows a close correlation (R^2=0.84) to a reciprocal of the ligand concentration that required to produce 40% B cell apoptosis (EC_{40}) (A). The effective 2D on-rate also shows a positive correlation (R^2=0.36) (B). The 2D off-rate shows a negative correlation (R^2=0.92) to $1/EC_{40}$ (C). The parameters used for the 2D kinetics are the mean values from the adhesion frequency assay and thermal fluctuation assay. The EC_{40} values are from previously conducted research[83].

4.2.4 Force-regulated dissociation kinetics of *in situ* 3.L2 TCR–pMHC interaction

In addition to the importance of TCR–pMHC interaction on a 2D membrane, several recent studies have proposed that the TCR recognize physical force to activate T-cells[38, 85-88]. In order to dissect the physical force contribution in T cell recognition, we conducted force-clamp assay to measure force-dependent dissociation kinetics. The

experiments were conducted in two difference T cell populations from mouse splenocytes to test the contribution of CD4. We isolated $CD4^+$ $CD8^-$ 3.L2 T cells (160 TCR/μm^2, 315 CD4//μm^2) and $CD4^-$ $CD8^+$ 3.L2 T cells (50 TCR/μm^2, 300 CD8/μm^2) from 3.L2 transgenic mouse splenocytes (**Figure 4.5**). When testing these two T cell populations in zero-force adhesion frequency assay, $CD8^+$ 3.L2 T cells showed a similar effective 2D affinity to $CD4^+$ 3.L2 T cells against APLs (**Figure 4.6**), further supporting CD4 does not contribute to TCR–pMHC interaction in zero-force condition.

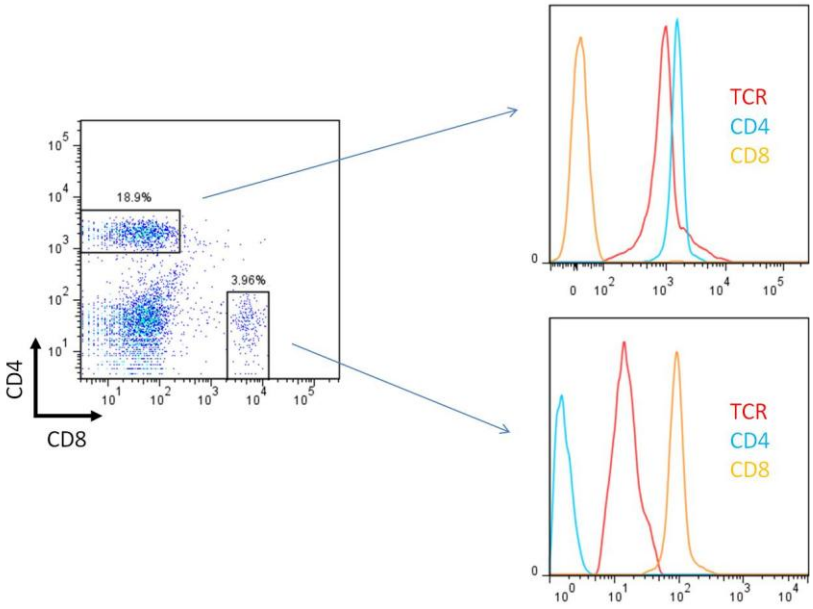

Figure 4.5: Flowcytometry analysis of $CD4^+$ $CD8^-$ and $CD4^-$ $CD8^+$ 3.L2 T cells Flowcytometry analysis shows distinct two populations based on the CD4 and CD8 dual staining. The $CD4^+$ $CD8^-$ and $CD4^-$ $CD8^+$ 3.L2 T cells were purified with respective purification protocols for adhesion frequency assay and force-clamp assay.

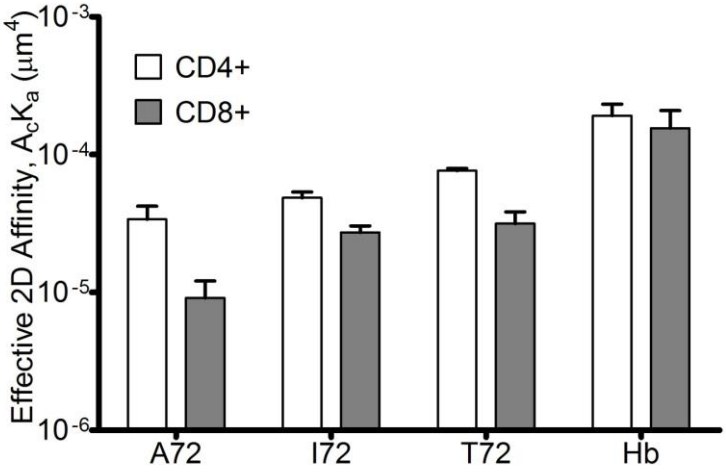

Figure 4.6: Comparison of the effective 2D affinity in CD4$^+$ and CD8$^+$ 3.L2 T cells From adhesion frequency assay, the effective 2D affinity of CD4$^+$ and CD8$^+$ 3.L2 T cells show similar level for APLs. Each bar is presented as mean ± SEM (n≥5).

However, the stiffness analysis from the force-clamp assay shows CD4 contribution under force. When plotting the histogram of the molecular bond stiffness from either CD4$^+$ or CD8$^+$ 3.L2 T cells (**Figure 4.7**), we were able to fit the histogram with single Gaussian distribution except Hb in CD4$^+$ 3.L2 T cells (**Figure 4.7A**). For the stiffness histogram of CD4$^+$ 3.L2 T cells binding to Hb, two-Gaussian distribution fit better than a single Gaussian distribution indicating the possibility of two kind of bond formation. However, the stiffness histogram of CD8$^+$ 3.L2 T cells binding to Hb showed a single Gaussian fit. Together, it suggested CD4 could contribute in TCR–pMHC interaction under force. However, this phenomenon was not detectable with other weaker ligands (**Figure 4.7C, D, E, F, G, and H**).

Next, from force-clamp assay we plotted force vs. bond lifetime curve (**Figure 4.8**). For agonist Hb, with or without CD4 condition showed catch-slip behavior where bond lifetime increases, reach a maximum then decrease to force. However, the magnitude of the peak bond lifetime was dependent on the presence of CD4. For CD4$^+$ T cell (red circle, **Figure 4.8A**) the peak bond lifetime reached maximum of 3.2s at 10pN whereas the peak bond lifetime with CD4 blocking antibody (yellow triangle, **Figure**

4.8A) or CD8+ T cell (blue square, **Figure 4.8A**) reached only 2s at 12pN. Thos events that had bond stiffness larger than the second peak (0.53pN/nm) in the stiffness analysis (green diamond, **Figure 4.8A**) indeed showed catch-slip behavior indicating the stiffening could be due to CD4 synergy. On the other hand, weaker ligands did not show CD4 dependency (**Figure 4.8B**). $CD4^+$ and $CD8^+$ T cells showed similar curve in force vs. bond lifetime analysis. Only weak agonist T72 showed small catch-slip behavior but the rest showed slip-only behavior. Together, agonist dependent CD4 synergy to TCR–pMHC interaction was observed under force.

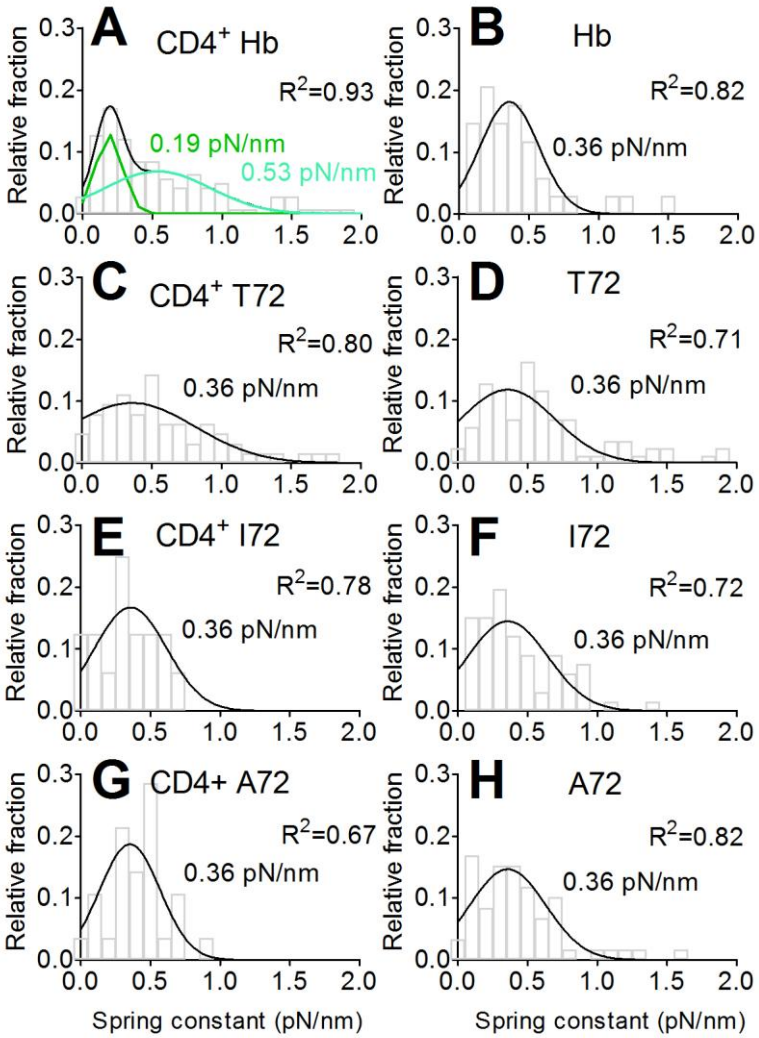

Figure 4.7: Molecular bond stiffness analysis of 3.L2 T cells Histogram (grey bar graph) of the molecular bond stiffness for APLs are plotted for $CD4^+$ (A, C, E, G) and $CD8^+$ (B, E, F, H) 3.L2 T cells. The histograms are fitted with a single Gaussian distribution (black line) except Hb binding to $CD4^+$ T cells which had better fit with sum of two Gaussian distribution (A, green and cyan line). The least mean square method was used to fit all the data to a single constraint mean of the indicated spring constant. Goodness of fit for each fitting is calculated in R^2. The sample size for each condition is listed as following: $CD4^+$ Hb (n=173), $CD4^+$ T72 (n=71), $CD4^+$ I72 (n=21), $CD4^+$ A72 (n=28), $CD8^+$ Hb (n=45), $CD8^+$ T72 (n=86), $CD8^+$ I72 (n=66), and $CD8^+$ A72 (n=59).

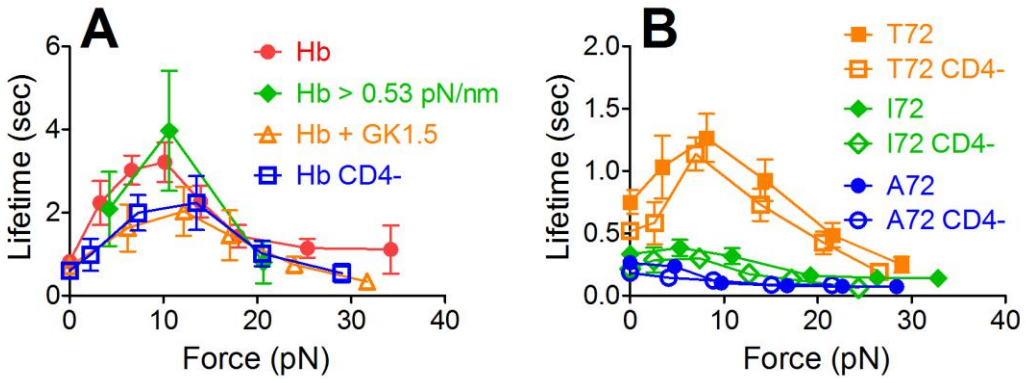

Figure 4.8: Force vs. bond lifetime analysis of 3.L2 system The force-clamp assay data are analyzed with force vs. bond lifetime curve. The strong agonist Hb shows CD4 dependent catch-slip behavior (A) whereas the weaker ligand does not show any CD4 synergy (B). Only weak agonist T72 shows small catch-slip behavior and the rest antagonists, I72 and A72, show slip-only behavior. Filled symbols represent the data from $CD4^+$ T cells and open symbols represent $CD8^+$ T cells or CD4 blocking conditions. The sample size for each condition is listed as following: $CD4^+$ Hb (n= 563), $CD4^+$ T72 (n=304), $CD4^+$ I72 (n=221), $CD4^+$ A72 (n=153), $CD8^+$ Hb (n=129), $CD8^+$ T72 (n=255), $CD8^+$ I72 (n=182), and $CD8^+$ A72 (n=151).

In order to test how force change the correlation of the bond lifetime to the ligand potency, we plotted the correlation curve between bond lifetime and the ligand concentration required to generate 40% B cell apoptosis (EC_{40}) from the previous research[83] (**Figure 4.9**). Like previously mentioned in zero-force correlation, the correlation of bond lifetime to EC_{40} only showed compressed correlation. In addition, the trend did not change much with (green) or without (blue) CD4 presence (**Figure 4.9**). However, when we correlate the bond lifetime at 10pN (force where the longest bond lifetime was observed) to EC_{40}, the correlation expanded a little allowing better dynamic

range than the zero-force. Also, the presence of CD4 (red) increased the expansion of the correlation allowing better dynamic power.

Further to answer how force contributes to the power of ligand discrimination, we plotted bond lifetime ratio of Hb/other peptide vs. force (**Figure 4.10**). The analyses for I72 (green) and A72 (blue) show that the ratio of bond lifetime increases till 10-15pN regime then decrease. This trend was similar but had slight difference when considering CD4. In the case of where CD4 was present the maximum ratio of bond lifetime for I72 was 1.5 times higher and for A72 1.6 times higher than the case where there was no CD4. For T72, the ratios of bond lifetime were lower compared to I72 and A72. These results further support that the force and the CD4 increases the power of ligand discrimination.

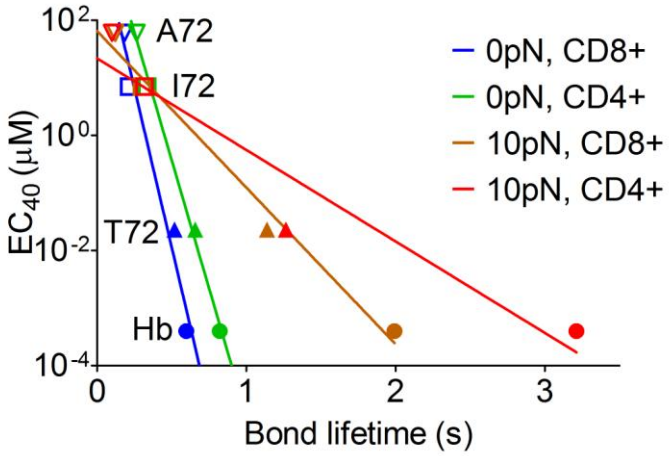

Figure 4.9: Bond lifetime vs. functional EC_{40} analysis of 3.L2 system The correlation between bond lifetime and the ligand concentration required to generate 40% B cell apoptosis (EC_{40}) from the previous research[83] show that force can expand the dynamic range of the correlation. The mean bond lifetime for Hb (filled circle), T72 (filled triangle), I72 (open square), and A72 (open triangle) are plotted with fitted lines for different conditions as color indicated.

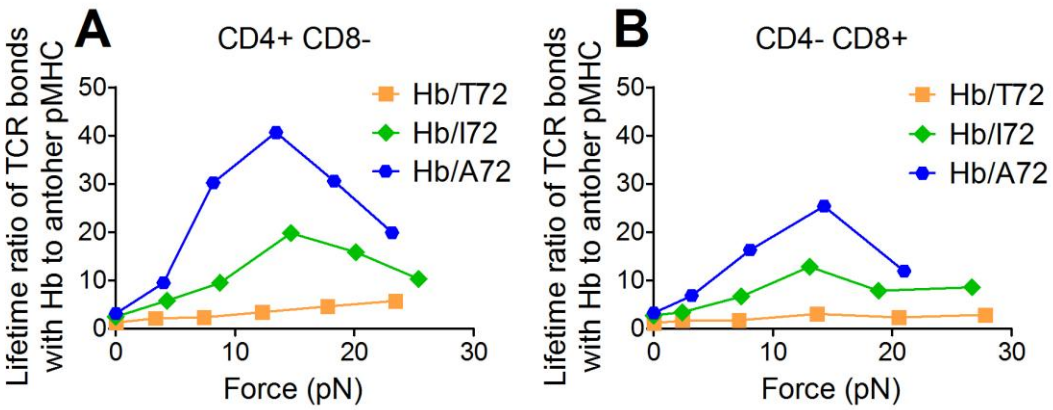

Figure 4.10: Bond lifetime ratio of TCR bonds with Hb to anther pMHC vs. force analysis of 3.L2 system The ratio of bond lifetime of Hb/other pMHC vs. force show increase power of ligand discrimination. Both results from $CD4^+$ $CD8^-$ (A) and $CD4^-$ $CD8^+$ (B) T cell population show increase of ratio for Hb/I72 (green) and Hb/A72 (blue). However, the magnitude of the ratio amplifies when there is CD4 (A). The data points from force vs. bond lifetime (**Figure 4.8**) were used to calculate the ratio.

4.3 Discussion

In this chapter, we took the advantage of micropipette apparatus to quantify *in situ* 2D kinetics and force-regulation of TCR–pMHC interaction and to correlate the measurements with those of the T cell function in a MHC class II-restricted system (3.L2) (

Table 3). Similar to the previous 2D kinetic measurements on a MHC class I-restricted system (OT-I)[1], the 2D kinetic parameters of the 3.L2 system had a wider dynamic range than the 3D kinetic parameters in terms of their correlation to ligand potency. Also, the measured 2D binding predicted T cell responses better than 3D binding. Even though the dynamic power was smaller in the 3.L2 system than the OT-I system, the 2D kinetic parameters correlated better with ligand potency than that of the 3D. When tested under force, 3.L2 system showed qualitative difference in the tested panel of altered peptide ligands. Force prolonged TCR–pMHC interaction for the strong agonist but not for the

weaker ligands. Lastly, CD4 synergistically contributed to TCR–pMHC interaction only under force for the strong agonist.

Table 3: Summary of 2D, 3D kinetics, and force-regulation of 3.L2 system

Peptide	Sequence	Classification of Ligand	Force -regulated lifetime	Effective 2D affinity A_cK_a (μm^4)	Effective 2D on-rate A_ck_{on} ($\mu m^4 s^{-1}$)	2D off-rate k_{off} (s^{-1})	3D affinity K_a (μM^{-1})	3D on-rate k_{on} ($M^{-1}s^{-1}$)	3D off-rate k_{off} (s^{-1})
Hb_{64-76}	GKKVITAFNEGLK	Agonist	Catch-slip	$19.2 \pm 4.1 \times 10^{-5}$	$23.3 \pm 5.6 \times 10^{-5}$	1.22 ± 0.13	0.030 ± 0.007	$15,183 \pm 3,017$	0.508 ± 0.019
T72	GKKVITAFTEGLK	Weak agonist	Catch-slip	$7.6 \pm 0.3 \times 10^{-5}$	$11.6 \pm 1.4 \times 10^{-5}$	1.52 ± 0.17	0.011 ± 0.002	$15,433 \pm 1,711$	1.370 ± 0.038
I72	GKKVITAFIEGLK	Antagonist	slip	$4.8 \pm 0.5 \times 10^{-5}$	$14.5 \pm 2.0 \times 10^{-5}$	2.99 ± 0.29	0.010 ± 0.002*	$17,833 \pm 2,371$*	1.753 ± 0.099*
A72	GKKVITAFAEGLK	Weak antagonist	slip	$3.4 \pm 0.8 \times 10^{-5}$	$12.9 \pm 3.6 \times 10^{-5}$	3.79 ± 0.54	0.013 ± 0.008*	$40,333 \pm 8,436$*	3.146 ± 1.046*

Recently, studies on 2D kinetics of the TCR–pMHC measurements using micropipette adhesion frequency assay have been well established. Other than previously mentioned studies on OT-I system[1, 40, 41], Sabatino et al.[42] used the micropipette adhesion frequency assay to detect the kinetics of polyclonal pMHC tetramer positive and negative $CD4^+$ cells that were responsive in self $MOG_{35–55}$ and pathogen $GP_{61–80}$ epitopes. This study showed that the micropipette adhesion frequency assay had better detection capabilities than 3D pMHC tetramer kinetic methods which rely on multivalent interaction (TCR avidity). Also, Adams et al. [43] used the micropipette adhesion frequency assay to detect difference in docking geometric in TCR–pMHC and found better correlation of 2D affinity with IL-2 activation than 3D tetramer affinity. Most recently, Liu et al.[89] reported 2D parameters of TCR–pMHC–CD8 interactions determine T cell tumor reactivity and suggested the possibility of 2D-based screening strategy for tumor immunotherapy. Overall, these findings show 2D kinetics have increased sensitivity than

3D kinetic measurements, and more accurately reflects the biology associated with T cell responses to antigen.

In addition to our observation, other previous studies also indicated different trends between the 2D and the 3D measurements[1, 43]. For example, the agonist peptides show high binding affinities, fast off-rates and on-rates in the 2D measurements but high binding affinities, low slow off-rates and on-rates in the 3D. These differences in binding kinetics between 2D and 3D for the same molecules raise unanswered questions[90, 91]. We believe that the different experimental conditions between the 2D and the 3D are beginning to provide some clues for these differences. For example, the 2D measurements are from membrane lipid anchored molecules that can be regulated by cytoskeleton and other proteins that can provide clustering or cooperativity between molecules. In contrast, the 3D measurements are typically from truncated forms of recombinant purified soluble molecules analyzed under conditions in flow that may not replicate the *in situ* molecular interaction. The importance of considering cellular microenvironment is supported by the recent cell-free 2D measurements that showed just the similar trend as the 3D measurements[92]. Although, off-rates have same unit of reciprocal time in both the 2D and the 3D, the direct conversion of on-rates and affinities between the 2D and the 3D is impossible due to different space dimensions of interacting molecules. This is an active area of research that would provide great insight into T cell triggering and response to antigens, but the direct conversion between 2D and 3D will be only possible when we can quantitatively measure the contribution of the cellular microenvironment in TCR–pMHC interaction.

Despite having similar TCR (~150 molecules/μm^2) and co-receptor (~300 molecules/μm^2) density on a T cell surface, the dynamic range of 2D kinetic parameters in the 3.L2 and the OT-I system showed discrepancies. The 2D kinetics of the 3.L2 had a single-log distribution that correlated to a six-log magnitude difference in the functional parameters. This trend in 3.L2 system differs from that in the OT-I system, which had

three orders of magnitude difference in 2D kinetics correlating to six orders of magnitude in T cell proliferation[1]. Compared to the OT-I system, the correlation of the 3.L2 system has lower dynamic range (i.e., compressed kinetics). The compressed 2D kinetics of the 3.L2 system seems unusual compared to the OT-I system, but this compactness was also observable in the 42F3 TCR system interacting with QL9:H2-L^d (MHC class I)-derived APLs, which ranged 0.2-1 × 10^{-4} μm^4 for 2D effective affinity[43]. Although the difference in dynamic range is difficult to comprehend, we know the mouse systems are different with different MHC class restriction, associating co-receptor, and maybe different surface organization.

We wanted to compare the binding characteristics of CD4 to that of CD8[40, 41]. However, effective 2D affinity for CD4 was measured to be less than 7.0 × 10^{-8} μm^4, which was lower than that of CD8–H-$2K^b$ (2.8-5.7 × 10^{-6} μm^4) and CD8–H-$2D^b$ (0.1-0.5 × 10^{-6} μm^4)[40]. Moreover, unlike CD8, CD4 did not exhibit a cooperative binding property[41] in the binding frequency assay, nor did it show any contribution to an increase in the binding frequency of TCR–pMHC. Even with more sensitive detection method we could only confirm that CD4 has minimal contribution in TCR–pMHC interaction under zero-force.

However, when force was applied to TCR–pMHC interaction, CD4 showed synergistic effect to prolong the lifetime with the strong agonist. From the stiffness analysis, the strong agonist binding data showed a two Gaussian distribution fit which indicated two populations in the molecular bond formation. This was verified from force vs. bond lifetime curve analysis where CD4 strengthened the catch-slip behavior. For the other weaker ligands, CD4 synergy was not observed. In addition, ligand dependent qualitative behavior was observed under force. Agonists showed catch-slip behavior with different peak lifetime whereas antagonists showed slip-only behavior that further allowed qualitative distinction based on the ligand potency. Lastly, the two bond lifetime related analyses we performed show force and CD4 increase dynamic range of

correlation to T cell function and increase the power of ligand discrimination. These results suggest that force in combination with CD4 enhances discrimination of the ligand potency by altering TCR–pMHC bond lifetime. Therefore, it is plausible to propose force-regulated TCR–pMHC interaction amplifies ligand discrimination and CD4 may have synergistic contribution.

In summary, we quantified the TCR–pMHC interaction in a cellular context for an MHC class II-restricted TCR system. Were we not only able to measure the 2D kinetic parameters but also were able to correlate the parameters to the T cell function. In addition, we found that because of their dynamic range, 2D kinetics were better able to distinguish ligand potency than 3D kinetics further supporting 2D kinetics as a reliable predictor of T cell function. We were not able to measure neither 2D kinetics nor cooperativity of CD4 in zero-force condition but when force was applied to TCR–pMHC interaction CD4 showed synergy in TCR–pMHC bond lifetime for a strong agonist. Lastly, force-regulated TCR–pMHC interaction showed qualitative ligand discrimination. This study supported a method of quantifying the receptor-ligand interaction under physical force and correlating the values with the cellular function that will enable us to continue research in an effort to explain the T cell recognition mechanism.

CHAPTER 5 CONSTRASTING CONTRIBUTION OF CO-RECEPTORS AND 2D KINETICS IN NAÏVE T CELLS AND THYMOCYTES

5.1 Introduction

Previous studies reported high sensitivity of thymocyte in inducing positive selection by either recognition of low dose[93, 94] or low affinity antigens[33, 47]. Also, pre-selection DP thymocytes but not SP T cells were responsive to a weak agonist antigen in CD69 up-regulation and calcium mobilization[95]. In addition to higher sensitivity in thymocytes, CD8 binds more avidly[96, 97] and enhances CD69 up-regulation and IL-2 production with weak agonists (lower affinity ligands)[2-4]. On the other hand, CD4 contribution may not be so dominant since positive selection can be possible in the absence of CD4[98]. Therefore, we anticipated to test the hypothesis of "TCR–pMHC interaction and co-receptor contribution may be different in naïve T cells and thymocytes." Three specific aims are tested: 1) Quantify and compare 2D kinetic parameters of 3.L2 and OT-I TCR binding to its respective APLs in naïve T cells and thymocytes; 2) Compare the contribution of co-receptors in TCR–pMHC interaction for these systems; 3) Measure intracellular calcium signaling to compare the sensitivity between naïve T cells and thmocyctes.

In this chapter, we measured and compared 2D kinetics of TCR–pMHC–CD4/CD8 binding on naïve T cells and DP thymocytes both in a MHC class I (OT-I)- or II (3.L2)-restricted systems. We used native DP thymocytes purified from a thymus of a transgenic OT-I or 3.L2 mouse. To derive the 2D binding kinetics, the altered peptide ligands were tested in the micropipette apparatus. The results showed that DP thymocytes had higher affinity than the naïve T cells. Also, in DP thymocytes CD8 contributed significantly from the early binding allowing no second step but a gradual contribution.

Consistent with the previous naïve OT-I data, CD8 cooperativity in DP thymocytes was signal dependent. However, CD4 did not show any contribution in TCR-pMHC binding in DP thymocytes. Lastly, concurrent calcium imaging with adhesion frequency assay showed higher sensitivity in DP thymoctes than naïve T cells.

5.2 Results

5.2.1 2D kinetic measurements of DP thymocytes

To compare the binding characteristics of DP thymocytes and naïve T cells, adhesion frequency assay was conducted to measure 2D kinetic parameters of DP thymocytes. DP thymocytes were purified from the thymus of 3.L2 and OT-I system as described in *Materials and Methods*. For 3.L2 system, we measured adhesion frequency level for APLs that were tested for naïve T cells in the previous chapter. The effective 2D affinity for DP thymocytes occurred over 4-fold range (5.0-19.5 × 10^{-4} μm^4) showing 10-times higher magnitude than that of the naïve T cells (**Figure 5.1A**). 2D off-rates (2.17-4.29 s^{-1}) showed little difference from that of the naïve T cells (**Figure 5.1B**). 2D on-rates were calculated over 4-fold range (1.5-9.6 × $10^{-3}\mu m^4 s^{-1}$) showing 10-times higher magnitude than that of the naïve T cells (**Figure 5.1C**). Except I72 that showed an outlier trend, 2D measurements in thymocytes also showed correlation with the ligand potency similar to that of naïve T cells.

Similarly, effective 2D affinity of APLs in DP OT-I thymocytes ranged more than 10-times higher than that of naïve T cells. The spectrum of effective 2D affinity of DP OT-I thymocytes spread with three-orders of magnitude (0.2-399.3 × 10^{-5} μm^4) whereas that of naïve T cells were much lower (0.1-25.6 × 10^{-6} μm^4) (**Figure 5.2**). Therefore, we were not only able to quantify 2D affinity in thymocytes and naïve T cells but also revealed 10-times higher affinity in thymocytes to that of naïve T cells.

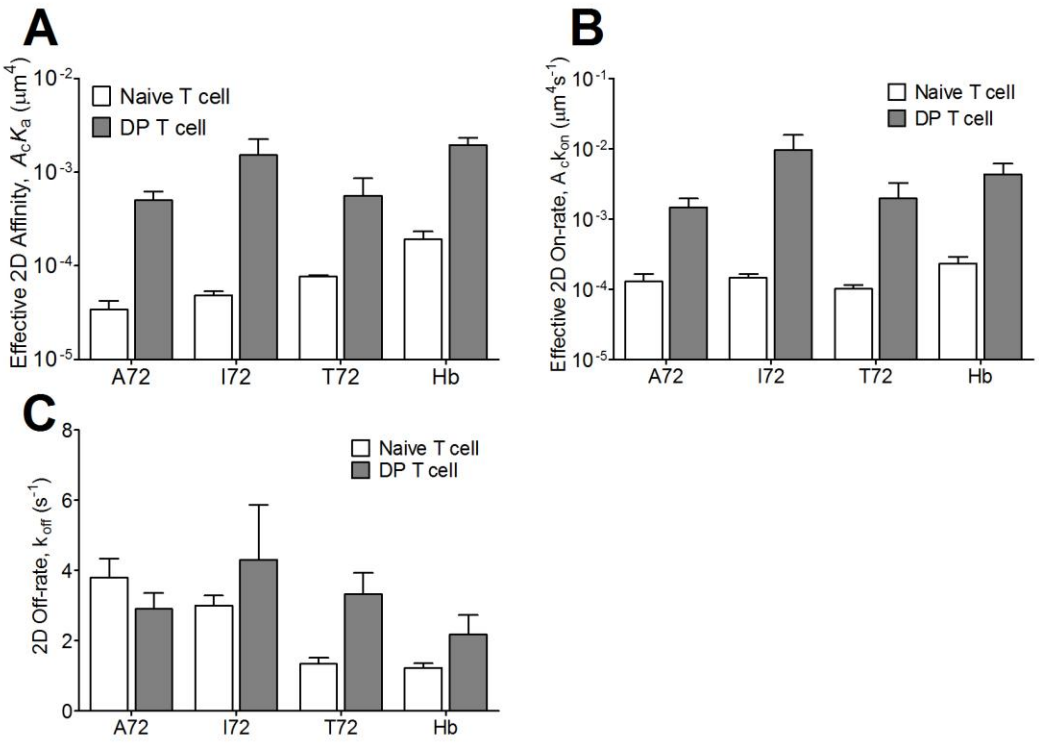

Figure 5.1: Comparison of 2D measurements in naïve and DP 3.L2 thymocyte The adhesion frequency assay for DP 3.L2 thymocytes was conducted through a panel of peptides (Hb_{64-76}, T72, I72, and A72) to derive effective 2D affinity (A), effective 2D on-rate (B), and 2D off-rate (C). The measured data were compared to that of the previously measured naïve T cells. Each 2D kinetic measurement is presented as mean ± SEM (n≥3).

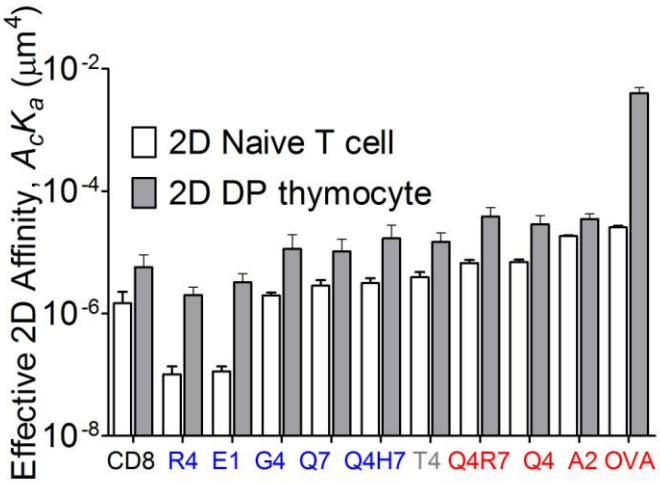

Figure 5.2: Comparison of effective 2D affinity in naïve and DP OT-I thymocyte The adhesion frequency assay for naïve and DP OT-I thymocytes was conducted through a

panel of peptides (OVA, A2, Q4, Q4R7, T4, Q4H7, Q7, G4, E1, R4, and VSV) to derive effective 2D affinity. Each 2D kinetic measurement is presented as mean ± SEM (n≥5).

5.2.2 Co-receptor contribution in DP thymocytes

Previous studies show that CD4 contribute to the delivery of Lck[81], the sensitivity[99], the IL-2 production for agonist peptides[100], the dimerization of the TCR-pMHC complex[101], but not significantly to the TCR binding energy[82]. In Chapter 4, however, CD4 did not contribute to TCR–pMHC interaction under zero-force. To further confirm the lack of CD4 cooperation on TCR–pMHC interaction, we conducted an adhesion frequency assay with and without blocking TCR and CD4 in 3.L2 DP thymocytes. We tested the effects of blocking TCR and CD4 by pre-incubating DP thymocytes with the anti-3.L2 clonotypic antibody (CAb) and the CD4 blocking antibody (GK1.5) and then performed the adhesion frequency assay against Hb_{64-76}:I-E^k-coated RBCs in the presence of the antibody in the experiment chamber. Adhesion frequency data showed that the GK1.5 treatment did not alter the binding frequency (**Figure 5.3A**). In contrast, the binding frequency disappeared when the cells were treated with CAb for Hb (**Figure 5.3B**). Therefore, consistent with the previous finding from naïve T cells, we conclude CD4 does not contribute to TCR-pMHC binding in DP thymocytes under zero-force.

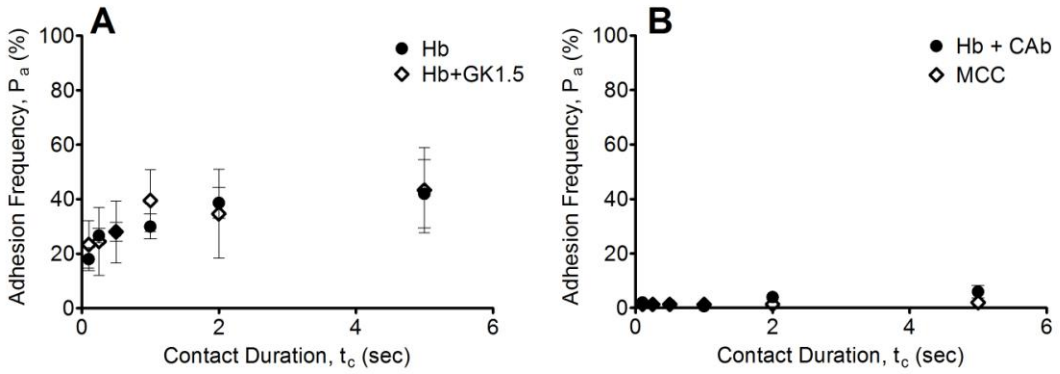

Figure 5.3: Contribution of CD4 in adhesion frequency of 3.L2 thymocytes No difference was observed in the adhesion frequency for the case of Hb and CD4 blocking (GK1.5) with Hb (A). However, CAb treatment resulted in a drop in the binding frequency (B). The irrelevant peptide MCC_{88-103}:I-E^k with high density did not show adhesion. The molecule densities tested at these representative data are as follows (TCR/μm^2:pMHC/μm^2): Hb_{64-76} (6:127), Hb_{64-76} + GK1.5 (6:127), Hb_{64-76} + CAb (6:127), MCC (2:5552, 86 for CD4). Each binding frequency measurement is presented as mean ± SEM (n≥3) for 50 touches each. The data are representative from at least two independent experiments.

Previously, Jiang et al.[41] found that CD8 synergistically enhances TCR-pMHC binding in naïve T-cells by observing a cooperative binding phenomenon in the adhesion frequency assay after one-second contact time. After CD8 formed a trimeric interaction with TCR–pMHC, the binding frequency increased abruptly (step-increase). We questioned whether this phenomenon also took place in OT-I DP thymocyte TCR–pMHC binding, so we tested the effect of blocking CD8 by pre-incubating DP thymocytes with the anti-CD8 antibody (CT-CD8a) and then performed an adhesion frequency assay on DP thymocytes against $OVA_{257-264}$:H-$2K^b$-coated RBCs in the presence of the antibody in the experiment chamber. Our adhesion frequency data showed that the CD8 blocking treatment reduced the binding frequency in all the measured contact times (**Figure 5.4**). In addition, CD8 cooperativity took place even during short contact times (0.1-0.5s). However, early CD8 cooperativity distinctly differed from that of naïve T-cells, in which CD8 cooperativity took place only during the longer contact times (after 1s) but not during the short contact times[41]. In addition, we tested whether CD8 cooperativity in DP thymocytes was signal dependent as in naïve T-cells. We used a PP2 treatment to inhibit Lck[41], which eliminated the contribution of CD8 to the TCR-pMHC binding frequency (**Figure 5.4**). The PP2 treatment abrogated the binding frequency to the same level as TCR binding to $OVA_{257-264}$:H-$2K^b$ α3A2. Therefore, CD8 in DP thymocytes contributed to the TCR-pMHC binding from the early binding stage depending on Lck signaling.

In terms of 2D affinity for CD8, the measurement in thymocytes ($5.73\pm 0.33 \times 10^{-6}$ μm^4) was 4-times higher than that in naïve T cells ($1.47 \pm 0.78 \times 10^{-6}$ μm^4) (**Figure 5.2**).

This quantitative observation of decrease in CD8 affinity due to development is already reported. Moody et al.[97] reported with using tetramer studies that CD8–MHC-I avidity decrease due to developmentally programmed O-glycan modification controlled by ST3Gal-I sialyltransferase during maturation.

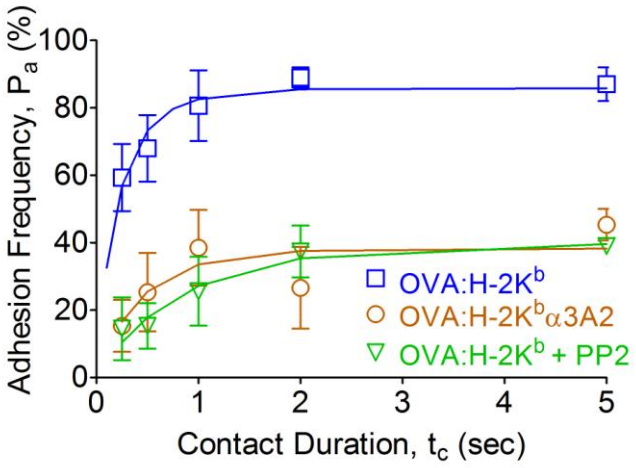

Figure 5.4: Contribution of CD8 in adhesion frequency of OT-I Adhesion frequency assay were conducted to test the contribution of CD8 in TCR–pMHC interaction. Experiment with wild-type OVA which could allow TCR–pMHC–CD8 interaction showed the highest adhesion level. However, mutant OVA which lack the binding site for MHC–CD8 interaction show a decreased adhesion level. When we treated Srk kinase inhibitor PP2 in testing wild-type OVA, the adhesion frequency dropped to the level of mutant OVA. The molecule densities tested at these representative data are as follows (TCR/μm^2:pMHC/μm^2): wild-type OVA (9:46), mutant OVA (9:42), wild-type OVA + 10μM PP2 (9:46). Each binding frequency measurement is presented as mean ± SEM (n≥3) for 50 touches each. The data are representative from at least two independent experiments.

5.2.3 Concurrent calcium imaging and adhesion frequency assay in naïve and DP 3.L2 thymocytes

In order to compare the sensitivity of naïve and DP thymocytes, concurrent calcium imaging system was implemented to the adhesion frequency assay (*see Materials and Methods*). Ratiometric readout of Fura2 for 10min time interval was normalized for continuous RBC and T cell binding with indicated contact duration (**Figure 5.5**). 0.5, 1, 2,

and 5s contact duration conditions were tested with indicated average adhesion frequency (**Figure 5.5**). However, the normalized Fura2 ratio did not show increase upon continuous adhesion events. Only for long contact duration, 5s and continuous engagement, it showed 20% increase in Fura2 ratio after 9min.

However, when we tested DP 3.L2 thymocytes the Fura2 showed significant difference to the results from naïve T cells. Same experiment with 3.L2 thymocytes resulted in much more fluctuation and increase in Fura2 ratio with similar level of adhesion frequency. For example, more than 30% increase in Fura2 ratio was observed just 3min after initial binding event for 5s contact duration condition (**Figure 5.6**). Other conditions also showed earlier increase of Fura2 ratio with magnitude reaching higher than that of naïve T cells. These results indicate that thymocytes are more responsive in fluxing calcium after TCR–pMHC engagement than naïve T cells, which further support previous report on higher sensitivity of thymocytes than naïve T cells in TCR stimulation[95].

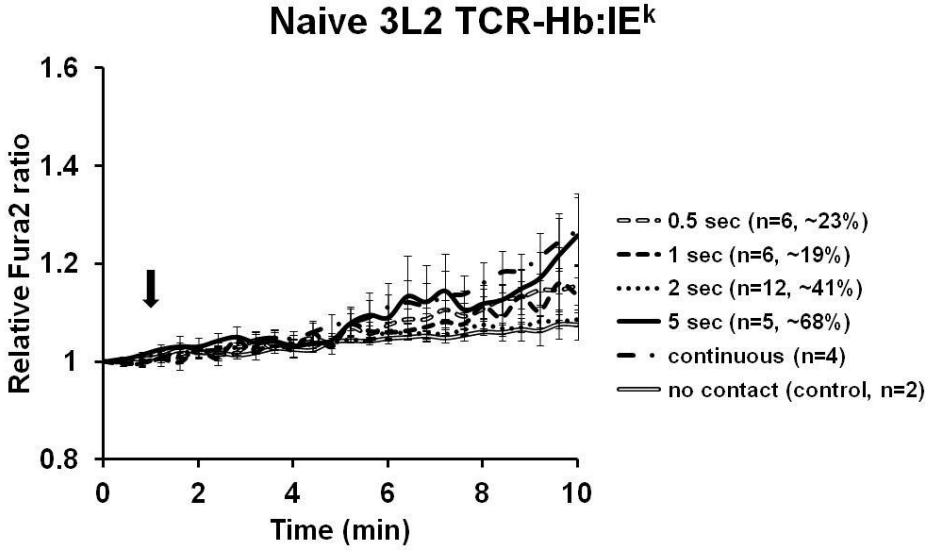

Figure 5.5: Normalized Fura2 ratio of naïve 3.L2 T cells Normalized Fura2 ratios of naïve 3.L2 T cells were measured from concurrent calcium imaging system in combination with adhesion frequency assay. Averaged normalized Fura2 ratios (mean ± SEM) from number for different cell pairs of different contact durations are plotted with

respective average adhesion frequency. We took images every 8s for 1min before the initial adhesion event (black arrow) and continued for 9min.

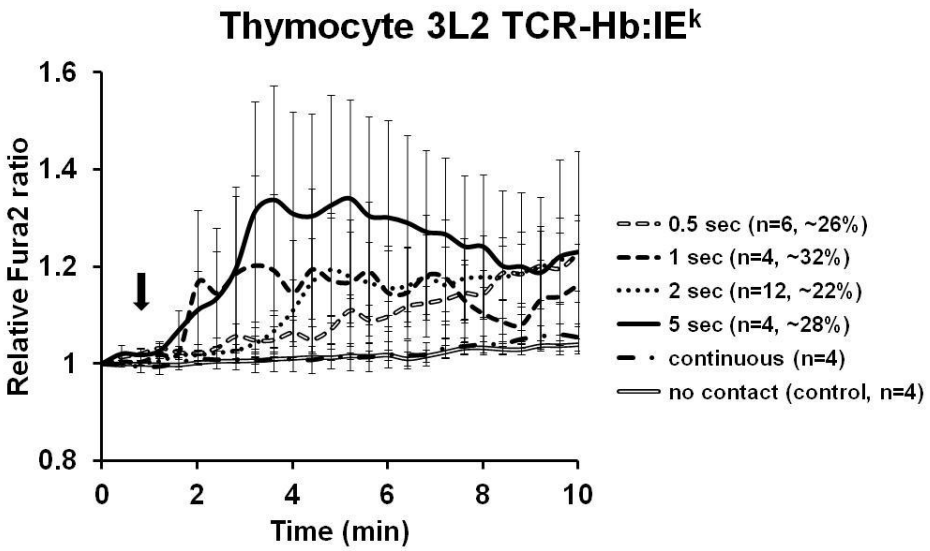

Figure 5.6: Normalized Fura2 ratio of DP 3.L2 thymocytes Normalized Fura2 ratios of FP 3.L2 thymocytes were measured from concurrent calcium imaging system in combination with adhesion frequency assay. Averaged normalized Fura2 ratios (mean ± SEM) from number for different cell pairs of different contact durations are plotted with respective average adhesion frequency. We took images every 8s for 1min before the initial adhesion event (black arrow) and continued for 9min.

5.3 Discussion

In this chapter, we successfully characterized the contribution of co-receptors in the TCR–pMHC–CD4/CD8 trimolecular interaction in thymocytes (in both MHC class I and II systems) and compared their contributions to naïve T-cells. Whereas CD4 did not contribute to TCR–pMHC interaction under zero-force, CD8 had signaling dependent early cooperativity and its 2D affinity on thymocytes was higher than that on naïve T cells. We also quantified the TCR–pMHC bimolecular interaction in DP thymocytes by effective 2D affinity and compared it to that of naïve T-cells. Our results showed the effective 2D affinity of all of the tested TCR–pMHC bimolecular interactions was about

10-times higher in DP thymocytes than in naïve T-cells. Lastly, concurrent calcium imaging demonstrated thymocytes were easier to stimulate than naïve T cells.

We know from flow cytometry analysis that even though the CD8 expression level of DP thymocytes is similar (~300/μm^2) to that of naïve T-cells, the TCR expression level of DP thymocytes is around 10-times lower (several tens of molecules/μm^2) than that of naïve T-cells. Based on this, it is questionable how thymocytes detect the ligand and initiate TCR signaling. In this context, higher 2D affinity of TCR–pMHC interaction in thymocytes and cooperativity of CD8 implies new information. Based on these data, we hypothesize that in contrast to naïve T-cells, DP thymocytes may compensate low level of TCR expression by higher affinity of TCR and early cooperativity of CD8 to have sufficient sensitivity for ligand recognition. For weaker ligands having similar or lower affinity than CD8, CD8 may even play a dominant role in TCR–pMHC recognition. We speculate these differences in thymocytes and naïve T-cells membrane may due to changes in composition or structural conformation of CD8 or TCR–CD8 complex during maturation. However, more in-depth research is required for verification.

More fundamental question in thymocyte context such as the mechanism of thymic selection can be asked. It has already been suggested that a 3D kinetic cutoff threshold correlates with negative selection[33, 52, 53]. However, for previously mentioned reasons 3D measurements may over simplify the physiologic TCR–pMHC interaction. Taking the advantage of 2D kinetics measurements, we can measure the 2D kinetics of DP thymocytes and relate them to the selection process to characterize how DP thymocytes quantify selection cues. Investigations related to this regard have been followed up in Chapter 6.

The study in this chapter showed a unique method of characterizing and quantifying the TCR–pMHC interaction in DP thymocytes in a cellular context. We were able to characterize the signaling-dependent CD8 cooperativity but not with CD4. In addition, we demonstrated higher sensitivity of TCR–pMHC interaction in thymocytes

with 2D affinity and concurrent calcium imaging. The findings of this study provide opportunities for research in T-cell development and recognition mechanism in DP thymocytes.

CHAPTER 6 FORCE-REGULATED BOND LIFETIME OF TCR–pMHC INTERACTION DETERMINES THYMIC SELECTION

6.1 Introduction

The repertoire of TCRs in the periphery is thought to be derived from thymocytes that have been selected from thymus by an optimal binding affinity window[10]. T cells with TCR that does not bind to self antigens die by neglect and those that bind too strongly undergo apoptosis to prevent potential autoimmune response. Only the T cells with optimal affinity TCR are positively selected. In this context, previous literature also suggests apparent affinity threshold for negative and positive selection discrimination[53]. Several approaches have been conducted to identify the thymic selection parameter such as kinetic threshold[33, 52-54], CD3 conformational change[56-59], signaling kinetics and compartmentalization[44, 52]. However, we only know that subtle differences in kinetics (i.e., less than two-fold difference in the selection border) or CD3 conformational change lead to distinct downstream signaling. In this chapter, we anticipated to test the hypothesis of "*in situ* 2D kinetics and force regulation of TCR–pMHC interaction better define thymic selection." This hypothesis is based on previous studies[1, 39] and our previous chapters that show 2D kinetic measurement better represent TCR–pMHC interaction. In addition, force could play a critical role in TCR–pMHC interaction due to continuous migration of thymocytes in thymus by encountering cortical (cTEC) and medulla thymic epithelial cells (mTEc)[5]. Three specific aims are tested: 1) Quantify zero-force 2D kinetic parameters of immature TCR–pMHC interaction in thymic selection; 2) Analyze force regulation in TCR–pMHC interaction in thymic selection; 3) Verify force regulation effect in thymic selection with endogenous ligands and in an alternative system.

In this chapter, we implemented mechanically based micropipette assays to study TCR-pMHC interaction considering co-receptor contribution and mechanical force

regulation in a native thymocyte environment to identify better physiologic predictor for thymic selection. We used negative and positive selecting ligands for transgenic OT-I mouse system to measure 2D binding characteristics, molecular bond stiffness, and force-lifetime relationship with micropipette apparatus[73, 76]. Our results show that normalized adhesion bonds, 2D effective affinity for TCR–pMHC, and zero-force synergy of CD8 do not show any significant difference among the tested ligands. However, when we applied force on the TCR–pMHC interaction we were able to observe significant difference between the two selecting ligand groups. Negative selecting ligands showed a catch-slip behavior (i.e., force induce longer lifetime until some degree then force induce shorter lifetime afterwards). On the other hand, positive selecting ligands showed only a slip behavior (i.e., force induce shorter lifetime). For verification, an alternative mouse system (2C) and endogenous peptide sequences were tested to demonstrate the same result. Based on these findings, we predict force induce longer lifetime for negative selecting ligands that can promote enough interval for signal initiation or accumulation for further downstream signaling. However, for positive selecting ligands force shortens bond lifetime restricting signaling to occur or accumulate. These results show a novel indicator that discriminates two selecting ligand groups based on force-lifetime relationship.

6.2 Results

6.2.1 Zero-force 2D kinetic measurements in thymic selection

In order to test correlation between 2D kinetics and thymic selection, we first anticipated to implement 2D adhesion technique to test a panel of pMHCs for a clear separation in 2D adhesion or kinetic parameters. For this purpose, we tested a panel of pMHCs (OVA, Q4, Q4R7, T4, Q4H7, Q7, and G4) that have been previously reported by Ed Palmer group[52, 53] that showed strong correlation in FTOC to negative (OVA, Q4,

Q4R7, and T4) and positive selection (Q4H7, Q7, and G4) (**Figure 6.1**). We used micropipette adhesion frequency assay to test the adhesion characteristics of these pMHCs to OT-I thymocytes (**Figure 6.2**). Since TCR and CD8 can both bind to pMHC on native thymocyte surface, we selectively tested TCR–pMHC interaction only by using either anti-CD8 blocking antibody (green triangle) or mutant MHC-I (H-2K^b α3A2) that limits CD8 binding to MHC-I (brown circle). Also, we tested TCR contribution in binding frequency by using anti-TCR blocking antibody (red diamond).

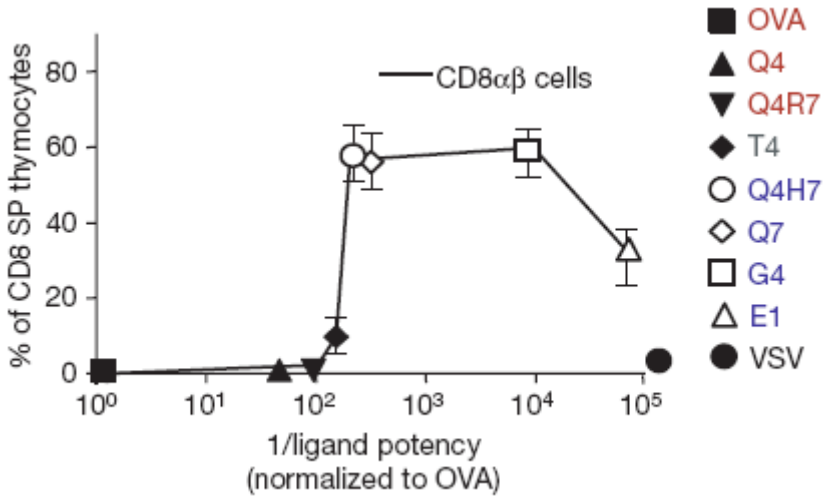

Figure 6.1: APLs for thymic selection Percentage of CD8 single-positive thymocytes generated in FTOC as a function of normalized ligand potency of OT-I system (adapted from Daniels et al. Nature, 2006)[52].

To compare directly among different ligands, binding frequency at each time point was converted to average adhesion bonds $\langle n \rangle = -\ln(1 - P_a)$ and normalized by pMHC density m_l for normalized adhesion bonds (**Figure 6.4**), or fitted by the probabilistic kinetic model $P_a = 1 - \exp[-m_r m_l A_c K_a \{1 - \exp(-k_{off} t_c)\}]$ [1, 41, 73] for effective 2D affinity (**Figure 6.3B**). As expected, normalized adhesion bonds (**Figure 6.4A and B**) and effective 2D affinity (**Figure 6.3B**) of MHC–CD8 measured from VSV ligand were lower than those of the other ligands where OVA showed the strongest normalized adhesion bonds and effective 2D affinity. However, the rest of selecting ligands were non-distinguishable.

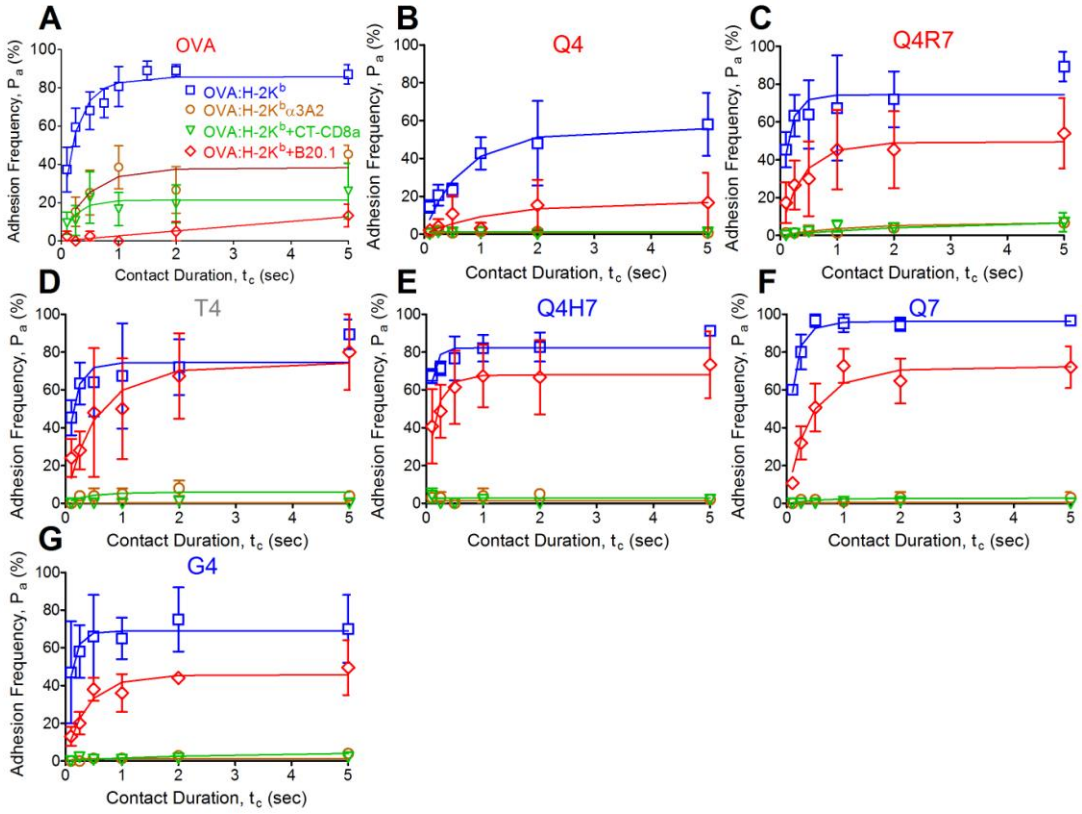

Figure 6.2: Adhesion frequency analysis in thymic selection Adhesion frequency assay for negative and positive selecting ligands were performed for four different conditions: wild-type H-2K^b (blue square), H-2K^b α3A2 (brown circle), wild-type H-2K^b in the presence of CD8 blocking antibody (CT-CD8a, green triangle), and wild-type H-2K^b in the presence of TCR blocking antibody (B20.1, red diamond). Similar level of pMHC density was used to compare measurements for indicated conditions in each ligand. However, the measurements for TCR–pMHC interaction in Q4-G4 (brown circle and green triangle) were not detectable with these pMHC densities. CD8–MHC interaction (red diamond) showed little lower level of binding frequency to the TCR–pMHC–CD8 trimolecular interaction (blue square). Each binding frequency measurement is presented as mean ± SEM (n≥3) for 50 touches each. The data are representatives from three independent experiments.

To measure 2D off-rate of TCR–pMHC interaction, we conducted thermal fluctuation assay with biomembrane force probe (BFP)[84] (**Figure 6.3A**). The slope of bond lifetime distribution yielded 2D off-rate from a first-order dissociation kinetics[1]. Whereas the 2D off-rate correlated inverse to the ligand potency (grey bar, **Figure 6.3C**),

the effective 2D on-rate (white bar, **Figure 6.3C**) tracked with the effective 2D affinity (grey bar, **Figure 6.3B**) both correlating with the ligand potency.

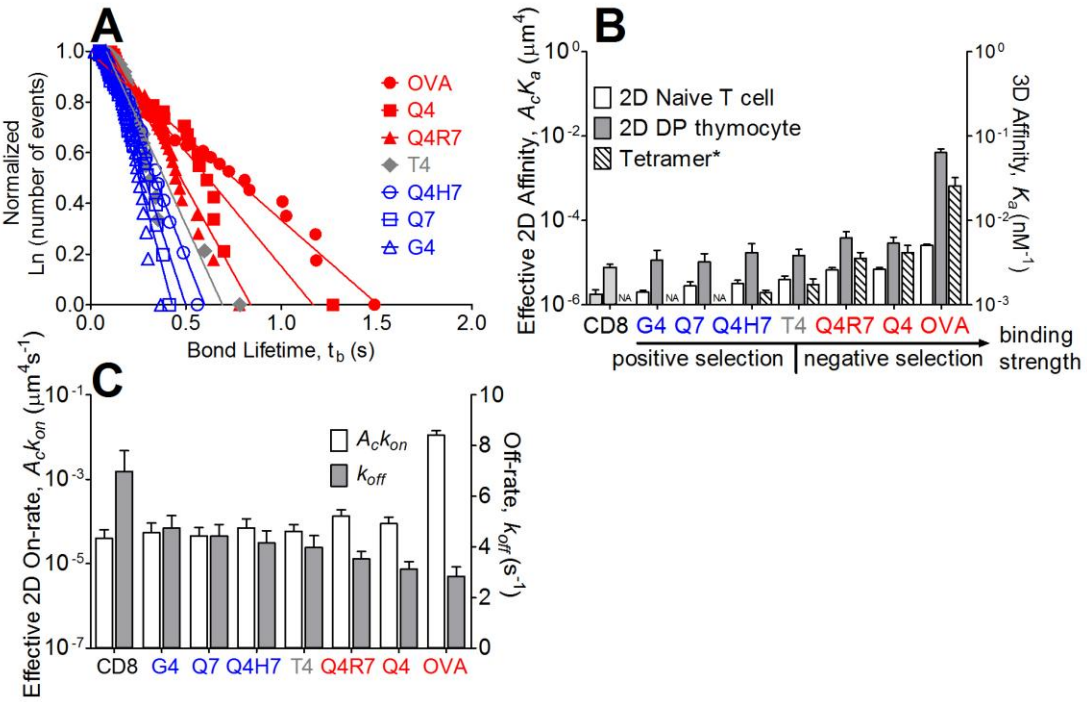

Figure 6.3: Thermal fluctuation assay and 2D kinetics analysis in thymic selection For 2D off-rate of TCR–pMHC interaction, thermal fluctuation assay was conducted with peptides bound to H-2K^b α3A2 (A). From the slope of distribution of bond lifetime, we can yield off-rates using first-order dissociation kinetics[1]. In addition, effective 2D affinities for the selecting ligands in naïve (white bar) and DP thymocytes (grey bar) are derived from adhesion frequency for comparison (B). Previous 3D affinity data (striped bar) using tetramer staining is plotted together for comparison[52]. The measured 2D off-rate and calculated effective 2D on-rate is plotted in bar graph for comparison among selecting ligands (C). Colored letters indicate thymic selection readout: red (negative selection), grey (selection threshold), and blue (positive selection)[52]. The sample size of bond lifetime for each ligand in thermal fluctuation data is listed as following: OVA (n=52), Q4 (n=39), Q4R7 (n=49), T4 (n=26), Q4H7 (n=31), Q7 (n=39), G4 (n=52), and VSV (n=20).Each bar in the effective 2D affinity is presented as mean ± SEM (n≥5).

For TCR–pMHC–CD8 trimolecular interaction, we calculated normalized adhesion bonds[41] by converting the adhesion frequency at the plateau level P_a to average adhesion bonds $\langle n \rangle = -\ln(1 - P_a)$ and normalizing it by pMHC density m_l (white bar,

Figure 6.4B) as well as the sum of normalized TCR–pMHC and MHC–CD8 bonds[73] by multiplying their effective 2D affinities by their respective TCR and CD8 site densities (grey bar, **Figure 6.4B**). The difference between the white and grey bar represents the synergy for the TCR–pMHC–CD8 trimolecular interaction for that ligand (**Figure 6.4C**). The larger the difference, the greater the synergy generated by the TCR–CD8 cooperation for pMHC binding[41]. Weaker ligands generated larger synergy than the strongest ligand OVA but their normalized adhesion bonds had no significant difference (p>0.5, one-way ANOVA). In summary, although the *in situ* 2D measurements were sensitive to detect bimolecular and trimolecular interaction in weaker ligands such as G4 and Q7, the dynamic range was comparable to the 3D measurements[52] (striped bar, **Figure 6.3B and Figure 6.4B**)

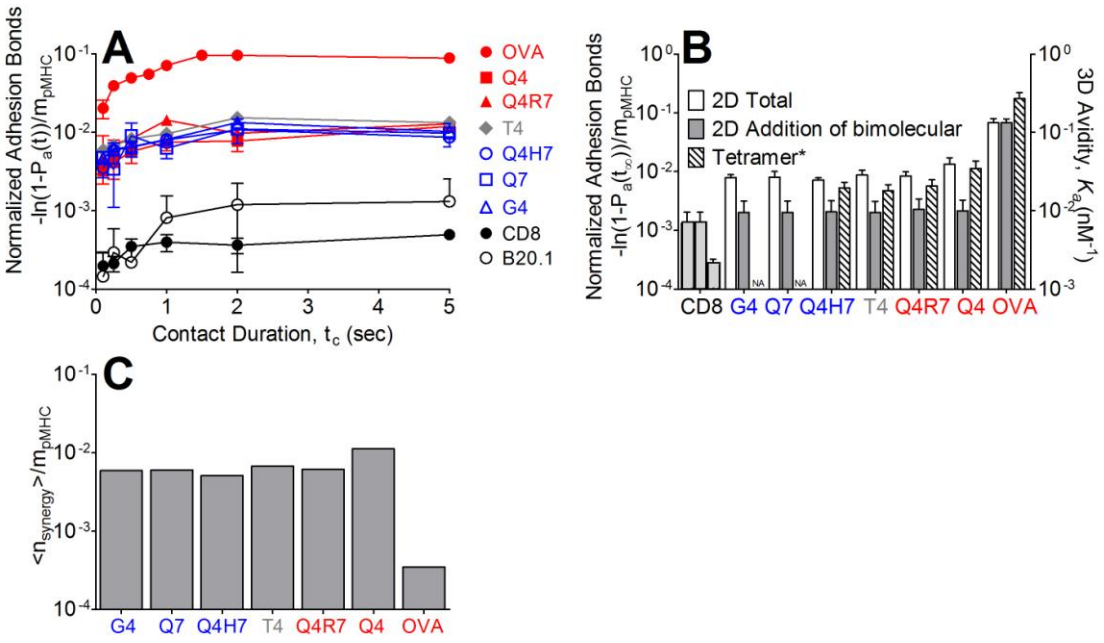

Figure 6.4: Normalized adhesion bonds and synergy analysis in thymic selection For direct comparison among different ligands, adhesion frequency data can be normalized by the pMHC density to yield normalized adhesion bonds. Except OVA, other selecting ligands have no significant difference in the time curve (A) or at the saturation level (white bar, B). To dissect the contribution in bond interactions, normalized adhesion bonds were measured from following conditions: pMHC with H-2K^b (mixture of TCR–pMHC–CD8, TCR–pMHC, and MHC–CD8), pMHC with H-2K^b α3A2 (TCR–pMHC),

and VSV:H-2K^b (MHC–CD8). Assuming these interactions occur independent to each other, $\langle n_{total} \rangle / m_l = \langle n_{TCR-pMHC} \rangle / m_l + \langle n_{CD8-MHC} \rangle / m_l + \langle n_{synergy} \rangle / m_l$[41]. The synergy of CD8 (C) can be calculated from the difference between the white bar and the grey bar from B. Previous 3D avidity data using tetramer staining is plotted together in B for comparison[52]. Colored letters indicate thymic selection readout: red (negative selection), grey (selection threshold), and blue (positive selection)[52]. Each point in the normalized adhesion bonds is presented as mean ± SEM (n≥3). The data are representatives from three independent experiments.

6.2.2 Molecular bond stiffness analysis and force-clamp assay in thymic selection

In addition to the importance of considering TCR–pMHC interaction in a 2D membrane surface, several recent studies have indicated that TCR recognize physical force to activate T-cells[38, 85-88]. For thymocytes, migration (10~20 μm/min) in cortex and medulla microenvironments, and continuous scanning on thymic epithelial cells can possibly exert physical force to TCR–pMHC interaction[5]. In addition, actin polymerization dependent retrograde flow on the cellular membrane may induce force to TCR–pMHC interaction[37, 102, 103].

We therefore first analyzed the molecular bond stiffness from the slope of the ramping phase of bond events in BFP force-clamp assay. The distributions of measured molecular bond stiffness were then fitted to either single or sum of two-Gaussian distributions using least mean square method to find the best parameter for fitting. The data demonstrated two distinct patterns separated by negative and positive selecting ligands. The histogram of molecular bond stiffness of O-T4:H-2K^b fitted well with sum of two-Gaussian distribution (**Figure 6.5A, B, C, and D**) that had constraint $mean_1$=0.17pN/nm and $mean_2$=0.51pN/nm. On the other hand, Q4H7-G4:H-2K^b fitted well with single Gaussian distribution (**Figure 6.5E, F, G, and H**) with a constraint mean=0.17pN/nm. However, when we tested the same analysis in the case of peptides bound to H-2K^b α3A2 the histogram of molecular stiffness for all ligands fitted with single Gaussian distribution (**Figure 6.6**) indicating the rise of the second population (higher stiffness) in negative selecting ligands is CD8 dependent.

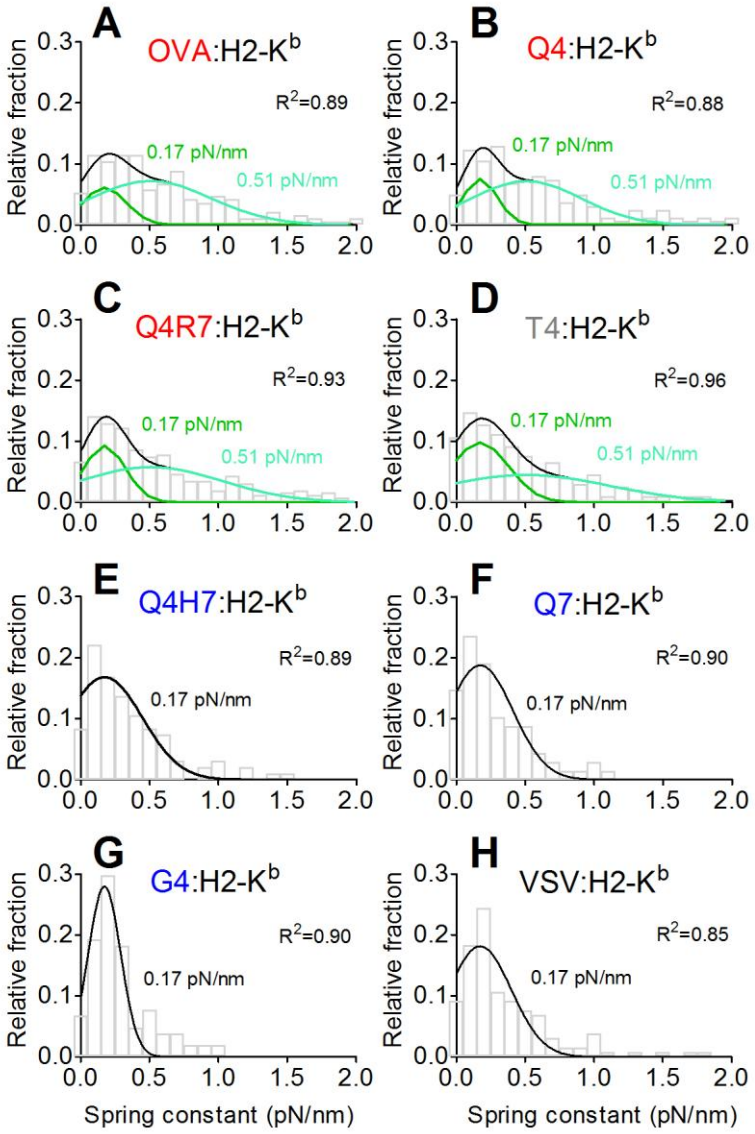

Figure 6.5: Molecular bond stiffness analysis in thymic selection with H-2K^{b}The molecular bond stiffness from the slope of the ramping phase of bond events in BFP force-clamp assay was collected for histogram analysis. The data fitted to either single or sum of two-Gaussian distributions using least mean square method to find the best parameter for fitting. Negative selecting ligands (OVA-T4) fitted well with sum of two-Gaussian distribution with constraint mean$_1$=0.17pN/nm and mean$_2$=0.51pN/nm, whereas positive selecting ligands (Q4H7-G4) and irrelevant ligand (VSV) fitted well with single Gaussian distribution with a constraint mean=0.17pN/nm. Goodness of fit for each fitting is calculated in R^2. Colored letters indicate thymic selection readout: red (negative selection), grey (selection threshold), and blue (positive selection)[52]. The sample size of

bond lifetime for each ligand is listed as following: OVA (n=192), Q4 (n=162), Q4R7 (n=254), T4 (n=197), Q4H7 (n=95), Q7 (n=68), G4 (n=104), and VSV (n=131).

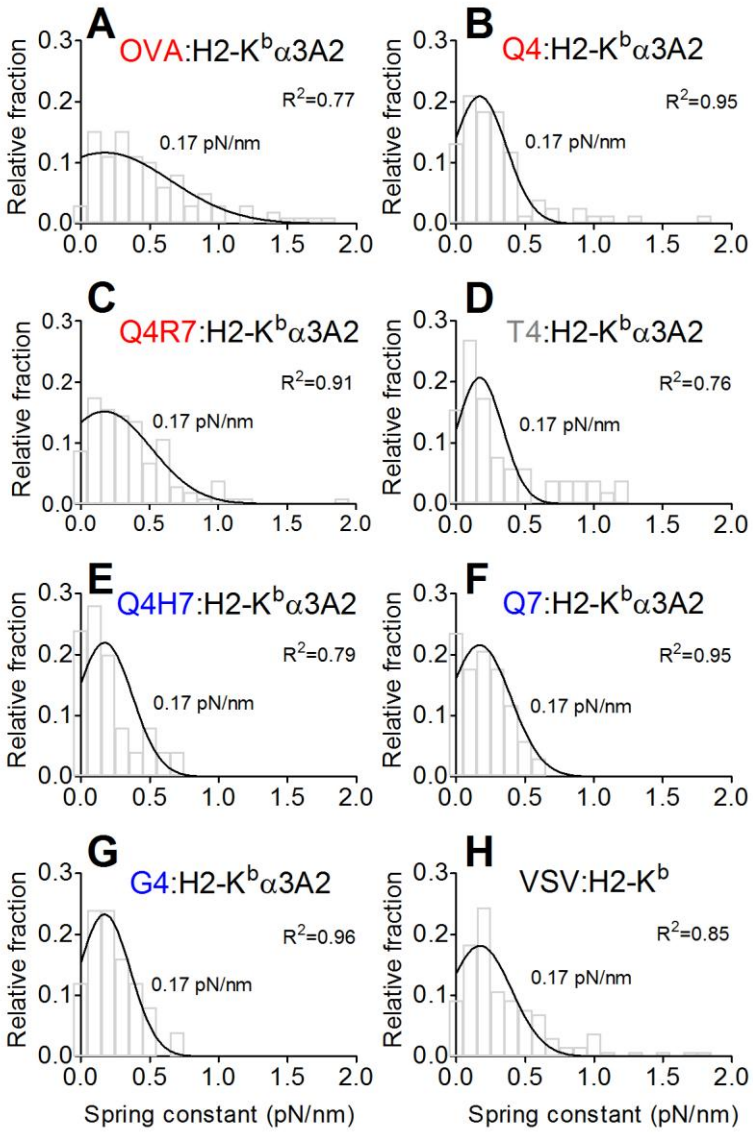

Figure 6.6: Molecular bond stiffness analysis in thymic selection with H-2K^b α3A2 In the case of neglecting CD8 binding to MHC by using H-2K^b α3A2, the stiffness histogram of all ligands fitted well with single Gaussian distribution with a constraint mean=0.17pN/nm. Goodness of fit for each fitting is calculated in R^2. Colored letters indicate thymic selection readout: red (negative selection), grey (selection threshold), and blue (positive selection)[52]. The sample size of bond lifetime for each ligand is listed as following: OVA (n=99), Q4 (n=76), Q4R7 (n=98), T4 (n=52), Q4H7 (n=25), Q7 (n=34), and G4 (n=25).

In the cases of two Gaussian fitting ligands with H-2K^b, the fraction of two Gaussian distributions can be calculated to show increase in the fraction of the second (higher stiffness or synergy) population as the negative selecting power gets stronger (**Figure 6.7A**). Also average of bond stiffness showed stiffer spring constant for negative selecting ligands with H-2K^b ("total", grey bar, **Figure 6.7B).** With knowing the fraction of synergistic TCR–pMHC–CD8 interaction and normalized adhesion bonds for TCR–pMHC and CD8–MHC from adhesion frequency assay, we were able to calculate the stiffness of synergistic TCR–pMHC–CD8 interaction ($k_{synergy}$) to be around 0.6pN/nm (striped bar, **Figure 6.7B**).

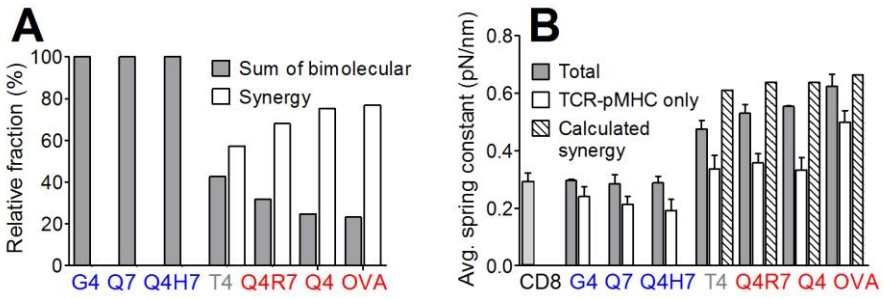

Figure 6.7: Fraction of synergy and average spring constant analysis in thymic selection The fraction of synergistic TCR–pMHC–CD8 interaction from stiffness analysis (A) and the average of molecular bond stiffness (B) are plotted for comparison in selecting ligands. Assuming bond interactions occur independent to each other, $\langle k_{total} \rangle$ = <fraction of mean$_1$ distribution in stiffness histogram>($\langle k_{TCR–pMHC} \rangle \langle n_{TCR–pMHC} \rangle_{ratio}/m_l$ + $\langle k_{CD8–MHC} \rangle \langle n_{CD8–MHC} \rangle_{ratio}/m_l$) + <fraction of mean$_2$ distribution in stiffness histogram>$\langle k_{synergy} \rangle$. With knowing the fraction of synergistic TCR–pMHC–CD8 interaction and normalized adhesion bonds for TCR–pMHC and CD8–MHC from adhesion frequency assay, $k_{synergy}$ is calculated (striped bar). Colored letters indicate thymic selection readout: red (negative selection), grey (selection threshold), and blue (positive selection)[52].

Next, we measured force-lifetime relationships in thymic selection using force-clamp assay[75, 76]. Like stiffness analysis, the result showed a selection-dependent characteristic. For TCR–pMHC–CD8 total interaction with H-2K^b, negative selecting

ligands (OVA-T4) formed catch-slip bonds where lifetime first increased, reached a maximum around 13pN, then decreased with increasing force (green square, **Figure 6.8A, B, C, and D**). If tested with H-2K^b α3A2 that only allowed TCR–pMHC bimolecular interaction, the catch-slip bond phenomenon was weakened for negative selecting ligands (brown circle, **Figure 6.8A, B, C, and D**) indicating the importance of CD8 for these ligands. In addition, most distinct ligand separation was observed in lifetime distribution in the 10-15pN regime which includes the maximum peak. In sharp contrast, positive selecting ligands (Q4H7-G4) presented by whether H-2K^b (total) or H-2K^b α3A2 (TCR–pMHC) formed slip bonds where lifetime was shortened by force (**Figure 6.8**), suggesting this type of force-dependent dissociation characteristics is important for peripheral exportation.

In fact, the lifetime measured with H-2K^b (total) include contributions from two bimolecular interactions, TCR–pMHC and CD8–MHC, and a synergistic TCR–pMHC–CD8 interaction: $\langle t_{total} \rangle$ = <fraction of mean$_1$ distribution in stiffness histogram>($\langle t_{TCR-pMHC} \rangle \langle n_{TCR-pMHC} \rangle_{ratio}/m_l$ + $\langle t_{CD8-MHC} \rangle \langle n_{CD8-MHC} \rangle_{ratio}/m_l$) + <fraction of mean$_2$ distribution in stiffness histogram>$\langle t_{synergy} \rangle$. Knowing the fraction of sum of bimolecular interactions and synergy, and normalized adhesion bonds from adhesion frequency assay, we can calculate lifetime of synergistic TCR–pMHC–CD8 interaction. Indeed, it shows a catch-slip bond for the negative selecting ligands (purple dash-line, **Figure 6.8A, B, C, and D**). To further support it is synergistic TCR–pMHC–CD8 interaction that derive catch-slip bond, only the bond lifetime events that had stiffness larger than the mean$_2$=0.51pN/nm from stiffness analysis were analyzed for force-lifetime relationship (orange diamond, **Figure 6.8**). Likewise, these events showed catch-slip bonds in negative selecting ligands but not in positive selecting ligands. Whereas the synergy in normalized adhesion bonds had no distinguishing power under zero-force, under force the synergistic TCR–pMHC–CD8 interaction was crucial for catch-slip behavior in negative selecting ligands (Q4, Q4R7 and T4).

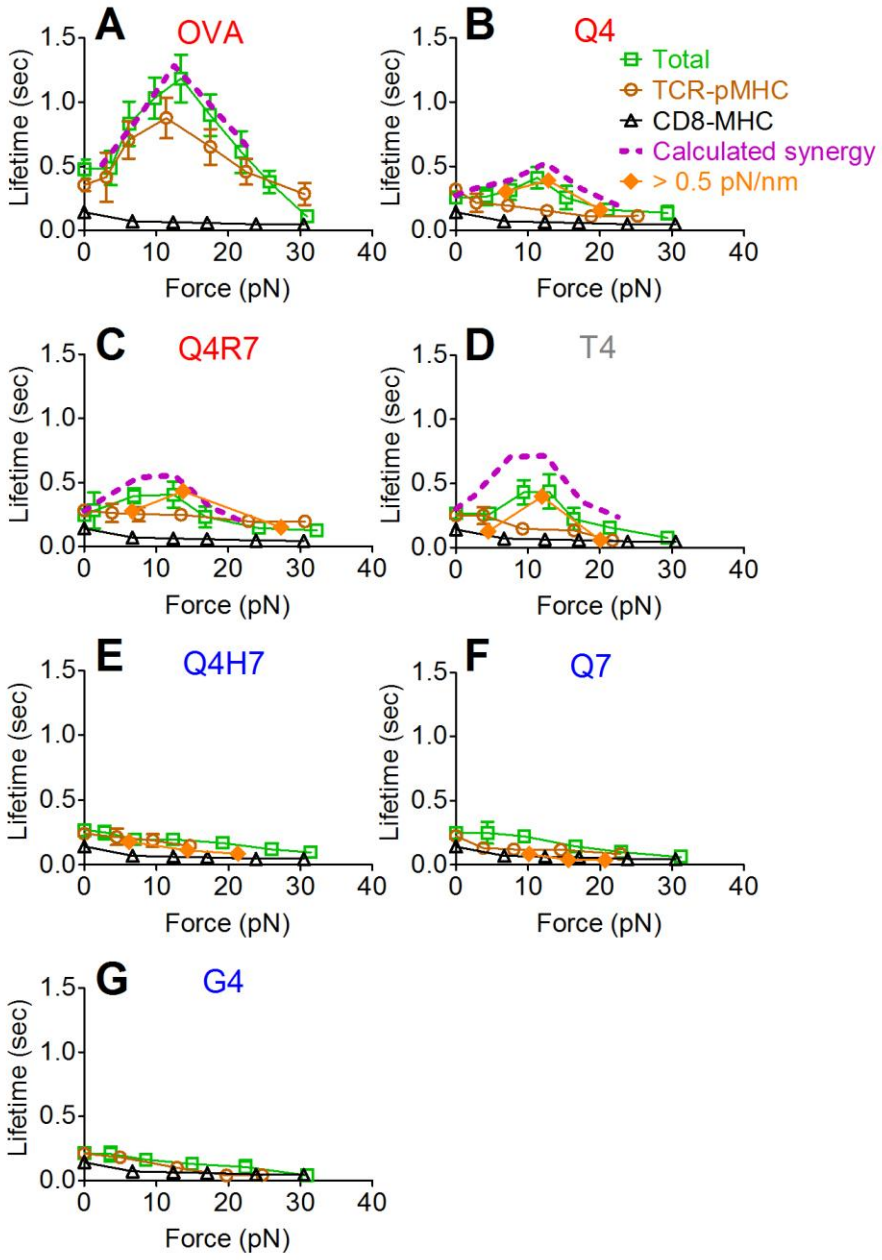

Figure 6.8: Force-lifetime analysis in thymic selection For TCR–pMHC–CD8 total interaction with H-2K^b (green square), negative selecting ligands (OVA-T4) formed catch-slip bonds whereas positive selecting ligands (Q4H7-G4) yielded slip bonds. However, in the case of Q4, Q4R7 and T4, both TCR–pMHC interaction with H-2K^b α3A2 (brown circle) and CD8–MHC interaction with VSV:H-2K^b (black triangle) only demonstrated slip bonds. Assuming these interactions are independent, $\langle t_{total} \rangle$ = <fraction of mean$_1$ distribution in stiffness histogram>($\langle t_{TCR-pMHC} \rangle \langle n_{TCR-pMHC} \rangle_{ratio}/m_l$ + $\langle t_{CD8-MHC} \rangle \langle n_{CD8-MHC} \rangle_{ratio}/m_l$) + <fraction of mean$_2$ distribution in stiffness histogram>$\langle t_{synergy} \rangle$. With previously calculated fraction of sum of bimolecular interactions and synergy, and normalized adhesion bonds from adhesion frequency assay,

we can calculate lifetime of synergistic TCR–pMHC–CD8 interaction (purple dash-line). To further test the contribution of synergistic TCR–pMHC–CD8 interaction, selective analysis with bond events with >0.51pN/nm showed catch-slip bonds for negative selecting ligands but not with positive selecting ligands. Colored letters indicate thymic selection readout: red (negative selection), grey (selection threshold), and blue (positive selection)[52]. The sample size for each ligand is listed as following: OVA:H-2K^b (n=707), OVA:H-2K^b α3A2 (n=375), Q4:H-2K^b (n=506), Q4:H-2K^b α3A2 (n=214), Q4R7:H-2K^b (n=694), Q4R7:H-2K^b α3A2 (n=367), T4:H-2K^b (n=620), T4:H-2K^b α3A2 (n=109), Q4H7:H-2K^b (n=460), Q4H7:H-2K^b α3A2 (n=104), Q7:H-2K^b (n=401), Q7:H-2K^b α3A2 (n=154), G4:H-2K^b (n=157), G4:H-2K^b α3A2 (n=118), and VSV:H-2K^b (n=112).

In order to investigate more on the effect of force-prolonged bond lifetime, we separated the lifetime events into different force regimes (0-5, 5-10, 10-15, and 15-20pN) and plotted normalized bond lifetime distributions (**Figure 6.9**). This analysis allows comparison of number of bonds that can survive at certain bond lifetime. For instance, in 0-5pN regime the trend of number of bond survival for the tested pMHCs show similar behavior (**Figure 6.9A**), but starting from 5-10pN regime negative ligands show longer survival than positive selecting ligands (**Figure 6.9B**). This trend of survival separation reaches peak at 10-15pN regime where all the negative selecting ligands show significant amount of bond survival even longer than 2s (**Figure 6.9C**). After reaching 10-15pN, the 15-20pN regime shows less discrete separation in the number of bond survival due to drop of Q4, Q4R7 and T4 (**Figure 6.9D**). The same analysis with H-2K^b α3A2 (**Figure 6.9E, F, G, and H**) showed overall similar trend to H-2K^b but the discrete separation of positive and negative selecting ligands was more obvious in 10-15pN of H-2K^b. These results indicate force-prolonged bond lifetime increases the bond survival separation between positive and negative selecting ligands.

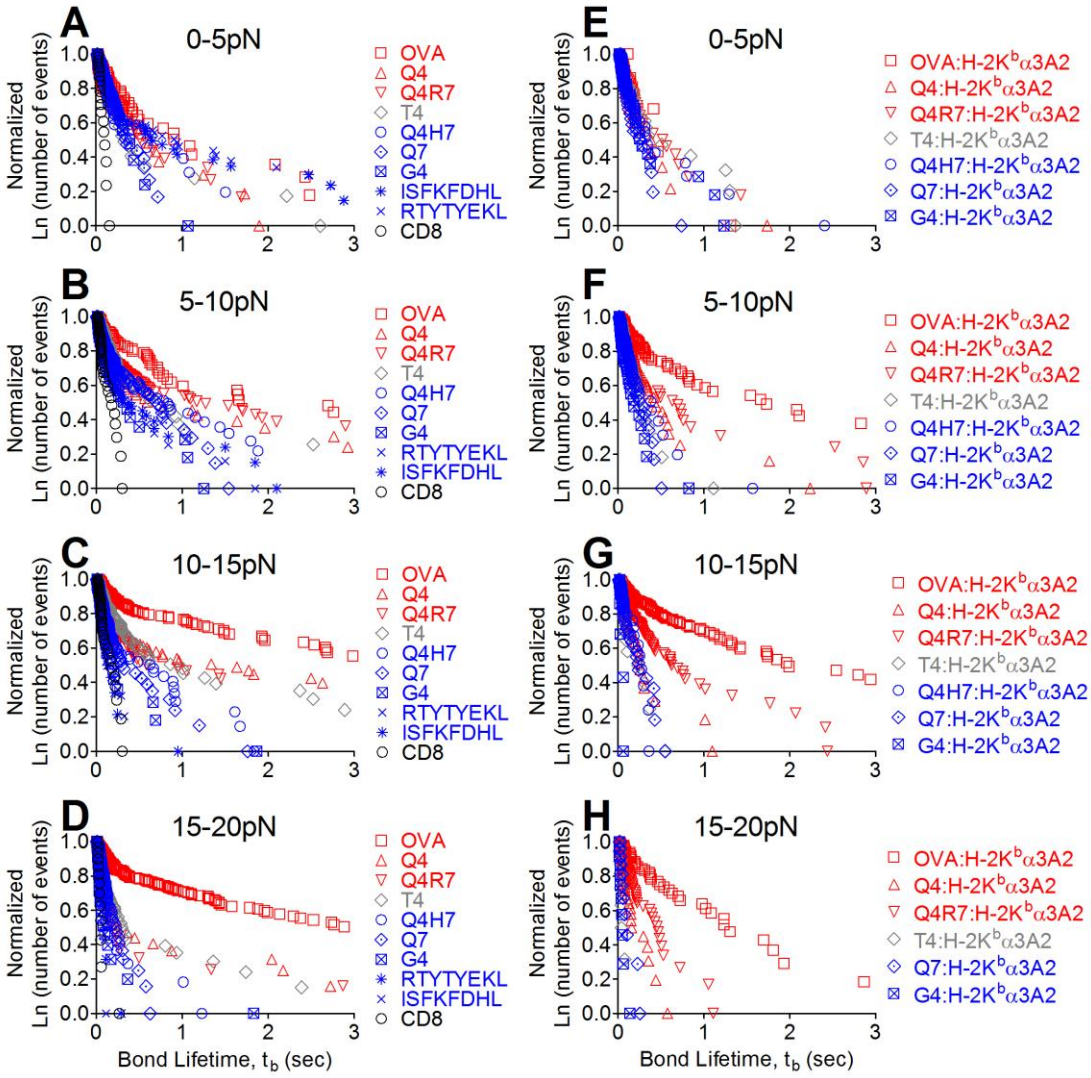

Figure 6.9: Normalized bond lifetime distribution of pMHCs with H-2K^b and H-2K^b α3A2 Normalized bond lifetime distributions are plotted in different force regimes (0-5, 5-10, 10-15, and 15-20pN). This allows comparison of number of bonds that can survive at certain bond lifetime in selecting ligands. As force increases (A, B, C, and D) in H-2K^b condition, the separation in the survival trend of selecting ligands are observed most discrete in 10-15pN (C). On the other hand, with H-2K^b α3A2 the separation is not so obvious (E, F, G, and H). Colored letters indicate thymic selection readout: red (negative selection), grey (selection threshold), and blue (positive selection)[52]. The sample size for each ligand is listed as following: OVA:H-2K^b (n=707), OVA:H-2K^b α3A2 (n=375), Q4:H-2K^b (n=506), Q4:H-2K^b α3A2 (n=214), Q4R7:H-2K^b (n=694), Q4R7:H-2K^b α3A2 (n=367), T4:H-2K^b (n=620), T4:H-2K^b α3A2 (n=109), Q4H7:H-2K^b (n=460), Q4H7:H-2K^b α3A2 (n=104), Q7:H-2K^b (n=401), Q7:H-2K^b α3A2 (n=154), G4:H-2K^b (n=157), G4:H-2K^b α3A2 (n=118), and VSV:H-2K^b (n=112).

For further analysis in this regard, we calculated the difference of Q4R7:H-2K^b and Q4H7:H-2K^b of the number of bonds that survived 4s lifetime. We chose 4s as a conservative time point for initiation of signaling after TCR stimulation from previous research where LAT phosphorylation was observed in 4s after stimulation[10, 104]. The calculation show that indeed at 10-15pN ΔQ4R7-QH7 had three-times more bond number than that of other force regimes (**Figure 6.10A**).

In addition, bond lifetime distribution can be fitted with two-state model[76, 105] for analysis of short-lived state and long-lived state. To investigate the contribution of long-lived states, we plotted the average spring constant (**Figure 6.10B**) and force-lifetime relationship (**Figure 6.10C**) with long-lived state only for Q4R7, T4 and Q4H7. For Q4R7 and T4, average spring constant showed 0.6pN/nm and catch-slip bonds whereas Q4H7 showed 0.2pN/nm and slip bonds. These measurements and trends in force-lifetime relationship coincide with the synergistic TCR–pMHC–CD8 interaction observed earlier. Furthermore, probability can be calculated for the percentage of events that had stiff bond with long lifetime. The probability of stiffer and long lifetime events out of total stiffer events can be calculated by P(long LT | high stiff) = P(high stiff | long LT) × P(long LT) / P(high stiff). Also, the probability of stiffer and long lifetime bonds out of total events can be calculated by P(high stiff | long LT) × P(long LT). The result show that both of the probabilities positively correlate to the power of the negative selection (**Figure 6.10D**). This further support the idea that force-induced synergistic TCR–pMHC–CD8 interaction gives rise to longer bond lifetime in negative selecting ligands.

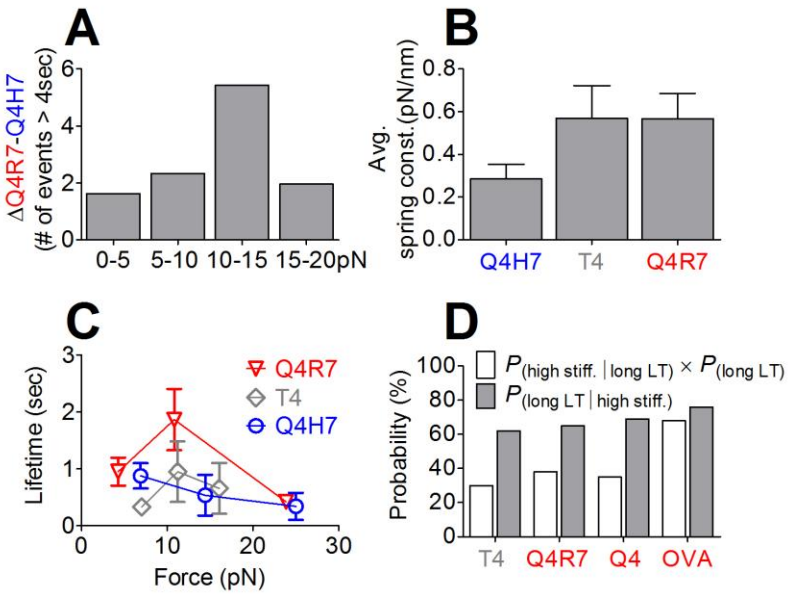

Figure 6.10: Other analyses in thymic selection The difference of Q4R7:H-2K^b and Q4H7:H-2K^b of number of bonds (ΔQ4R7-QH7) that survived 4s lifetime showed three-times more bond number at 10-15pN regime than that of other force regimes (A). Fitting the bond lifetime distribution with two-state model allowed the analysis of long-lived states for average spring constant (B) and force-lifetime relationship (C). Lastly, probabilities are calculated for the percentage of events that had stiff bond with long lifetime. Colored letters indicate thymic selection readout: red (negative selection), grey (selection threshold), and blue (positive selection)[52].

Further to answer how force contributes to the power of ligand discrimination, we plotted bond lifetime ratio of OVA/other peptide vs. force (**Figure 6.11**). In the presence of CD8, the analyses for negative selecting ligands (warm colors) and positive selecting ligands (cold colors) showed drastic discrimination with the highest separation occurring at 10-15pN regime. The difference in the ratio between negative and positive selecting ligands was 3 to 4 times at this force regime. However, in the absence of CD8 the ligand separation was not observed which further indicates that CD8 cooperativity under force is critical for ligand discrimination in thymic selection.

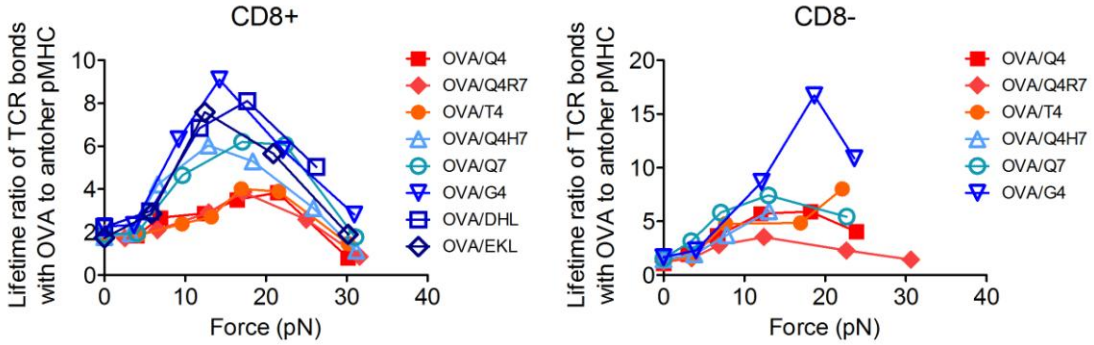

Figure 6.11: Bond lifetime ratio of TCR bonds with OVA to anther pMHC vs. force analysis of OT-I system The ratio of bond lifetime of OVA/other pMHC vs. force show increase power of ligand discrimination. The negative and positive selecting ligand show discrete separation in the presence of CD8 (A). However, in the absence of CD8, the strong separation of the ratio is not observed anymore (B). The data points from force vs. bond lifetime (**Figure 6.8**) were used to calculate the ratio.

6.2.3 Verification of force regulation effect in thymic selection

In order to test our findings in more physiologic condition, endogenous ligands that have been identified previously to give positive selection in FTOC were tested in force-clamp assay. These results were further supportive to our findings as slip bonds were observed in endogenous positive selecting ligands, $Catnb_{329\text{-}336}$ (β-catenin, RTYTYEKL) and $Capp1_{92\text{-}99}$ (F-actin capping protein A, ISFKFDHL)[67, 68]. When comparing endogenous peptides only, the difference in the force-regulated dissociation characteristics was more distinct between negative (OVA) and positive (RTYTYEKL and ISFKFDHL) selecting ligands (**Figure 6.12**).

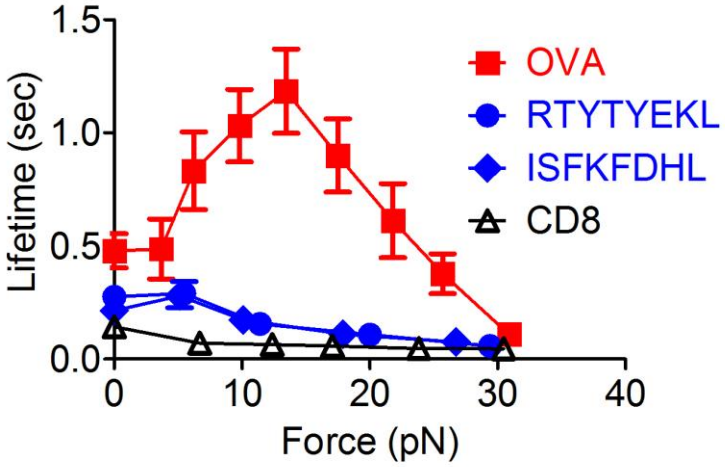

Figure 6.12: Force-lifetime analysis for endogenous ligands in thymic selection Consistent with our previous finding, endogenous positive selecting ligands show slip bonds. Colored letters indicate thymic selection readout: red (negative selection) and blue (positive selection)[52]. The sample size for each ligand is listed as following: OVA:H-2K^{b} (n=707), RTYTYEKL:H-2K^{b} (n=230), ISFKFDHL:H-2K^{b} (n=242), and VSV:H-2K^{b} (n=112).

To further verify our observation in an alternative TCR system, 2C TCR system was tested with negative selecting ligands, SIYR:H-2K^{b} and dEV8:H-2K^{bm3}, and positive selecting endogenous ligands, dEV8:H-2K^{b}, EVSV:H-2K^{b}, and p2Ca:H-2K^{b} [35, 70-72]. Results from stiffness analysis, force-lifetime relationship, and bond lifetime distribution further supported our findings: the two negative selecting ligands showed CD8-dependent stiffer population in stiffness histogram (**Figure 6.13A, B, and G**) and catch-slip bond in force-lifetime relationship (**Figure 6.14A and D**) whereas the three positive selecting ligands showed no observation of stiffer population (**Figure 6.13C, D, E, F, and H**) and slip bond in force-lifetime relationship (**Figure 6.14B, C, and D**). Consistent with OT-I system, normalized bond lifetime distribution of 2C system showed discrete separation of negative and positive ligands at 10-15pN regime and the discrimination power dropped when neglecting CD8 contribution (**Figure 6.15**).

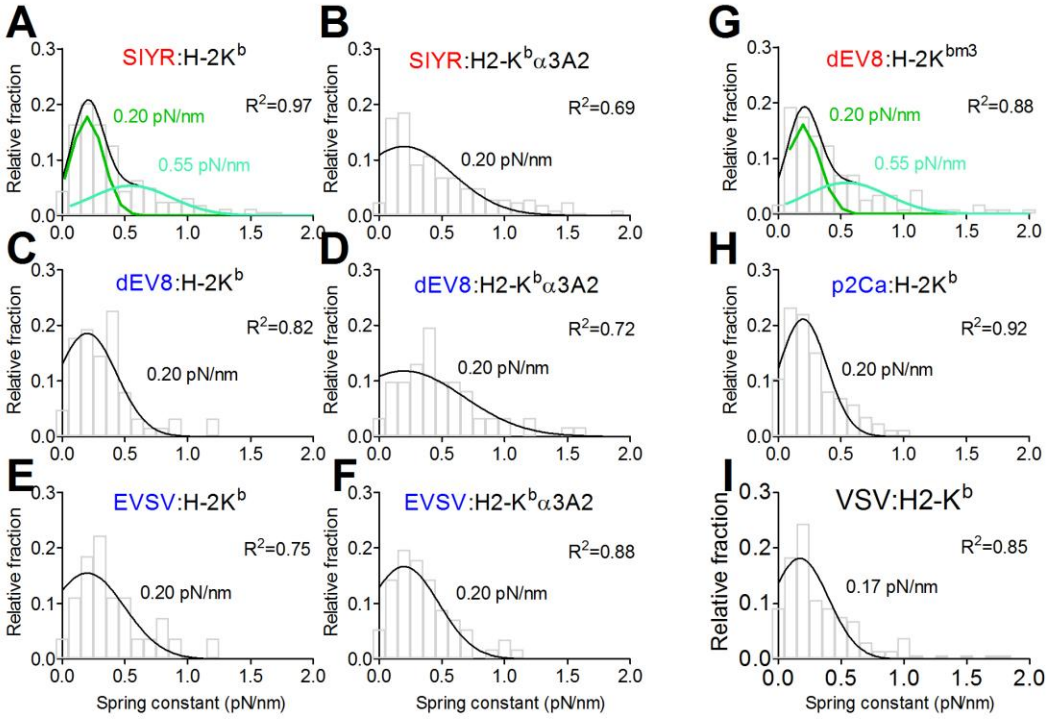

Figure 6.13: Molecular bond stiffness analysis in 2C system The molecular bond stiffness from the slope of the ramping phase of bond events in BFP force-clamp assay was collected for histogram analysis. The data fitted to either single or sum of two-Gaussian distributions using least mean square method to find the best parameter for fitting. Negative selecting ligands (SIYR and dEV8:H-2K^{bm3}) fitted well with sum of two-Gaussian distribution with constraint mean$_1$=0.20pN/nm and mean$_2$=0.55pN/nm (A and G), whereas positive selecting ligands (dEV8, EVSV, and p2Ca) (C, D, and H) and irrelevant ligand (VSV) (I) fitted well with single Gaussian distribution with a constraint mean. Goodness of fit for each fitting is calculated in R^2. In the case of neglecting CD8 binding to MHC by using H-2K^b α3A2 (B, D, and F), the stiffness histogram of all ligands fitted well with single Gaussian distribution with a constraint mean=0.20pN/nm. Goodness of fit for each fitting is calculated in R^2. Colored letters indicate thymic selection readout: red (negative selection) and blue (positive selection)[35, 70-72]. The sample size of bond lifetime for each ligand is listed as following: SIYR:H-2K^b (n=158), SIYR:H-2K^b α3A2 (n=205), dEV8:H-2K^b (n=62), dEV8:H-2K^b α3A2 (n=61), EVSV:H-2K^b (n=27), EVSV:H-2K^b α3A2 (n=56), dEV8:H-2K^{bm3} (n=114), p2Ca:H-2K^b (n=86), and VSV (n=131).

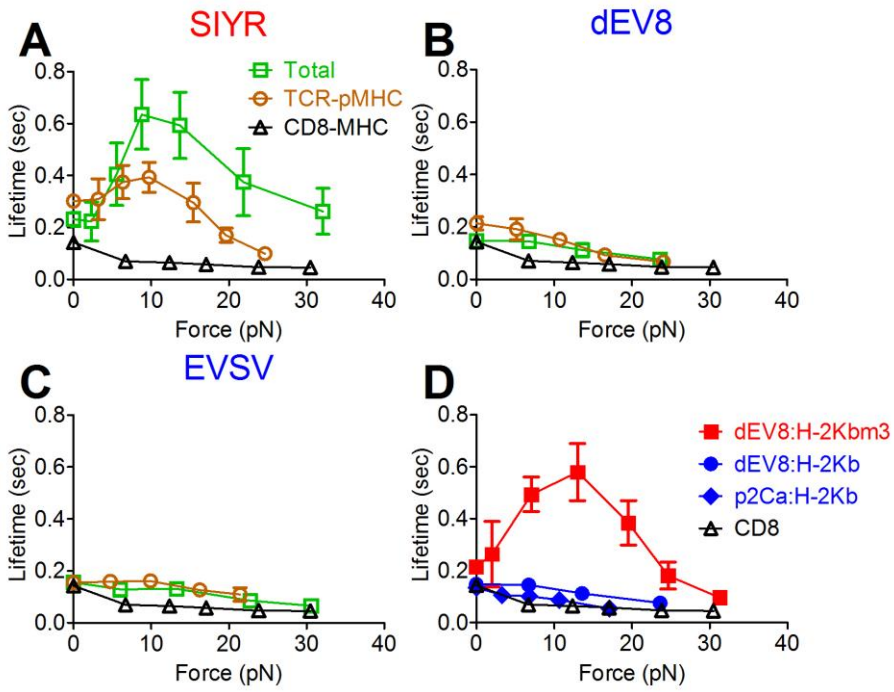

Figure 6.14: Force-lifetime analysis in 2C system For TCR–pMHC–CD8 total interaction (green square), negative selecting ligands (SIYR and dEV8:H-2K^{bm3}) formed catch-slip bonds whereas positive selecting ligands (dEV8, EVSV, and p2Ca) yielded slip bonds. The trend was similar in TCR–pMHC interaction (brown circle). Colored letters indicate thymic selection readout: red (negative selection) and blue (positive selection)[35, 70-72]. The sample size of bond lifetime for each ligand is listed as following: SIYR:H-2K^{b} (n=360), SIYR:H-2K^{b} α3A2 (n=363), dEV8:H-2K^{b} (n=184), dEV8:H-2K^{b} α3A2 (n=187), EVSV:H-2K^{b} (n=187), EVSV:H-2K^{b} α3A2 (n=187), dEV8:H-2K^{bm3} (n=402), p2Ca:H-2K^{b} (n=151), and VSV (n=112).

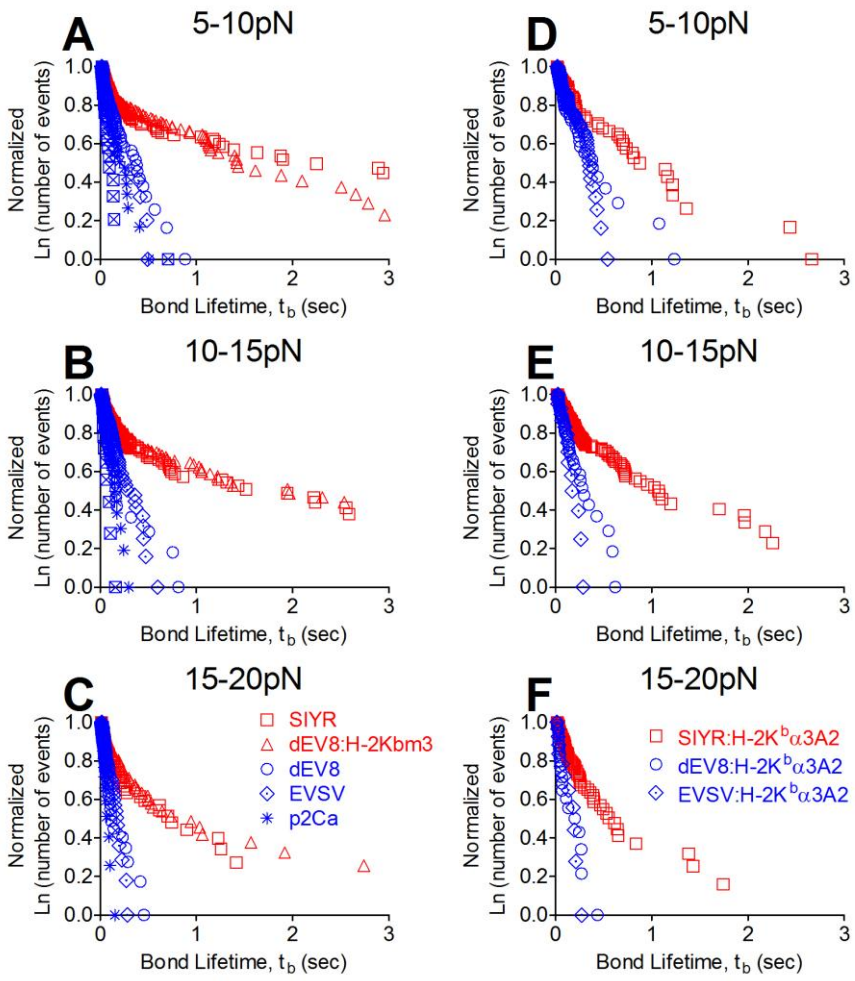

Figure 6.15: Normalized bond lifetime distribution of pMHCs in 2C system To compare number of bonds that survive certain lifetime, normalized bond lifetime distributions are plotted in different force regimes (0-5, 5-10, and 10-15). The separation in the survival trend between the selecting ligands is observed as increasing force (A, C, and C). With H-2K^b α3A2, the separation is still present but in lower power than H-2K^b (D, E, and F). Colored letters indicate thymic selection readout: red (negative selection) and blue (positive selection)[35, 70-72]. The sample size of bond lifetime for each ligand is listed as following: SIYR:H-2K^b (n=360), SIYR:H-2K^b α3A2 (n=363), dEV8:H-2K^b (n=184), dEV8:H-2K^b α3A2 (n=187), EVSV:H-2K^b (n=187), EVSV:H-2K^b α3A2 (n=187), dEV8:H-2K^{bm3} (n=402), p2Ca:H-2K^b (n=151), and VSV (n=112).

6.3 Discussion

In this chapter, 2D kinetics that previously showed better sensitivity than the 3D[1, 42] was determined for thymic selection. However, neither the effective 2D affinity for

TCR–pMHC bimolecular interaction nor the normalized adhesion bonds or synergy for TCR–pMHC–CD8 trimolecular interaction showed sufficient differences among negative and positive selecting ligands that induce drastically different fates in T-cells. However, when force was applied to TCR–pMHC–CD8 interaction two distinct patterns emerged on bond stiffness histogram and force-dependent dissociation characteristics. For both engineered and endogenous peptides, negative selecting ligands had synergistic TCR–pMHC–CD8 interaction that formed catch-slip bonds whereas positive selecting ligands did not have that population only to form slip-only bonds (summarized in **Table 4**).

Table 4: Summary of OT-I and 2C system

System	Ligands	TCR↑ MHC↓ ↓ ↓ ↑ ↓ ↑ ↑ ↓ 1 2 3 4 5 6 7 8	T cell response	Thymic selection	Force-lifetime	Lifetime @ 10-15pN (s)
OT-I	$OVA_{257-264}$:H-$2K^b$	S I I N F E K L	Agonist	Negative	Catch-slip	1.18
	Q4:H-$2K^b$	S I I Q F E K L	Weak agonist	Negative	Catch-slip	0.41
	Q4R7:H-$2K^b$	S I I Q F E R L	Weak agonist	Negative	Catch-slip	0.40
	T4:H-$2K^b$	S I I T F E K L	Weak agonist	Minimal Negative	Catch-slip	0.43
	Q4H7:H-$2K^b$	S I I Q F E H L	Weak agonist	Positive	Slip	0.20
	Q7:H-$2K^b$	S I I N F E Q L	Weak agonist	Positive	Slip	0.15
	G4:H-$2K^b$	S I I G F E K L	Weak ag. / antag.	Positive	Slip	0.13
	$Capp1_{92-99}$:H-$2K^b$	I S F K F D H L	Null	Positive	Slip	0.17
	$Catnb_{329-336}$:H-$2K^b$	R T Y T Y E K L	Null	Positive	Slip	0.15
	VSV:H-$2K^b$	R G Y V Y Q G L	Null	Null	Slip	0.06
2C	SIYR:H-$2K^b$	S I Y R Y Y G L	Super agonist	Negative	Catch-slip	0.64
	dEV8:H-$2K^{bm3}$	E Q Y K F Y S V	Agonist	Negative	Catch-slip	0.58
	dEV8:H-$2K^b$	E Q Y K F Y S V	Weak agonist	Positive	Slip	0.11
	EVSV:H-$2K^b$	R G Y V Y Q E L	Antagonist	Positive	Slip	0.13
	p2Ca:H-$2K^b$	L S P F P F D L	Null	Positive	Slip	0.09

Mechanosensing behavior of TCR has been previously reported. Judokusumo et al.[86] showed a positive correlation of IL-2 production of naïve T cells with

polyacrylamide gel substrate stiffness. Kim et al.[53] reported 50pN of tangential force on CD3 induced by optical trap could influx calcium for T cell activation. Li et al.[87] reported shear and pulling force on CD3 complex using micropipette could influx calcium. In addition, some evidence even argue that upon TCR engagement force is generated[85]. Recently catch bond observed in antigen-specific TCR–pMHC interaction has been demonstrated to trigger T-cell signaling (Liu and Chen et al. accepted to Cell). Our conclusion from this chapter further supports the importance of force-regulated TCR–pMHC bond interaction for thymic selection.

Other than our observation, the counter-intuitive characteristic of catch bonds are observed in number of biological systems: P-selectin[106], L-selectin[107], bacterial adhesive protein FimH[108], integrins[76, 109], platelet GP1b[110], actin[111], and TCR (Liu and Chen et al. in press). Although specific detail of molecular mechanism of this behavior is still not fully understood, some models based on molecular dynamic simulation has been proposed to understand physiologic relevance[112]. In this regard, our finding of catch-slip bond in negative selecting ligands opens question for molecular mechanism and biological relevance. It could be possible that force with negative selecting ligands may increase bond lifetime to induce phosphotase segregation on the contact surface for favoring kinase activity ("kinetic segregation model")[113] and/or it may alter conformation of TCR-CD3 complex for access of Lck to the ITAMs[57]. Other possibility is that the force could alter membrane surface for actin remodeling that is required for initiation of full TCR signaling[114]. On the other hand, force on positive selecting ligands may only give sufficient bond lifetime for survival signaling.

In fact, two-photon microscopy study on thymocyte migration in medulla eludes some connection with single bond lifetime and cellular migration[115]. In the presence of a negative selecting ligand, thymocytes slowed down, became confined to a region of 30μm in diameter where they had increased contact with surrounding dendritic cells[115]. Considering our findings, it is possible that the reduction of the speed of thymocytes and

confinement area could be due to prolonged bond lifetime due to force regulation. More related study is necessary for further understanding.

We know in force-free condition, CD8 on a naïve T-cell binds to TCR–pMHC cooperatively with 1s delay in a Srk kinase dependent way[41]. However, in DP thymocytes, CD8 cooperativity was observed as early as the shortest contact time tested (0.1s) but still in a signaling dependent manner as it was eliminated by the Src kinase inhibitor PP2. In addition, CD8 in DP thymocytes binds higher affinity to MHC-I possibly because of developmentally programmed O-glycan modification controlled by ST3Gal-I sialyltransferase[96, 97]. Also, regions for CD8 association to TCR (such as CD3δ and α-CPM[59]) were identified to be critical in positive selection[58]. Based on these and our findings of CD8-dependent synergistic effect in force-regulated bond lifetime, we can imagine CD8 plays a critical role in thymic selection. It is plausible to propose the dominant expression level and early cooperativity of CD8 in thymocyte membrane can contribute significantly to the binding of self-pMHC, possibly acting as decision maker under force where newly binding sites are available to enhance strong binding for initiation of signaling events for negative selecting ligands but no such effect for positive selecting ligands. More careful experiments are necessary to test this hypothesis and to understand the mechanism.

The study in this chapter showed a novel observation in characterizing and quantifying the TCR–pMHC interaction in thymic selection. We were able to characterize CD8-dependent synergistic TCR–pMHC–CD8 interaction under force for negative selecting ligands but not for positive selecting ligands. The findings of force-regulation on TCR–pMHC interaction provide new conceptual advance in thymic selection.

CHAPTER 7 CONCLUSIONS AND FUTURE DIRECTIONS

In this thesis, we showed that co-receptor and force regulated 2D TCR-pMHC interaction determine T cell function. We have tested two systems to show in the absence or presence of force what parameters influence the ligand discrimination for T cell activation or thymic selection. Using ultrasensitive 2D mechanical assays, *in situ* 2D kinetic measurements showed better sensitivity than the SPR 3D kinetic measurements in gauging the ligand potency and thymic selection. In addition, force-regulated bond lifetime of TCR–pMHC interaction amplified the discrimination of APLs and thymic selection. When force was applied to TCR–pMHC–CD4/8 bonds, two distinct patterns emerged: agonist/negative selecting ligands formed CD4/8-dependent catch-slip bonds, whereas antagonist/positive selecting ligands formed slip-only bonds. In thymic selection, CD8-dependent synergistic effect was critical for negative selection. We speculate that force-prolonged bond lifetime in agonist/negative selecting ligands may allow sufficient time window for signaling molecules such as Lck and Zap70 to accumulate to the TCR proximal for the cascade of downstream signaling events.

In continuation of this study, following questions could be addressed: 1) How would the signaling molecules accumulate in force-prolonged TCR-pMHC interaction; 2) What is the structural mechanism for synergistic TCR-pMHC-CD4/8 interaction under force; 3) How much physiologic force can T cell or thymocytes exert on TCR; 4) Is force critical in actually thymic selection; 5) How does force contribute to “agonist selection;” 6) Can force contribute to on-rate change; 7) Is there CD4 synergy in thymic selection.

To test how force-regulated bond lifetime relate to T cell signaling, our colleagues have measured concurrent calcium imaging for TCR–pMHC interaction (Liu and Chen et al. in press). They have reported that in single-cell analysis calcium flux requires early and rapid accumulation of bond lifetimes whereas low calcium corresponds to high frequency of short lifetimes. Although the study is state of art, calcium is still in the late

stage of T cell signaling and many other proximal signaling activities are missing. In addition, how co-receptors contribute to the initiation of force-regulated TCR signaling is the key question that is not clearly answered. In addition to our force study, fluorescent-based early signaling molecule study is necessary to answer these questions.

In an attempt to study the mechanism of co-receptor dependent catch-slip bonds, disrupting or blocking experiments can be conducted. We have conducted preliminary study with disrupting microfilament using latrunculin A on force-clamp assay. The data show that latrunculin A treatment reduces the bond lifetime somewhat but the overall trend holds for negative selecting ligands (**Figure 7.1**). Other cytoskeleton disrupting reagents such as blebbistatin (inhibitor for myosin II), or cholesterol depletion agent like methyl-β-cyclodextrin or cholesterol oxidase can be used to test its significance in force-lifetime relationship. However, these attempts only show indirect evidence for the force-regulated TCR characteristics. Alternatively, molecular dynamic simulation with protein structure could give more direct information on the mechanism. In these studies, force can be applied to TCR–pMHC–CD4/8 complex and important residues for rebinding or unbinding can be identified. Based on the simulation results, we can further reverse engineer mutate potentially critical residues and verify in experiments. In fact, unpublished data from colleagues (Liu et al.) show that force induces new interaction in TCR–pMHC interaction and also in CD4–MHC interaction. This result support that force may induce conformational change or reveal a cryptic site for a new stronger interaction. For further reveal structural mechanism, more in-depth study is required.

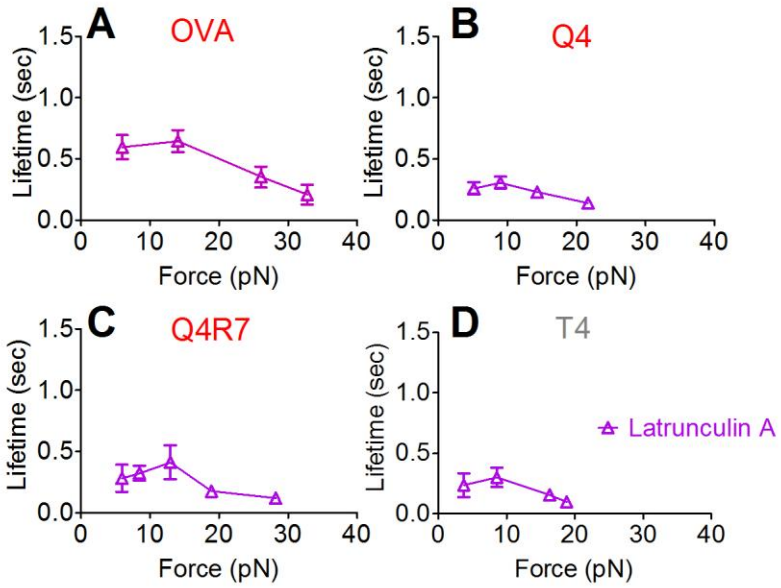

Figure 7.1: Latrunculin A treatment in force-lifetime relationship Latrunculin A treatment lowered bond lifetime somewhat but the overall trend was consistent with no treatment. The sample size of bond lifetime for each ligand is listed as following: OVA (n=350), Q4 (n=129), Q4R7 (n=258), and VSV (n=110).

One of technical advancements in recent years is to manipulate DNA with single-molecule fluorescence resonance energy transfer (smFRET) to measure single-molecule force in the order of pico newtons[116-118]. Recent single molecular force study show that cell apply ~40pN at single integrin-ligand peak tension and less than 12pN is required to activate Notch receptors[119]. This technique could be implemented to answer how much force is actually applied to TCR. It is possible with these DNA force probes that we can read forces being applied on the TCR in a cell culture environment. In addition, we can restrict the force field on the TCR–pMHC by designing the base pair of DNA for further studying force contribution in cellular function. Active study is undergoing with collaboration with Dr. Khalid Salaita's lab in Emory University.

Our results indicated CD8-dependent synergistic TCR–pMHC–CD8 interaction is critical for negative selection. We have verified the findings with endogenous ligands and even in an alternative CD8 system. However, it will be interesting to study the

contribution of CD4 in thymic selection. From our CD4 study, we know that CD4 behave differently to CD8 with no cooperativity under zero-force. However, when force is applied CD4 also enhances the interaction of TCR–pMHC with agonist ligand. Kao et al. [98] previously reported that the antagonist peptide can mediate positive selection in the absence of CD4. How CD4 may contribute to thymic selection will be very interesting. Some studies have reported thymic selection study with APLs[120] and endogenous ligands[121, 122]. Our preliminary force-lifetime assay on AND system show consistent findings with OT-I where catch-slip bond for negative selecting ligand MCC (red square) and slip bond for positive selecting ligand gp250 (blue triangle) (**Figure 7.2**). More thorough experiments are required. In addition, how force on TCR–pMHC interaction regulates "agonist selection" will be very interesting area for future studies.

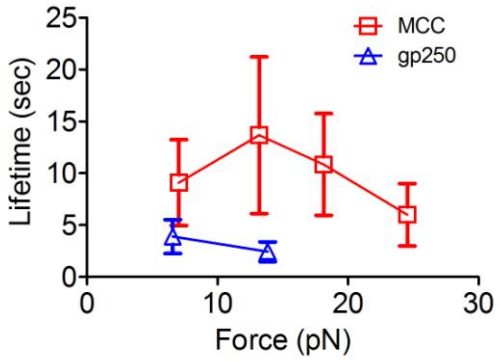

Figure 7.2: Force-lifetime analysis in AND system Preliminary force-regulated bond lifetime data of TCR–pMHC–CD8 interaction in AND system with endogenous negative selecting ligand (MCC, red quare) and positive selecting ligand (gp250, blue triangle)[122]. The sample size of bond lifetime for each ligand is listed as following: MCC (n=57), and gp250 (n=13).

Our results in this thesis successfully identified physiologic characterization of *in situ* TCR–pMHC interaction with considering cellular membrane restrictions and physical force contribution to correlate with cellular function. Our findings highlight an important role of mechanical force in ligand discrimination and suggest a new

mechanism for T activation and thymic selection that is distinct from previous models based on 3D measurements. This work has made a conceptual advance in the field since this is first study to show force-regulated TCR–pMHC–CD4/8 (trimolecular) bond lifetime correlates with T cell activation or thymic selection. The novel findings include measurement of CD4 contribution in TCR-pMHC binding under force, measurement of bond lifetime and stiffness for thymic TCR-pMHC interaction under force, measurement of signaling dependent thymic CD8 cooperativity and synergistic effect under force.

Although there was no single universal indictor for ligand discrimination, it seems like the discrimination mechanism can be affected at least by force level, co-receptor cooperativity, and maturation state. I believe this work has opened a new level of understanding for molecular base of T cell recognition.

REFERENCES

1. Huang, J. et al. The kinetics of two-dimensional TCR and pMHC interactions determine T-cell responsiveness. *Nature* **464**, 932-6 (2010).

2. Yachi, P.P., Ampudia, J., Gascoigne, N.R. & Zal, T. Nonstimulatory peptides contribute to antigen-induced CD8-T cell receptor interaction at the immunological synapse. *Nat Immunol* **6**, 785-92 (2005).

3. Yachi, P.P., Lotz, C., Ampudia, J. & Gascoigne, N.R. T cell activation enhancement by endogenous pMHC acts for both weak and strong agonists but varies with differentiation state. *J Exp Med* **204**, 2747-57 (2007).

4. Holler, P.D. & Kranz, D.M. Quantitative analysis of the contribution of TCR/pepMHC affinity and CD8 to T cell activation. *Immunity* **18**, 255-64 (2003).

5. Ladi, E., Yin, X., Chtanova, T. & Robey, E.A. Thymic microenvironments for T cell differentiation and selection. *Nat Immunol* **7**, 338-43 (2006).

6. Davidson, A. & Diamond, B. Autoimmune diseases. *N Engl J Med* **345**, 340-50 (2001).

7. Kamradt, T. & Mitchison, N.A. Tolerance and autoimmunity. *N Engl J Med* **344**, 655-64 (2001).

8. Nankivell, B.J. & Alexander, S.I. Rejection of the kidney allograft. *N Engl J Med* **363**, 1451-62.

9. Murphy, K., Travers, P. & Walport, M. Janeway's immunobiology (Garland Science, 2008).

10. Palmer, E. & Naeher, D. Affinity threshold for thymic selection through a T-cell receptor-co-receptor zipper. *Nat Rev Immunol* **9**, 207-13 (2009).

11. Singer, A., Adoro, S. & Park, J.H. Lineage fate and intense debate: myths, models and mechanisms of CD4- versus CD8-lineage choice. *Nat Rev Immunol* **8**, 788-801 (2008).

12. Acuto, O., Di Bartolo, V. & Michel, F. Tailoring T-cell receptor signals by proximal negative feedback mechanisms. *Nat Rev Immunol* **8**, 699-712 (2008).

13. Oh-hora, M. & Rao, A. Calcium signaling in lymphocytes. *Curr Opin Immunol* **20**, 250-8 (2008).

14. Konig, R., Huang, L.Y. & Germain, R.N. MHC class II interaction with CD4 mediated by a region analogous to the MHC class I binding site for CD8. *Nature* **356**, 796-8 (1992).

15. Cammarota, G. et al. Identification of a CD4 binding site on the beta 2 domain of HLA-DR molecules. *Nature* **356**, 799-801 (1992).

16. Gibbings, D. & Befus, A.D. CD4 and CD8: an inside-out coreceptor model for innate immune cells. *J Leukoc Biol* **86**, 251-9 (2009).

17. Dustin, M.L. Cell adhesion molecules and actin cytoskeleton at immune synapses and kinapses. *Curr Opin Cell Biol* **19**, 529-33 (2007).

18. Smith-Garvin, J.E., Koretzky, G.A. & Jordan, M.S. T cell activation. *Annu Rev Immunol* **27**, 591-619 (2009).

19. Feske, S. Calcium signalling in lymphocyte activation and disease. *Nat Rev Immunol* **7**, 690-702 (2007).

20. Nel, A.E. T-cell activation through the antigen receptor. Part 1: signaling components, signaling pathways, and signal integration at the T-cell antigen receptor synapse. *J Allergy Clin Immunol* **109**, 758-70 (2002).

21. Seminario, M.C. & Bunnell, S.C. Signal initiation in T-cell receptor microclusters. *Immunol Rev* **221**, 90-106 (2008).

22. Fooksman, D. et al. Functional Anatomy of T Cell Activation and Synapse Formation. *Annual Review of Immunology* **28**, 79-105 (2009).

23. Lee, K.H. et al. The immunological synapse balances T cell receptor signaling and degradation. *Science* **302**, 1218-22 (2003).

24. Lee, K.H. et al. T cell receptor signaling precedes immunological synapse formation. *Science* **295**, 1539-42 (2002).

25. Lewis, R.S. Calcium signaling mechanisms in T lymphocytes. *Annu Rev Immunol* **19**, 497-521 (2001).

26. Randriamampita, C. & Trautmann, A. Ca2+ signals and T lymphocytes; "New mechanisms and functions in Ca2+ signalling". *Biol Cell* **96**, 69-78 (2004).

27. Zarnitsyna, V. & Zhu, C. T cell triggering: insights from 2D kinetics analysis of molecular interactions. *Phys Biol* **9**, 045005 (2012).

28. Choudhuri, K. & van der Merwe, P.A. Molecular mechanisms involved in T cell receptor triggering. *Semin Immunol* **19**, 255-61 (2007).

29. Morris, G.P. & Allen, P.M. How the TCR balances sensitivity and specificity for the recognition of self and pathogens. *Nat Immunol* **13**, 121-8 (2012).

30. Stone, J.D., Chervin, A.S. & Kranz, D.M. T-cell receptor binding affinities and kinetics: impact on T-cell activity and specificity. *Immunology* **126**, 165-76 (2009).

31. Davis, M.M. et al. Ligand recognition by alpha beta T cell receptors. *Annu Rev Immunol* **16**, 523-44 (1998).

32. Gascoigne, N.R., Zal, T. & Alam, S.M. T-cell receptor binding kinetics in T-cell development and activation. *Expert Rev Mol Med* **2001**, 1-17 (2001).

33. Alam, S.M. et al. T-cell-receptor affinity and thymocyte positive selection. *Nature* **381**, 616-20 (1996).

34. Alam, S.M. et al. Qualitative and quantitative differences in T cell receptor binding of agonist and antagonist ligands. *Immunity* **10**, 227-37 (1999).

35. Degano, M. et al. A functional hot spot for antigen recognition in a superagonist TCR/MHC complex. *Immunity* **12**, 251-61 (2000).

36. Kersh, G.J., Kersh, E.N., Fremont, D.H. & Allen, P.M. High- and low-potency ligands with similar affinities for the TCR: the importance of kinetics in TCR signaling. *Immunity* **9**, 817-26 (1998).

37. Yi, J., Wu, X.S., Crites, T. & Hammer, J.A., 3rd. Actin retrograde flow and actomyosin II arc contraction drive receptor cluster dynamics at the immunological synapse in Jurkat T cells. *Mol Biol Cell* **23**, 834-52 (2012).

38. Kim, S.T. et al. The alphabeta T cell receptor is an anisotropic mechanosensor. *J Biol Chem* **284**, 31028-37 (2009).

39. Huppa, J.B. et al. TCR-peptide-MHC interactions in situ show accelerated kinetics and increased affinity. *Nature* **463**, 963-7 (2010).

40. Huang, J., Edwards, L.J., Evavold, B.D. & Zhu, C. Kinetics of MHC-CD8 interaction at the T cell membrane. *J Immunol* **179**, 7653-62 (2007).

41. Jiang, N. et al. Two-Stage Cooperative T Cell Receptor-Peptide Major Histocompatibility Complex-CD8 Trimolecular Interactions Amplify Antigen Discrimination. *Immunity* **34**, 13-23 (2011).

42. Sabatino, J.J., Jr., Huang, J., Zhu, C. & Evavold, B.D. High prevalence of low affinity peptide-MHC II tetramer-negative effectors during polyclonal CD4+ T cell responses. *J Exp Med* **208**, 81-90 (2011).

43. Adams, J.J. et al. T Cell Receptor Signaling Is Limited by Docking Geometry to Peptide-Major Histocompatibility Complex. *Immunity* (2011).

44. Werlen, G., Hausmann, B., Naeher, D. & Palmer, E. Signaling life and death in the thymus: timing is everything. *Science* **299**, 1859-63 (2003).

45. Moran, A.E. & Hogquist, K.A. T-cell receptor affinity in thymic development. *Immunology* **135**, 261-7 (2012).

46. Palmer, E. Negative selection--clearing out the bad apples from the T-cell repertoire. *Nat Rev Immunol* **3**, 383-91 (2003).

47. Hogquist, K.A. et al. T cell receptor antagonist peptides induce positive selection. *Cell* **76**, 17-27 (1994).

48. Baldwin, T.A., Hogquist, K.A. & Jameson, S.C. The fourth way? Harnessing aggressive tendencies in the thymus. *J Immunol* **173**, 6515-20 (2004).

49. Fontenot, J.D. & Rudensky, A.Y. Molecular aspects of regulatory T cell development. *Semin Immunol* **16**, 73-80 (2004).

50. Gapin, L. The making of NKT cells. *Nat Immunol* **9**, 1009-11 (2008).

51. Leishman, A.J. et al. Precursors of functional MHC class I- or class II-restricted CD8alphaalpha(+) T cells are positively selected in the thymus by agonist self-peptides. *Immunity* **16**, 355-64 (2002).

52. Daniels, M.A. et al. Thymic selection threshold defined by compartmentalization of Ras/MAPK signalling. *Nature* **444**, 724-9 (2006).

53. Naeher, D. et al. A constant affinity threshold for T cell tolerance. *J Exp Med* **204**, 2553-9 (2007).

54. Williams, C.B., Engle, D.L., Kersh, G.J., Michael White, J. & Allen, P.M. A kinetic threshold between negative and positive selection based on the longevity of the T cell receptor-ligand complex. *J Exp Med* **189**, 1531-44 (1999).

55. King, C.G. et al. T cell affinity regulates asymmetric division, effector cell differentiation, and tissue pathology. *Immunity* **37**, 709-20 (2012).

56. Risueno, R.M., van Santen, H.M. & Alarcon, B. A conformational change senses the strength of T cell receptor-ligand interaction during thymic selection. *Proc Natl Acad Sci U S A* **103**, 9625-30 (2006).

57. Gil, D., Schrum, A.G., Alarcon, B. & Palmer, E. T cell receptor engagement by peptide-MHC ligands induces a conformational change in the CD3 complex of thymocytes. *J Exp Med* **201**, 517-22 (2005).

58. Werlen, G., Hausmann, B. & Palmer, E. A motif in the alphabeta T-cell receptor controls positive selection by modulating ERK activity. *Nature* **406**, 422-6 (2000).

59. Doucey, M.A. et al. CD3 delta establishes a functional link between the T cell receptor and CD8. *J Biol Chem* **278**, 3257-64 (2003).

60. McCarty, N. et al. Signaling by the kinase MINK is essential in the negative selection of autoreactive thymocytes. *Nat Immunol* **6**, 65-72 (2005).

61. Lo, W.L., Donermeyer, D.L. & Allen, P.M. A voltage-gated sodium channel is essential for the positive selection of CD4(+) T cells. *Nat Immunol* **13**, 880-7 (2012).

62. Fu, G. et al. Themis controls thymocyte selection through regulation of T cell antigen receptor-mediated signaling. *Nat Immunol* **10**, 848-56 (2009).

63. Brockmeyer, C. et al. T cell receptor (TCR)-induced tyrosine phosphorylation dynamics identifies THEMIS as a new TCR signalosome component. *J Biol Chem* **286**, 7535-47 (2011).

64. Fu, G. et al. Themis sets the signal threshold for positive and negative selection in T-cell development. *Nature* **504**, 441-5 (2013).

65. Puls, K.L., Hogquist, K.A., Reilly, N. & Wright, M.D. CD53, a thymocyte selection marker whose induction requires a lower affinity TCR-MHC interaction than CD69, but is up-regulated with slower kinetics. *Int Immunol* **14**, 249-58 (2002).

66. Kozono, H., White, J., Clements, J., Marrack, P. & Kappler, J. Production of soluble MHC class II proteins with covalently bound single peptides. *Nature* **369**, 151-4 (1994).

67. Hogquist, K.A. et al. Identification of a naturally occurring ligand for thymic positive selection. *Immunity* **6**, 389-99 (1997).

68. Santori, F.R. et al. Rare, structurally homologous self-peptides promote thymocyte positive selection. *Immunity* **17**, 131-42 (2002).

69. Nathenson, S.G., Geliebter, J., Pfaffenbach, G.M. & Zeff, R.A. Murine major histocompatibility complex class-I mutants: molecular analysis and structure-function implications. *Annu Rev Immunol* **4**, 471-502 (1986).

70. Tallquist, M.D., Yun, T.J. & Pease, L.R. A single T cell receptor recognizes structurally distinct MHC/peptide complexes with high specificity. *J Exp Med* **184**, 1017-26 (1996).

71. Kuhns, S.T., Tallquist, M.D., Johnson, A.J., Mendez-Fernandez, Y. & Pease, L.R. T cell receptor interactions with class I heavy-chain influence T cell selection. *Proc Natl Acad Sci U S A* **97**, 756-60 (2000).

72. Pawlowski, T.J., Singleton, M.D., Loh, D.Y., Berg, R. & Staerz, U.D. Permissive recognition during positive selection. *Eur J Immunol* **26**, 851-7 (1996).

73. Chesla, S.E., Selvaraj, P. & Zhu, C. Measuring two-dimensional receptor-ligand binding kinetics by micropipette. *Biophys J* **75**, 1553-72 (1998).

74. Chen, W., Zarnitsyna, V.I., Sarangapani, K.K., Huang, J. & Zhu, C. Measuring Receptor-Ligand Binding Kinetics on Cell Surfaces: From Adhesion Frequency to Thermal Fluctuation Methods. *Cell Mol Bioeng* **1**, 276-288 (2008).

75. Chen, W., Lou, J., Evans, E.A. & Zhu, C. Observing force-regulated conformational changes and ligand dissociation from a single integrin on cells. *J Cell Biol* **199**, 497-512 (2012).

76. Chen, W., Lou, J. & Zhu, C. Forcing switch from short- to intermediate- and long-lived states of the alphaA domain generates LFA-1/ICAM-1 catch bonds. *J Biol Chem* **285**, 35967-78 (2010).

77. Lou, J. et al. Flow-enhanced adhesion regulated by a selectin interdomain hinge. *J Cell Biol* **174**, 1107-17 (2006).

78. Marshall, B.T. et al. Measuring molecular elasticity by atomic force microscope cantilever fluctuations. *Biophys J* **90**, 681-92 (2006).

79. Persaud, S.P., Donermeyer, D.L., Weber, K.S., Kranz, D.M. & Allen, P.M. High-affinity T cell receptor differentiates cognate peptide-MHC and altered peptide ligands with distinct kinetics and thermodynamics. *Mol Immunol* **47**, 1793-801 (2010).

80. Krogsgaard, M. et al. Agonist/endogenous peptide-MHC heterodimers drive T cell activation and sensitivity. *Nature* **434**, 238-43 (2005).

81. Artyomov, M.N., Lis, M., Devadas, S., Davis, M.M. & Chakraborty, A.K. CD4 and CD8 binding to MHC molecules primarily acts to enhance Lck delivery. *Proc Natl Acad Sci U S A* **107**, 16916-21 (2010).

82. Xiong, Y., Kern, P., Chang, H. & Reinherz, E. T Cell Receptor Binding to a pMHCII Ligand Is Kinetically Distinct from and Independent of CD4. *J Biol Chem* **276**, 5659-67 (2001).

83. Kersh, G.J. & Allen, P.M. Structural basis for T cell recognition of altered peptide ligands: a single T cell receptor can productively recognize a large continuum of related ligands. *J Exp Med* **184**, 1259-68 (1996).

84. Chen, W., Evans, E.A., McEver, R.P. & Zhu, C. Monitoring receptor-ligand interactions between surfaces by thermal fluctuations. *Biophys J* **94**, 694-701 (2008).

85. Husson, J., Chemin, K., Bohineust, A., Hivroz, C. & Henry, N. Force generation upon T cell receptor engagement. *PLoS One* **6**, e19680.

86. Judokusumo, E., Tabdanov, E., Kumari, S., Dustin, M.L. & Kam, L.C. Mechanosensing in T lymphocyte activation. *Biophys J* **102**, L5-7 (2012).

87. Li, Y.C. et al. Cutting Edge: mechanical forces acting on T cells immobilized via the TCR complex can trigger TCR signaling. *J Immunol* **184**, 5959-63 (2010).

88. Ma, Z. & Finkel, T.H. T cell receptor triggering by force. *Trends Immunol* **31**, 1-6 (2010).

89. Liu, B. et al. 2D TCR-pMHC-CD8 kinetics determines T-cell responses in a self-antigen-specific TCR system. *Eur J Immunol* (2013).

90. Huang, J., Meyer, C. & Zhu, C. T cell antigen recognition at the cell membrane. *Mol Immunol* **52**, 155-64 (2012).

91. Edwards, L.J., Zarnitsyna, V.I., Hood, J.D., Evavold, B.D. & Zhu, C. Insights into T cell recognition of antigen: significance of two-dimensional kinetic parameters. *Front Immunol* **3**, 86 (2012).

92. Robert, P. et al. Kinetics and mechanics of two-dimensional interactions between T cell receptors and different activating ligands. *Biophys J* **102**, 248-57 (2012).

93. Ashton-Rickardt, P.G. et al. Evidence for a differential avidity model of T cell selection in the thymus. *Cell* **76**, 651-63 (1994).

94. Sebzda, E. et al. Positive and negative thymocyte selection induced by different concentrations of a single peptide. *Science* **263**, 1615-8 (1994).

95. Davey, G.M. et al. Preselection thymocytes are more sensitive to T cell receptor stimulation than mature T cells. *J Exp Med* **188**, 1867-74 (1998).

96. Daniels, M.A. et al. CD8 binding to MHC class I molecules is influenced by T cell maturation and glycosylation. *Immunity* **15**, 1051-61 (2001).

97. Moody, A.M. et al. Developmentally regulated glycosylation of the CD8alphabeta coreceptor stalk modulates ligand binding. *Cell* **107**, 501-12 (2001).

98. Kao, H. & Allen, P.M. An antagonist peptide mediates positive selection and CD4 lineage commitment of MHC class II-restricted T cells in the absence of CD4. *J Exp Med* **201**, 149-58 (2005).

99. Li, Q.J. et al. CD4 enhances T cell sensitivity to antigen by coordinating Lck accumulation at the immunological synapse. *Nat Immunol* **5**, 791-9 (2004).

100. Hampl, J., Chien, Y.H. & Davis, M.M. CD4 augments the response of a T cell to agonist but not to antagonist ligands. *Immunity* **7**, 379-85 (1997).

101. Hamad, A.R. et al. Potent T cell activation with dimeric peptide-major histocompatibility complex class II ligand: the role of CD4 coreceptor. *J Exp Med* **188**, 1633-40 (1998).

102. Yu, C.H., Wu, H.J., Kaizuka, Y., Vale, R.D. & Groves, J.T. Altered actin centripetal retrograde flow in physically restricted immunological synapses. *PLoS One* **5**, e11878 (2010).

103. Babich, A. et al. F-actin polymerization and retrograde flow drive sustained PLCgamma1 signaling during T cell activation. *J Cell Biol* **197**, 775-87 (2012).

104. Huse, M. et al. Spatial and temporal dynamics of T cell receptor signaling with a photoactivatable agonist. *Immunity* **27**, 76-88 (2007).

105. Kong, F. et al. Cyclic mechanical reinforcement of integrin-ligand interactions. *Mol Cell* **49**, 1060-8 (2013).

106. Marshall, B.T. et al. Direct observation of catch bonds involving cell-adhesion molecules. *Nature* **423**, 190-3 (2003).

107. Yago, T. et al. Catch bonds govern adhesion through L-selectin at threshold shear. *J Cell Biol* **166**, 913-23 (2004).

108. Thomas, W. Catch bonds in adhesion. *Annu Rev Biomed Eng* **10**, 39-57 (2008).

109. Kong, F., Garcia, A.J., Mould, A.P., Humphries, M.J. & Zhu, C. Demonstration of catch bonds between an integrin and its ligand. *J Cell Biol* **185**, 1275-84 (2009).

110. Yago, T. et al. Platelet glycoprotein Ibalpha forms catch bonds with human WT vWF but not with type 2B von Willebrand disease vWF. *J Clin Invest* **118**, 3195-207 (2008).

111. Lee, C.Y. et al. Actin depolymerization under force is governed by lysine 113:glutamic acid 195-mediated catch-slip bonds. *Proc Natl Acad Sci U S A* **110**, 5022-7 (2013).

112. Lou, J. & Zhu, C. A structure-based sliding-rebinding mechanism for catch bonds. *Biophys J* **92**, 1471-85 (2007).

113. Davis, S.J. & van der Merwe, P.A. The kinetic-segregation model: TCR triggering and beyond. *Nat Immunol* **7**, 803-9 (2006).

114. Tan, Y.X. et al. Inhibition of the kinase Csk in thymocytes reveals a requirement for actin remodeling in the initiation of full TCR signaling. *Nat Immunol* **15**, 186-94 (2014).

115. Le Borgne, M. et al. The impact of negative selection on thymocyte migration in the medulla. *Nat Immunol* **10**, 823-30 (2009).

116. Stabley, D.R., Jurchenko, C., Marshall, S.S. & Salaita, K.S. Visualizing mechanical tension across membrane receptors with a fluorescent sensor. *Nat Methods* **9**, 64-7 (2012).

117. Liu, Y., Yehl, K., Narui, Y. & Salaita, K. Tension sensing nanoparticles for mechano-imaging at the living/nonliving interface. *J Am Chem Soc* **135**, 5320-3 (2013).

118. Hohng, S. et al. Fluorescence-force spectroscopy maps two-dimensional reaction landscape of the holliday junction. *Science* **318**, 279-83 (2007).

119. Wang, X. & Ha, T. Defining single molecular forces required to activate integrin and notch signaling. *Science* **340**, 991-4 (2013).

120. Kersh, G.J., Engle, D.L., Williams, C.B. & Allen, P.M. Ligand-specific selection of MHC class II-restricted thymocytes in fetal thymic organ culture. *J Immunol* **164**, 5675-82 (2000).

121. Ebert, P.J., Jiang, S., Xie, J., Li, Q.J. & Davis, M.M. An endogenous positively selecting peptide enhances mature T cell responses and becomes an autoantigen in the absence of microRNA miR-181a. *Nat Immunol* **10**, 1162-9 (2009).

122. Lo, W.L. et al. An endogenous peptide positively selects and augments the activation and survival of peripheral CD4+ T cells. *Nat Immunol* **10**, 1155-61 (2009).